VILNIUS TECH
Vilniaus Gedimino technikos universitetas

Povilas DABRILA

STRUCTURAL ANALYSIS OF INNOVATIVE STEEL CABLE-STAYED-STRING BRIDGE

DOCTORAL DISSERTATION

TECHNOLOGICAL SCIENCES
CIVIL ENGINEERING (T 002)

Vilnius, 2025

2025-026-M

VILNIUS GEDIMINAS TECHNICAL UNIVERSITY

Povilas DABRILA

STRUCTURAL ANALYSIS OF INNOVATIVE STEEL CABLE-STAYED-STRING BRIDGE

DOCTORAL DISSERTATION

TECHNOLOGICAL SCIENCES
CIVIL ENGINEERING (T 002)

Vilnius, 2025

The doctoral dissertation was prepared at Vilnius Gediminas Technical University in 2020–2025.

Supervisor

Prof. Dr Algirdas JUOZAPAITIS (Vilnius Gediminas Technical University, Civil Engineering – T 002).

The Dissertation Defence Council of the Scientific Field of Civil Engineering of Vilnius Gediminas Technical University:

Chairman

Prof. Dr Darius BAČINSKAS (Vilnius Gediminas Technical University, Civil Engineering – T 002).

Members:

Assoc. Prof. Dr Tomas GEČYS (Vilnius Gediminas Technical University, Civil Engineering – T 002),

Dr Virginijus MARCINKEVIČIUS (Vilnius University, Informatics Engineering – T 007),

Prof. Dr Habil. Hartmut PASTERNAK (Brandenburg University of Technology, Germany, Civil Engineering – T 002),

Prof. Dr Antanas ŠAPALAS (Vilnius Gediminas Technical University, Civil Engineering – T 002).

The dissertation will be defended at the public meeting of the Dissertation Defence Council of the Scientific Field of Civil Engineering in the *Aula Doctoralis* Meeting Hall of Vilnius Gediminas Technical University at **9 a.m. on 6 June 2025**.

Address: Saulėtekio al. 11, LT-10223 Vilnius, Lithuania.
Tel.: +370 5 274 4956; fax +370 5 270 0112; e-mail: doktor@vilniustech.lt

A notification on the intended defence of the dissertation was sent on 5 May 2025. A copy of the doctoral dissertation is available for review at Vilnius Gediminas Technical University repository https://etalpykla.vilniustech.lt and the Library of Vilnius Gediminas Technical University (Saulėtekio al. 14, LT-10223 Vilnius, Lithuania).

Vilnius Gediminas Technical University book No 2025-026-M

https://doi.org/10.20334/2025-026-M

povilas.dabrila@vilniustech.lt

VILNIAUS GEDIMINO TECHNIKOS UNIVERSITETAS

Povilas DABRILA

INOVATYVAUS VANTINIO-STYGINIO PLIENO TILTO KONSTRUKCIJŲ ANALIZĖ

DAKTARO DISERTACIJA

TECHNOLOGIJOS MOKSLAI,
STATYBOS INŽINERIJA (T 002)

Vilnius, 2025

Disertacija rengta 2020–2025 metais Vilniaus Gedimino technikos universitete.

Vadovas

prof. dr. Algirdas JUOZAPAITIS (Vilniaus Gedimino technikos universitetas, Statybos inžinerija – T 002).

Vilniaus Gedimino technikos universiteto Statybos inžinerijos mokslo krypties disertacijos gynimo taryba:

Pirmininkas

prof. dr. Darius BAČINSKAS (Vilniaus Gedimino technikos universitetas, Statybos inžinerija – T 002).

Nariai:

doc. dr. Tomas GEČYS (Vilniaus Gedimino technikos universitetas, Statybos inžinerija – T 002),

dr. Virginijus MARCINKEVIČIUS (Vilniaus universitetas, Informatikos inžinerija – T 007),

prof. habil. dr. Hartmut PASTERNAK (Brandenburgo technologijos universitetas, Vokietija, Statybos inžinerija – T 002),

prof. dr. Antanas ŠAPALAS (Vilniaus Gedimino technikos universitetas, Statybos inžinerija – T 002).

Disertacija bus ginama viešame Statybos inžinerijos mokslo krypties disertacijos gynimo tarybos posėdyje **2025 m. birželio 6 d. 9 val.** Vilniaus Gedimino technikos universiteto *Aula Doctoralis* posėdžių salėje.

Adresas: Saulėtekio al. 11, LT-10223 Vilnius, Lietuva.
Tel.: (0 5) 274 4956; faksas (0 5) 270 0112; el. paštas doktor@vilniustech.lt

Pranešimai apie numatomą ginti disertaciją išsiųsti 2025 m. gegužės 5 d.

Disertaciją galima peržiūrėti Vilniaus Gedimino technikos universiteto talpykloje https://etalpykla.vilniustech.lt ir Vilniaus Gedimino technikos universiteto bibliotekoje (Saulėtekio al. 14, LT-10223 Vilnius, Lietuva).

Abstract

Cable-stayed bridges are a type of bridge structure with a rich history spanning a couple of centuries. They are known for their distinctive architectural expression and ability to span some of the longest distances in the world. It is essential to recognise that beneath the elegant aesthetics of cable-stayed bridges lies a complex interaction of forces that can lead to undesirable behavioural issues. Engineers and scientists actively seek new solutions, design innovative forms of these bridges, and develop methodologies to evaluate them. One such example is the application of pedestrian bridges with intersecting cable-stays. Although these structural solutions show promise, they remain relatively new. It is noted that detailed analysis of bridge behaviour and calculation methodologies are lacking.

This dissertation examines a novel structural system for a cable-stayed-string steel bridge with intersecting cables and intermediate pylons. Its behaviour is investigated through experimental model studies and numerical and analytical analysis. The work aims to develop an innovative pedestrian bridge design with crossed cables and create a calculation methodology for its analysis.

The First Chapter provides a brief history of cable-stayed pedestrian bridges, the current research outlook, and a literature review of their structures and load-bearing elements. It also discusses methods for calculating cable-stayed bridges and inclined cables.

The Second Chapter introduces the calculation methodology for two types of bridge constructions: one with a stiffening beam and another with a string. The composition of the hybrid cable-stayed-string bridge is performed, and rational parameters are identified. The rational heights and arrangements of pylons are provided. A proposed assembly sequence for construction is provided.

The Third Chapter analyses the behaviour of the intersecting cable system using experimental model studies and numerical analysis. It presents the stresses and displacements of symmetrically and asymmetrically loaded bridge systems and compares the results of physical experiments and numerical analyses. The influence of pretensioning in the string and intersecting cable-stays on the bridge structure's behaviour is demonstrated.

The dissertation findings have been published in two scientific articles in peer-reviewed journals, and the results of the research conducted in the dissertation have been presented at two scientific conferences.

Reziumė

Vantiniai tiltai – tiltų konstrukcijos tipas, turintis turtingą, porą šimtmečių besitęsiančią istoriją bei garsėjantis išskirtine architektūrine išraiška ir gebėjimu įveikti vienus ilgiausių atstumų pasaulyje. Tačiau po elegantiška vantinių tiltų estetika slypi sudėtinga jėgų sąveika, kuri gali sukelti nepageidaujamų problemų. Inžinieriai ir mokslininkai aktyviai ieško naujų sprendimų, kuria naujas šio tipo tilto formas ir metodikas šioms formoms vertinti. Toks naujas sprendinys yra kryžminių vantų pėsčiųjų tiltai. Nors tokie konstrukciniai sprendiniai yra perspektyvūs, jie vis dar yra ganėtinai nauji. Pastebima, kad trūksta detalesnės tiltų elgsenos analizės ir skaičiavimo metodikų.

Disertacijoje aptariama nauja vantinio-styginio plieninio tilto konstrukcinė sistema su kryžminiais vantais ir tarpiniais pilonais. Tilto elgesena nagrinėjama atliekant eksperimentinio modelio tyrimą, skaitinę ir analitinę analizę. Darbo tikslas – sukurti inovatyvią kryžminių vantų pėsčiųjų tilto konstrukciją bei parengti jos inžinerinę skaičiavimo metodiką.

Pirmame skyriuje pateikiama trumpa vantinių pėsčiųjų tiltų istorija, dabartinė tyrimų kryptis bei jų konstrukcijų ir laikančiųjų elementų literatūros apžvalga. Apžvelgiamos vantinių tiltų, pasvirusių lynų skaičiavimo metodikos.

Antrame skyriuje pristatoma dviejų tipų tilto konstrukcijų – su standumo sija ir su styga – inžinerinė skaičiavimo metodika. Atliekamas vantinio-styginio tilto komponavimas ir parenkami racionalūs parametrai. Pateikti racionalūs pilono aukščiai ir galimas jų išdėstymas.

Trečiame skyriuje analizuojama kryžminių vantų sistemos elgesena vykdant modelio eksperimentą ir skaitinę analizę. Pateikiamos simetriškai ir asimetriškai apkrautos tilto sistemos įrąžos ir poslinkiai, palyginami fizinio eksperimento ir skaitinės analizės rezultatai. Parodyta stygų ir kryžminių vantų išankstinio įtempimo įtaka tilto konstrukcijos elgsenai.

Disertacijos medžiaga paskelbta dviejuose moksliniuose straipsniuose, kurie yra recenzuojamuose mokslo žurnaluose, o disertacijoje atliktų tyrimų rezultatai – dviejose mokslinėse konferencijose.

Notations

Symbols

α, β, γ – the angle between the pylon and cable (liet. *kampas tarp pilonų ir vantų*);
A_{vi} – cable cross-section area (liet. *vantų skerspjūvio plotas*);
Δf_{0i} – cable initial sag (liet. *vanto pradinis įsviris*);
Δ_{pi} – beam deflection caused by external force (liet. *išorinės jėgos sukeltas sijos įlinkis*);
δ_{ci} – beam deflection caused by cable support reactions (liet. *palaikančiųjų jėgų sukeltas sijos įlinkis*);
Δf_{vi} – cable sag (liet. *vanto įsviris*);
Δf – middle cable/string displacement (liet. *stygos / vanto vidurio įlinkis*);
Δl_i – elongation of a cable (liet. *vanto pailgėjimas*);
E_{vi} – cable elastic modulus (liet. *tamprumo modulis*);
$F_{support}$ – support reaction at the cable-stay connection point (liet. *vantų palaikančioji jėga jų jungimo vietoje*);
F_{zi} – supportive reaction at the cable's end in the z-axis (liet. *vanto galų palaikančioji jėga z ašyje*);
H – tension force (liet. *ašinė jėga*);
M_i – internal moment (liet. *lenkimo momentas*);
$N_{pi_{min}}$ – minimal axial prestress force (liet. *minimalus išankstinis įtempimas*);
N_i – axial cable-stay force (liet. *ašinė vanto jėga*);
N_{pi} – prestress force (liet. *išankstinio įtempimo jėga*);
p_l – cable own weight (liet. *vanto svoris*);

P – girder axial force (liet. *ašinė sijos jėga*);

q_z; q_x – cable own weight load in the z and x-axis (liet. *vanto soris z ir x ašyse*);

S_m – combined distributed load (liet. *suminė išskirstytoji apkrova*);

w_l, M_l – deflections and bending moments obtained with linear calculation (liet. *tiesiškai apskaičiuoti įlinkiai ir lenkimo momentai*);

w_n, M_n – deflections and bending moments, considering nonlinear effects (liet. *netiesiškai apskaičiuoti įlinkiai ir lenkimo momentai*).

Abbreviations

FEM – finite element method (liet. *baigtinių elementų metodas)*;

L-BFGS – limited memory variant of BFGS (liet. *Broyden–Fletcher–Goldfarb–Shanno metodas ribotos atminties sistemoms*);

BFGS – Broyden–Fletcher–Goldfarb–Shanno method (liet. *Broyden–Fletcher–Goldfarb–Shanno metodas*).

Contents

Introduction

Problem formulation

Cable-stayed bridges with intersecting cable-stays are relatively new and marked with geometrically nonlinear behaviour. The literature overview of previously published works on the discussed structure did not present a design methodology or detailed design guidelines. Furthermore, coupled with a prestressed string, its behaviour becomes even more complex and less studied. Currently, the following questions about the intersecting cable-stayed bridge system remain:

- Rational shape parameters of the system are unknown: the number of internodes (pylons), the shape of the pylon outline, etc.;
- A methodology to determine displacements and stresses in the system is lacking;
- The behaviour of this bridge structure at asymmetrical pedestrian loading has not been thoroughly researched;
- Geometrical nonlinear behaviour during symmetrical and asymmetrical loading has not been researched.

Relevance of the dissertation

With growing populations worldwide, there is a rising need for sustainable infrastructure. Minimising the depletion of natural resources, carbon footprint, and considerations about the well-being of communities using this infrastructure become inseparable from built environment development. These goals demand effective solutions throughout the process, including bridges.

Cable-stayed bridges hold a unique position in construction due to their efficient design and striking architectural presence. They are also effectively employed in pedestrian bridges with shorter spans. Nevertheless, these bridges come with certain limitations. First, they are susceptible to displacements under asymmetrical loads and require relatively hefty stiffening girders. Second, the effectiveness of cable-stayed bridges is constrained by the minimum angle at which the cables can be inclined. Furthermore, constraints posed by urban or economic factors may restrict the height of pylons, thereby limiting the system's adaptability.

Amidst these challenges, innovative solutions such as replacing the stiffening girder with a string and implementing the configuration of the intersecting cable stays (sometimes referred to as an inverted fink truss) offer mitigations of these challenges. In particular, the intersecting cable solution helps maintain the bridge's initial shape during asymmetrical loading by efficiently distributing loads, reducing material usage, and improving resistance to dynamic loads. Although this structure shows promise, it remains relatively unexplored, with only a handful of examples constructed so far. Despite its potential, there is a notable absence of established calculation methodologies for this type of structure. Designing such bridges with rational parameter solutions is challenging without calculation methods or experimental data.

Research object

The dissertation's research object is the stresses and deformations of a pedestrian cable-stayed-string bridge structural system with intersecting cable stays and load-bearing elements.

Aim of the dissertation

The dissertation aims to create a new cable-stayed-string bridge with intersecting cable stays and analyse this structure's stress and deformation state.

Tasks of the dissertation

The following tasks have to be solved to achieve the aim of the dissertation:

1. To compose the structural system of the new cable-stayed bridge and analyse its behaviour.
2. To develop a calculation methodology for stresses and deflections of the load-bearing elements of a cable-stayed bridge with (1) a stiffening girder and (2) a cable.
3. To perform a numerical analysis of the behaviour of the new cable-stayed bridge structure under static symmetrical and asymmetrical static pedestrian loads.
4. To carry out experimental studies of the model of the steel cable-stayed-string bridge structure.
5. To compare analysis results with FEM data.

Research methodology

The following research analytical methods were chosen to investigate the object: static behaviour analysis, which assesses geometrically nonlinear behaviour; numerical modelling (finite element) methods, and physical experimentation.

Scientific novelty of the dissertation

During the preparation of the dissertation, the following new results were obtained for civil engineering:

1. A novel cable-stayed-string bridge structure was proposed.
2. A calculation methodology for the strains and displacements of the load-bearing elements of an intersecting cable-stay pedestrian bridge with a stiffening girder and a string has been prepared.
3. The first experimental study of the new cable-stayed-string steel bridge structure model was carried out.

Practical value of the research findings

A new cable-stayed bridge with intersecting cables and a string was created. Furthermore, the proposed methodology for designing intersecting cable-stay bridges provides a systematic approach to determining the geometry and selecting

appropriate cross-sections for supporting elements. This methodology simplifies the development of a balanced structural outline, aids in preparing a numerical model, and shortens the initial design process.

Defended statements

The following statements based on the results of the present investigation may serve as defended statements:

1. Intersecting cable-stayed pedestrian bridges effectively redistributes asymmetrical pedestrian loads, reducing displacements and bending moments in the stiffening beam compared to conventional cable-stayed designs.
2. Proper prestressing of both cross-cables and strings in an intersecting cable bridge is essential to stabilise its initial shape.
3. The calculation method for cable-stayed and cable-string bridges demonstrates less than a 4% discrepancy from numerical analyses, allowing for an accurate assessment of internal stresses and deflections under both symmetrical and asymmetrical loads.
4. Finite element analyses of cable-stayed bridge prototypes validate experimental measurements with internal forces and displacement values aligning within a 9–10% range, thereby underscoring the reliability of the modelling approach.

Approval of the research findings

Five scientific articles in peer-reviewed scientific journals on the topic of the dissertation were published, two of which are in the publications of the *Web of Science* database with a citation index, one article in the publication of other international databases, and two articles in conference proceedings. The list of the author's publications is given on page 98. The author has made two presentations at two scientific conferences:

- XIV International Conference on Metal Structures (ICMS, 2021), 2021, Poznań, Poland.
- IABSE Congress Nanjing 2022 – Bridges and Structures: Connection, Integration, and Harmonisation, 2022, Nanjing, China.

Structure of the dissertation

The dissertation consists of an introduction, three chapters, and a summary of the results. The volume of the work is 121 pages, excluding appendices, 102 numbered formulas, 64 figures, and 16 tables used in the text. The dissertation used 108 literature sources.

Acknowledgement

The author expresses his sincere gratitude and acknowledgement to his supervisor, Professor Dr Algirdas Juozapaitis, for his guidance and assistance.
Special thanks are given to “Peikko Lietuva” and IDDO, who provided him with the materials necessary for the bridge model experiment.
Finally, the author would like to thank his family and friends for their constant support and encouragement.

1

Overview of cable-stayed and string bridge structures

This chapter reviews existing research on cable-stayed bridges, focusing on their structural analysis methods, design principles, and experimental studies. Special attention is given to studies addressing cable-stayed systems with intersecting cable stays. Based on this analysis, the chapter concludes with summarised insights, formulating the research objectives and tasks of this dissertation. On the topic of this chapter, 1 scientific publication was published (Dabrila & Juozapaitis, 2024a).

1.1. Literature overview

The cable-stayed bridges are defined by their load-bearing deck, which is supported by cables anchored in a pylon structure (Strasky, 2005). Cable-stayed footbridges exhibit significant flexibility and are lightweight, leading to vibration-prone structures (Ferreira, 2019). Various classifications exist for cable-stayed bridge systems. First, they can be categorised based on the arrangement of the cable stays (Fig. 1.1). Traditional classifications include Harp and Fan layouts. Fan-type cables extend from the top of the pylon, each at a distinct angle, while harp-type cables are consistently inclined with the overlay. Additionally, semi-fan

systems are common, featuring fan cables distributed along the pylon's length for easier installation and connection. However, closely spaced installation points on the pylon can mimic fan behaviour. The conventional harp system, though, complicates construction efforts while balancing lateral and central spans (Gimsing, 2011).

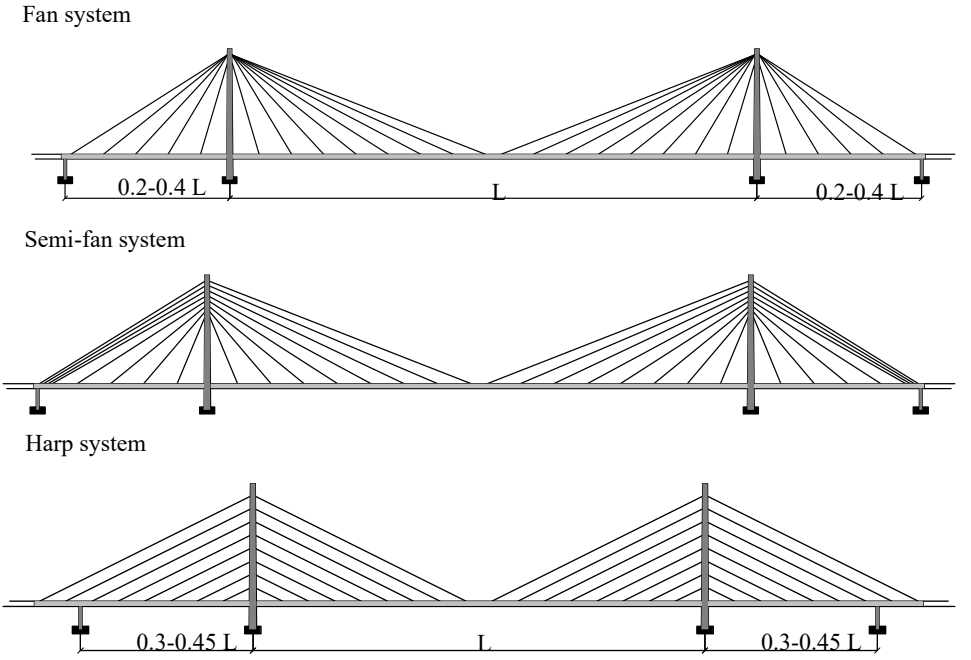

Fig. 1.1. Arrangement of the cable stays (Gimsing, 2012)

Pylon types also distinguish cable-stayed systems, with the pylon's shape and mass primarily dictated by the cable arrangement (Fig. 1.2). Due to bending moments, harp system pylons tend to be bulkier and more rigid than fan-type pylons. Furthermore, the placement of fan-supporting cables offers structural support.

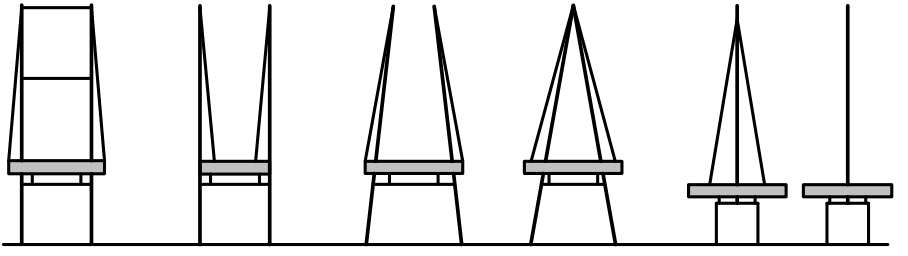

Fig. 1.2. Pylon types (Notkus, 2010)

The pylon's shape can vary across the bridge based on traffic volume, static forces, cable tie points, material selection, anchor requirements, and economic and architectural considerations (Walther, 1999).

1.1.1. Brief history of cable stay structures

The first designs of the cable-stayed bridge were proposed relatively early. The idea of such a bridge, whose stiffness beam is supported by links, can be found as early as in 16th-century literature. The Machine Novae by the Venetian inventor Fausto Verenzio presents a possible two-pylon bridge with girders supported by chains (Triplett, 2012). Despite the absence of a physical bridge, this concept reveals a surprisingly sophisticated theoretical understanding of bridge-building even centuries ago (Fig. 1.3).

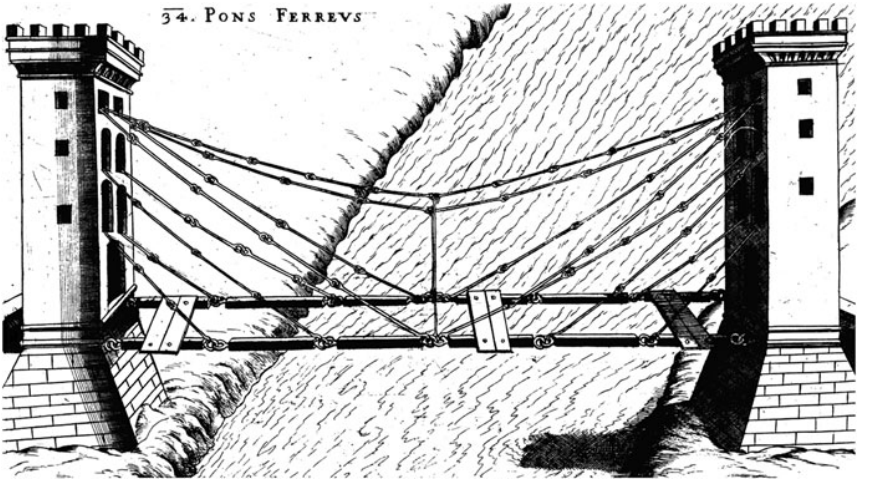

Fig. 1.3. System proposed by Fausto Verenzio (Gazola, 2015)

The 19th century saw a surge in bridge building, with designs blurring the lines between suspension and cable-stayed forms. Early suspension bridges, like the Dryburgh Abbey Bridge (Stevenson, 1821) and the Brooklyn Bridge (McCullough, 1972), incorporated elements of the cable-stayed method for additional stability.

Modern cable-stayed bridges emerged around 1950. Their efficient design and economical construction made them ideal for spanning large distances. This need became especially pressing after World War II due to two factors: the high demand for bridges and limited material resources. The Stromsund Bridge in Sweden was built in 1955. It is considered the first modern cable-stayed bridge,

designed by Franz Dischinger and built by AB Skånska Cementgjuteriet (Wai-Fah, 2000). This bridge has three spans: a main span of 182.6 meters and two side spans of 74.7 meters each.

Fig. 1.3. Stromsund Bridge (Eriksson, 1955)

Changtai Yangtze River Bridge in Jiangsu, China (Fig. 1.4) currently holds the record for the longest cable-stayed bridge span, with a central span of 1208 meters. (Guo, 2023).

Fig. 1.4. Changtai Yangtze River Bridge (Yang, 2025)

Steel box girder decks have been used for these very long spans to improve aerodynamic stability, increase strength, and reduce dead weight (Pedro, 2016; Wang, 2021). This feat of engineering pushes the boundaries of what is possible, showcasing the continuous advancements in materials and design principles. This

coincides with the growing bridge sector and increasing demand for infrastructure (Chinchane, 2020).

1.1.2. Current research outlook

Renowned for their captivating architectural elegance and efficient structural engineering (Schlaich et al., 2005; Strasky, 2007; Xiaoyu, 2021), cable-stayed bridges have become iconic landmarks worldwide. However, beyond their graceful appearance lies a complex interplay of forces, posing significant challenges (Gimsing et al., 2012; Walther, 1999), especially if the structure is asymmetrical (Jutila, 2021; Malinowski, 2018). Despite their widespread acclaim and functional application, cable-stayed bridges face structural challenges (Svensson, 2012; Ferrera et al., 2019), ranging from susceptibility to asymmetric loads to the intricacies of their massive components (Cid et al., 2018). Addressing these challenges demands meticulous attention and innovative solutions to ensure longevity and safety (Innocenzi, 2022; Palheriya, 2018).

Modern cable-stayed bridge construction involves assembling an almost unlimited variety of deck, pylon, and cable elements in many ways (Kanok-Nukulchai, 1992). Furthermore, recent advances in structural analysis techniques and construction technologies have made it possible to build cable-stayed bridges with main spans of up to 1000 meters. As the span lengths of these bridges increase, there is a need for more precise and accurate analysis methods that account for both material and geometric nonlinearities to predict the realistic behaviour of the structures (Kulbach, 2006; Wang, 2018). Material nonlinearity arises from the nonlinear stress-strain behaviour of the materials used. In contrast, geometric nonlinearity is due to effects such as cable sag, the interaction between axial forces and bending moments in the girder and tower, and large displacements (Thai, 2011). While it is necessary to account for certain material nonlinearities in the analysis of cable-stayed bridges, most nonlinear responses in steel cable-stayed bridges primarily arise from geometric factors (Wu, 2015). Due to the nonlinear elastic behaviour of cable-stayed bridges, which stems from the presence of cables, optimisation algorithms necessitate frequent nonlinear analyses (Hassan, 2013). Precision is vital for determining the tensile forces in the cables, which significantly influence the rigidity and strength of the entire bridge. While specific sources of material nonlinearity, such as layered bearings or specific seismic devices, might need to be accounted for, the primary cause of nonlinear response in steel cable-stayed bridges is typically geometric. Three primary sources of geometric nonlinearity in cable-stayed bridges include the beam-column effect, large displacements, and cable-stay sag. Cable-stay sag is often considered the most significant and must be included in the design of cable-stayed bridges, even in simplified models and for smaller spans (Bayraktar, 2017).

The structural safety of a bridge depends, among other things, on the number of vehicles passing on its deck, their weights, and the distribution of loads to their axes (Machelski, 2021; Zhou, 2019). Selecting partial factors for permanent loads and cable preload significantly impacts cost-effectiveness and can influence project feasibility. Although various design approaches exist, many designers treat the uncertainties of these two factors as correlated, leading them to apply the same partial factor to both actions simultaneously (Kaufmann, 2021).

During the structural analysis of cable-stayed bridges, unique construction challenges emerge that are not typically encountered with other bridge types (Atmaca, 2012; Hoffman, 2022). Any slight deviation from the proposed erection procedure at any stage can significantly alter the final geometry, which, in turn, can affect properties such as vibration frequencies. Regarding the construction method, the cantilever method is commonly used for the girder erection of cable-stayed bridges due to their self-anchored cable systems. This method is incredibly convenient for constructing large-span cable-stayed bridges (Pipinato, 2011). One such challenge is determining the optimal sequence for tensing the stay cables. This unique aspect of cable-stayed bridge design requires a distinct approach, adding a layer of challenge and excitement to the structural engineer's work (Janjic, 2003). Traditional methods involve bulky hydraulic jacks for collective tensioning, making the process intricate. However, technological advancements have introduced remarkably lightweight hydraulic jacks for individual strand tensioning (Spasojević-Šurdilović, 2014).

Designing large-span cable-stayed bridges requires cable adjustments during various construction phases and for the completed structure. Various regulatory approaches exist, such as establishing design geometry (primarily for smaller-span pedestrian bridges), optimising shear or moment diagrams in the construction of roadways, and reducing maximum tensile or compressive stresses in structural elements (Song, 2018). Typically, selecting mechanical and geometric parameters for the main load-bearing components – cables, stiffness girders, and pylons – which influence the bridge's flexibility is an iterative process driven by structural engineering expertise (Straupe, 2012).

Analysing the initial tension in stay cables is often complex, particularly in steel cable-stayed bridges. This complexity arises from factors such as the cable sag effect and the inelastic behaviours that must be considered. These behaviours include the stress-strain relationship of steel materials and the interaction between axial forces and bending moments in steel pylons and girders. Additionally, interest has been growing among researchers in optimising stay cable designs in recent years. This focus aims to minimise the overall costs of the stay cable system while ensuring the performance of the bridge remains uncompromised (Ha, 2018). The ability of the stay-cables to perform these tasks entirely depends on the appropriate post-tensioning forces (PTF) applied to the stay-cables. Under the effects of

dead loads of bridges' components, the deck's vertical displacement and the pylon's horizontal displacement must be close to zero. They must be under the limit values given in national codes under service loads. Using the trial-and-error method to determine the PTF of stay-cables is a time-consuming procedure, and most of the time, unable to find the optimum solution. Therefore, obtaining proper PTF of stay-cables takes cognizance of one of the most significant difficulties at the design stage of cable-supported bridges (Song, 2023).

Moreover, obtaining the PTF of stay-cables and finding the minimum cross-sectional area of stay-cables to ensure strength and serviceability requirements together may be challenging (Atmaca, 2021). The increasing spans of cable-stayed bridges pose fresh challenges for engineers. As the main span of cable-stayed bridges grows, the cable sag effect is believed to become more pronounced. Railway bridges typically feature heavier stay cables and a larger live-to-dead load ratio than their highway counterparts (Wen, 2022). However, the pylon could be inclined to compensate for dead loads with its weight (Crusells-Girona, 2016). The examination of construction for cable-stayed bridges holds significant importance in ensuring the safety of these structures. This is because the stresses and deflections experienced during construction may surpass those encountered during service. While certain commercial software can simulate these scenarios, they often utilise the stage superposition principle, making it challenging to analyse intermediate stages independently. Furthermore, this approach complicates the adjustment of tensioning processes in response to deviations in cable stresses measured on-site (Farr´e-Checa, 2022; Cho, 2013).

Effective cable arrangement can be crucial to system effectiveness, and researchers are looking for novel solutions, too (Malwiya, 2017). Among these, branched cable-stayed bridges were proposed. This design effectively handles asymmetric loads, which is crucial for minimising bridge element cross-sections. Additionally, it requires fewer cables, contributing to its efficiency (Stragys, 2018). An alternative solution involves employing crossing stay cables originating from both neighbouring towers and extending to the central portion of each span, like the design of the Queensferry Crossing Bridge (Arellano, 2018). This configuration offers several advantages, notably in effectively mitigating bending moments in the towers to acceptable levels. Moreover, it aids in reducing bending moments in the deck through the overlap of stay cables. As recommended, it is optimal for the crossed cables to extend approximately 20% of the span length beyond the centre of the span (Cid, 2018).

Another important factor is reliability analysis methods (Bas, 2017). They can be divided into two main groups: analytical and simulation techniques. Analytical techniques, such as first-order reliability (FORM) and second-order

reliability (SORM), enable the estimation of structural reliability using the means and variances of random variables and the definition of the limit state function (LSF) at the most probable points (MPP) (Truong, 2017). Current studies focus on reliability and cable breakage (Mozos, 2011; Park, 2023) and their dynamic effects (Chen, 2023; Abdelaziz, 2024; Ali, 2020). In the last decade, dynamic identification and FE model updating have become standard practices in structural engineering (Briseghella, 2021). In cable-stayed bridges, parametric excitation is highly likely due to numerous low frequencies within the deck, towers, and stay cables (Wang, 2021). When a local mode (from the cables) and a global mode (from the entire structure) become coupled, even minimal movement of the deck or tower can lead to dynamic instability, resulting in significantly large vibration amplitudes in the stay cables (Ouni, 2012). Wind effects bring the challenge of decreasing critical velocities for wind-induced flutter, posing significant survival risks for these bridges in areas with extreme wind conditions (Zheng, 2023).

In recent years, many structural health monitoring (SHM) systems have been implemented to investigate the dynamic properties of cable-stayed bridges (Ni, 2021; Xu, 2021). Studies have been undertaken to develop monitoring systems for cable-stayed bridges to assess their performance using measurement data (Nicoletti, 2023; Jana, 2021). However, most of these studies have relied on extensive measurement data for evaluation and primarily focused on estimating local responses. To address these constraints, a new approach called Structural Responses Analysis using a Limited amount of multi-response data (SRALMR) has been recently introduced and validated using simple structural models like beams and trusses (Byun, 2022). Measuring tension and damping of stay cables is standard practice during construction, as well as regular assessments and long-term health monitoring of bridges. These measurements offer valuable insights to bridge owners regarding safety, potential damages, structural changes, and deterioration. Various methods have been employed to determine cable tension, broadly classified into direct and indirect methods. Direct methods, like the lift-off test, provide consistent tension values with high accuracy but require substantial equipment, skilled labour, and high costs. In contrast, the indirect method, such as vibration testing, is widely used for cable force estimation due to its simplicity, non-destructive nature, and relatively low cost. This makes vibration testing a preferred option for frequently monitoring cable tension (Le, 2022).

Optimising cable-stayed bridges presents a complex challenge for structural engineers (Hassan, 2013; Lakshmi Poornima, 2017). Research in this area began over 40 years ago; interest has surged recently, with more than half of the relevant studies emerging in the past decade (Ma, 2024). Historically, optimisation efforts focused primarily on adjusting cable forces and achieving

cost-effective designs, accounting for 80% of past research. However, the past ten years have seen a broadening of focus. Engineers apply optimisation algorithms to various new areas, including designing hybrid reinforced polymeric decks and cables, monitoring and assessing existing bridges and developing passive and active control devices to improve earthquake resilience (Martins, 2020). The optimal design of cable-stayed bridges is a complex endeavour. The vast array of design parameters, stringent constraints dictated by design codes, significant geometric nonlinearity, and the impactful role of post-tensioning cable forces render traditional design methods inadequate for this task (Hassan, 2014). In most practical engineering applications, the forces in the stay cables are optimised to ensure that the bridge's displacements or internal forces reach predefined states. These methods include the zero-displacement method, force equilibrium method, and load method, among others. The zero-displacement method aims for zero displacements at the anchorage points between the stay cables and the girder. Initially, the stay cables in the model are not tensioned, and the vertical displacements of the girder, along with the stay cable forces, are determined following a gravity analysis. Subsequently, the stay cables are tensioned using the previously obtained cable forces, and a second gravity analysis is conducted. This process aims to achieve the desired configuration of the girder. However, in most instances, the resulting stay cable forces could be better, and the girder displacements do not reach zero, indicating potential areas for optimisation (Guo, 2023).

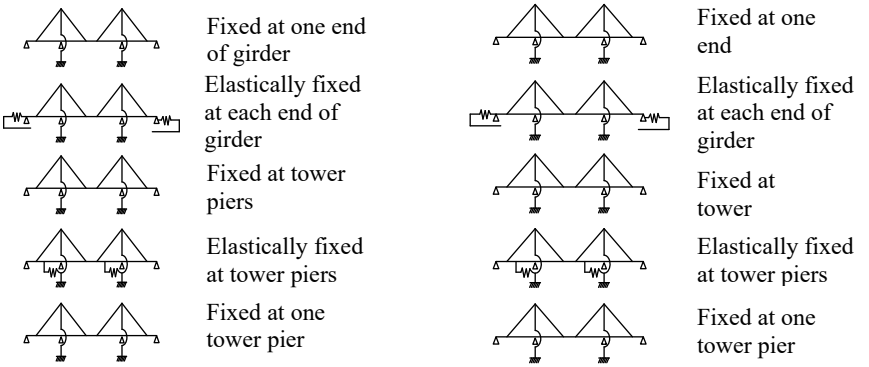

Fig. 1.5. Cable-stayed bridge configurations (Ito, 2005)

Cable-girder anchorage structures in cable-stayed bridges under long-term service have attracted much attention (Wang, 2021; Chen, 2023). The choice of supports for longitudinal movement is quite flexible due to the presence of stay cables and pliant towers. This flexibility along the bridge axis allows for more extended natural periods of motion, reducing seismic inertia forces (Martínez-

Rodrigo, 2015; Valdebenito, 2006). However, this reduced constraint on the girder's longitudinal movement can lead to significant bending moments in the towers and greater displacement of the girder itself. The figure shows the common combinations of support conditions for spans typically found in long-span cable-stayed bridges (Ito, 2005). Additionally, the impact of temperature changes must also be considered.

Carbon fibre reinforced polymer (CFRP), an advanced structural material, has found widespread application in aerospace, aircraft structures, yachts, vehicles, and related industries worldwide. This popularity stems from its exceptional mechanical and chemical properties, including lightweight construction, high strength-to-weight ratio, significant flexibility, robust corrosion resistance, high fatigue resistance, and ease of customisation. Since the late 1980s, Japan and several European countries have pioneered the initial use of CFRP tendons in various applications, including short-span cable-stayed bridges, prestressed concrete structures, structural strengthening, and structural optimisation (Xie, 2016).

1.1.3. Current footbridge research

Early suspension bridges, often used as footbridges, were constructed using cables from twisted vines or tightly drawn hides to minimise sagging. The ends of these cables were secured to trees or other stable structures situated along riverbanks or at the edges of gorges and other natural barriers. The bridge deck, typically made from roughly cut planks, was placed directly on these cables. This bridge construction method dates to ancient times and was prevalent in regions such as China, Japan, India, and Tibet. It was also employed by the Aztecs in Mexico, the Incas in Peru, and indigenous populations in other parts of South America. Such bridges are still found in some of the world's more secluded areas (Podolny, 1980).

Footbridges offer a more intimate interaction with their users, as pedestrians directly walk on, touch, and observe them closely, unlike road and railroad bridges (Svenson, 2012). This direct engagement influences their design significantly, demanding that they be crafted on a human scale. Unlike road and railroad bridges, which typically aim to connect two points as directly as possible, footbridges provide opportunities to break away from this straightforward approach. They can incorporate pedestrian "desire lines" into their design, profoundly affecting their layout. Options such as movable bridges, curved and cable-supported decks, or intersecting multiple decks can create a unique spatial experience (Idelberger, 2011). In footbridge design, factors such as location, length, and elevation are not predetermined but should be carefully explored by the designer. Bridges also shape future urban or

environmental developments based on their integration into existing environments. In these respects, the input from architects can be invaluable (Schlaich, 2005). In this development, footbridges create pathways and can become attractive public spaces (Baus, 2008).

In recent years, footbridges have become a crucial component of urban infrastructure for ensuring safe pedestrian movement, particularly in densely populated cities (Hassan, 2020; Chen, 2014). Various types of footbridges, such as beam, truss, arch, suspension, and cable-stayed, have been constructed worldwide, depending on their superstructure design (Strasky, 2005). Among these, the cable-stayed footbridge (CSFB) is particularly favoured in modern cities due to its aesthetic appeal, visual lightness, cost-effectiveness, and ease of construction. The primary structural components of a CSFB include the deck, pylon, stay cables, and foundation. The stay-cables are vital in distributing the deck's dead and live loads throughout the bridge structure. They are also instrumental in managing the vertical and horizontal displacements of the deck and pylon, respectively (Atmaca, 2021).

However, with the advent of advanced design methods and high-strength materials, footbridges have become increasingly slender. As a result, these structures are now more susceptible to dynamic vibrations caused by pedestrian traffic, which can compromise their comfort and serviceability (Bassoli, 2017). Pedestrian movement over bridge decks is unpredictable, and in response, various scientific and technical studies aim to assist in modelling pedestrian dynamic loads. These models support both the structural design and dynamic testing of footbridges. While international guidelines offer some recommendations on this topic, it is important to note that the study of pedestrian-induced vibrations is still an evolving area of research and is far from being fully resolved (Nicoletti, 2023).

1.1.4. Intersecting cable stays system

Amidst these challenges, innovative approaches such as substituting stiffening girders with strings (Unitsky, 2019; Pipinato, 2015) and intersecting cable configurations offer substantial advantages. Particularly, intersecting cables enhance structural stability under asymmetric loads, reducing material usage and improving resistance to dynamic forces (Pearce & Jobson, 2002). Despite promising results, this approach remains relatively underexplored, with only a few examples implemented (Table 1.1).

A couple of bridges were more thoroughly described, such as the Royal Victoria Dock Bridge in the United Kingdom (Pearce & Jobson, 2002), the Passerelle du Grand Large Bridge in Dunkirk (Robin et al., 2014) (Fig. 1.6), and the Taiping North Road Pedestrian Bridge (Brownie et al., 2008).

Table 1.1. Intersecting Cable Bridges

Bridge	Country	Main span length [m]	Year built
Royal Victoria Dock Pedestrian Bridge	United Kingdom	127.5	1998
Forthside Footbridge	United Kingdom	88.2	2009
Passerelle du Grand Large	France	112.5	2014
Frank Gehry Bridge	Spain	76.9	2014
Moody Pedestrian Bridge	USA	42.4	2015
Zhangjiatang	China	55.0	2018
Grand Canal	China	150.0	2024
Hickory Riverwalk	USA	105.0	2024

Fig. 1.6. Passerelle du Grand Large (Janberg, 2022)

Nevertheless, the absence of established design methodologies for such structures is notable (Racić, 2006). Designing these bridges with rational parameters proves challenging without analytical frameworks, calculation methods, or experimental data. Engineers typically calculate geometry and cable-stay pretension based on simple laws to avoid compression in the cable stays at the Service Limit State while permitting relaxation of central cable-stays at the Ultimate Limit State. This approximation, treating the bridge as two cantilevers, leads to imprecise evaluations of deflections and stresses, highlighting the necessity for detailed research (Robin et al., 2014).

1.2. Methods of calculation of string and cable-stayed structures

Although four methodologies were suggested for cable-stayed bridges and their elements (Gazzola, 2015; Wu, 2019; Costa, 2021; Sharry, 2022; Zhang, 2022), no abundance exists in the calculation methodology for string structures. Although examples can be found.

Beivydas and others presented a methodology for calculating the prestressing force considering the operational requirements (Beivydas, 2023). A flexible and elastic string may be either prestressed or non-prestressed. A non-prestressed string acts as a suspended element with its initial length equal to the span length ($s_0 = l$). It is assumed that any forces and displacements resulting from applied loads occur without prestressing, meaning the string undergoes no additional tensile force from pre-tensioning.

The equilibrium condition of such a flexible structure, between tension force H and internal moment $M(x)$, particularly concerning the midpoint of the span, can be formulated as follows:

$$H = \frac{M(x)}{\Delta f}; \tag{1.1}$$

$$M(x) = \frac{(g+v)l^2}{8}\left(\frac{4x}{l} + \frac{4x^2}{l^2}\right). \tag{1.2}$$

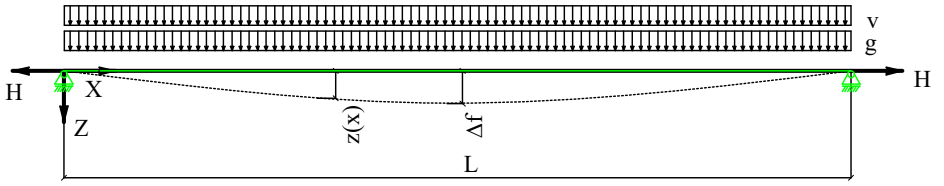

Fig. 1.7. Symmetrically loaded string (Beivydas, 2023)

Beivydas describes a method for calculating the displacement at the midpoint of a span in a symmetrically (Fig. 1.7) loaded string:

$$\Delta f = \sqrt[3]{\frac{(g+v)l^2}{64EA}}. \tag{1.3}$$

Analogously, it is possible to get a direct solution for calculating the tensile force:

$$\mathrm{H} = \sqrt[3]{\frac{(g+v)^2 l^2 EA}{64EA}}. \tag{1.4}$$

The equations demonstrate that it is feasible to calculate both the displacement at the mid-span and the tension force of a non-stressed string directly, without iterative methods, provided that the loads on the string, the span length, and the axial stiffness are known. Once the elastic displacement of the string, denoted as Δf, is established, the tensile force can be calculated accordingly. It is evident that the string's tension force depends on the displacement magnitude and will be significantly higher compared to a cable with similar characteristics but with an initial sag.

The analysis should also consider an elastic string asymmetrically loaded with live loads and symmetrically with dead loads (Fig. 1.9). It is important to highlight that, unlike a cable, the flexible string functions as a suspension element without any initial sag ($f_0 = 0$). As a result, under asymmetric loading, the string does not experience kinematic displacements. Instead, only elastic displacements affect the string, and the curve of its deformed axis can be described by the sum of two elastic displacement curves:

$$z(x) = \frac{\Delta f_{as}}{1 + 0.5\gamma}\left[\left(\frac{4x}{l} + \frac{4x^2}{l^2}\right) + \frac{\gamma}{2}\left(\frac{6x}{l} + \frac{6x^2}{l^2}\right)\right], 0 \le x \le \frac{l}{2}. \tag{1.5}$$

The equations reveal that the curve of the deformed axis for the left part, which is asymmetrically loaded, consists of the sum of two quadratic parabolas. In contrast, the right part combines a quadratic parabola with a straight line.

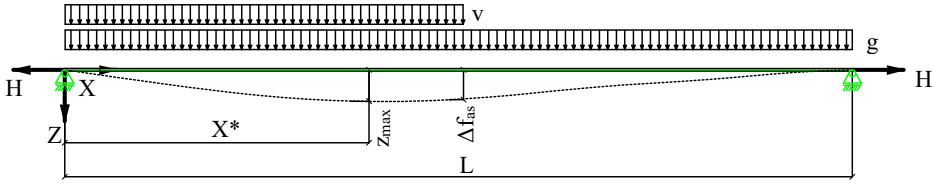

Fig. 1.8. Asymmetrically loaded string (Beivydas, 2023)

The displacement of asymmetrically loaded string at the mid-span and its tensile force are calculated as follows:

$$\Delta f_{as} = \sqrt[3]{\frac{3g(1+0.5\gamma)l^4}{64EA}}; \tag{1.6}$$

$$\mathrm{H}_{as} = \sqrt[3]{\frac{g^2l^2(1+0.5\gamma)}{24}\left[\left(1+\gamma+\frac{5\gamma^2}{16}\right)/\left(1+\gamma+\frac{5\gamma^2}{16}\right)\right]}. \tag{1.7}$$

Asymmetric equations are like their symmetrical counterparts, with the main difference being that they also assess the influence of the γ ratio, which represents the proportion of asymmetric to symmetric loads on displacements and tensile forces. Under the same initial conditions, the displacement and tensile force in an asymmetrically loaded string will be lower than those in a symmetrically loaded string.

The elastic string may be prestressed to minimise its displacements. The level of prestressing force is chosen based on operational needs and the loads it will bear. It is presumed that the string is prestressed before applying the dead load. Displacements for such a prestressed string at the midpoint of the span are computed like that of a non-stressed string. In this scenario, the elastic elongation is calculated and considered. N_0, the prestressing force. However, this calculation methodology considers only one span without considering deflections or forces affecting the string in the multi-span case.

Strasky (2006), in his analysis, assumes that a cable with a cross-sectional area A and modulus of elasticity E functions as a perfectly flexible member capable only of withstanding normal forces. Under this assumption, the cable's response to a load is influenced by the application of this load along the cable and a predefined horizontal force, H. For a specific load $q(x)$ and the chosen horizontal force H, the shape of the cable curve is defined by the coordinates $y(x)$, the sag $f(x)$, the tangent slope $y'(x)=\tan\phi(x)$, and the radius of curvature $R(x)$. These parameters are calculated based on the general equilibrium conditions of the cable segment ds. The cable experiences a normal force $N(x)$, which is broken down into its vertical $V(x)$ and horizontal $H(x)$ components (Fig. 1.9).
When q(x) is constant,

$$p^0(x) = \frac{1}{H}\left(\frac{1}{2}ql - qx\right) = \frac{q}{2H}(l-2x); \tag{1.13}$$

$$p(x) = p^0(x) + \frac{h}{l} = p^0(x) + \tan\beta; \tag{1.14}$$

$$f(x) = \frac{M(x)}{H} = \frac{1}{H}\left(\frac{1}{2}qlx - \frac{1}{2}qx^2\right) = \frac{q}{2H}x(l-x). \tag{1.15}$$

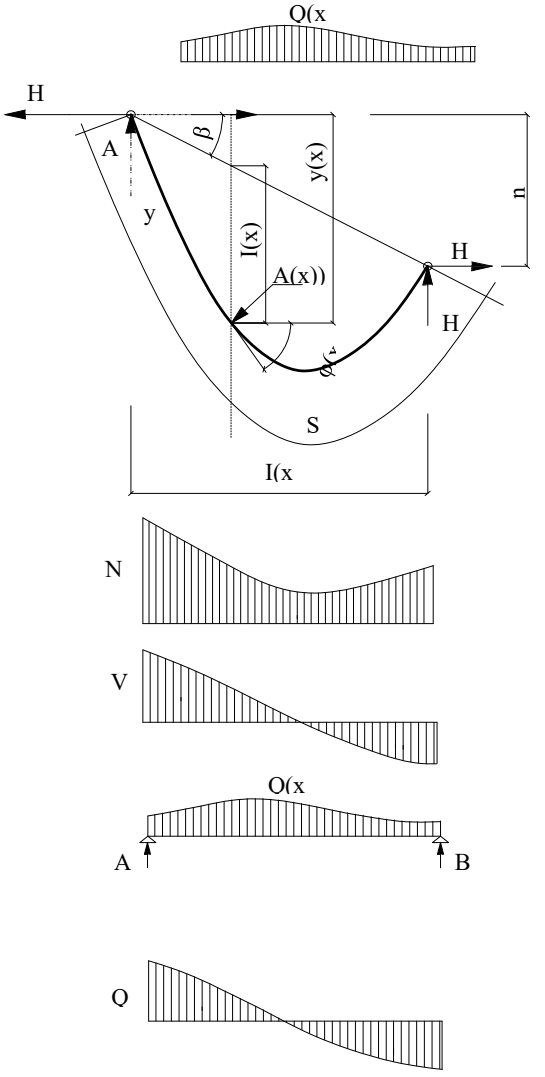

Fig. 1.9. Basic characteristics of a single cable (Strasky, 2006)

In this instance, the length of the cable:

$$s = \int_0^s ds = \int_0^l \sqrt{dx^2 + dy^2}. \tag{1.16}$$

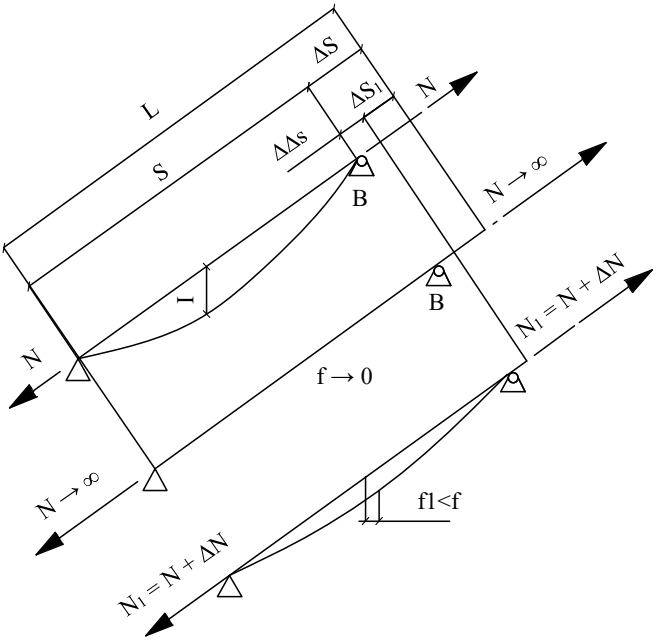

Fig. 1.10. Effects of prestress (Walther, 1999)

Additionally, Walther (1999) describes the specific stress-strain relationship for a cable supported by a series of frictionless supports, preventing deflection (Fig. 1.10). This relationship is characterised by its modulus of elasticity E, henceforth referred to as E_e. An idealised modulus of elasticity E_i can be calculated:

$$E_i = \frac{\sigma}{\varepsilon_f + \varepsilon_e}. \tag{1.17}$$

By introducing into the equation the moduli E_f and E_e such that:

$$\varepsilon_f = \frac{\sigma}{E_f};\ \varepsilon_e = \frac{\sigma}{E_e}. \tag{1.18}$$

Then E_i can be expressed like this:

$$E_i = \frac{E_f E_e}{E_f + E_e} = \frac{E_e}{1 + E_e/E_f}. \tag{1.19}$$

If the ratio of the catenary shape f/s is sufficiently low (less than 1/12), it should be approximated as a parabola. Based on this assumption, Ernst derived the modulus E_f.

$$E_f = \frac{12\sigma^3}{(\gamma l)^2}. \tag{1.20}$$

Incorporating this value into the previously discussed equation yields the idealised modulus of elasticity for a cable with a horizontal span of l and a tensile force σ.

$$E_i = \frac{E_e}{1 + (\gamma l)^2 E_e/12\sigma^3}. \tag{1.21}$$

The modulus E_i, as defined in equation 1.21, applies only to a single value of stress σ. Considering that this stress value can significantly vary with live loads, an equivalent modulus for a cable that operates between two stress levels is defined. σ_{low} and σ_{up}. Ernst, therefore, postulated a secant modulus:

$$E_f = \frac{12\sigma_m^3}{(\gamma l)^2}\frac{16\mu^2}{(1+\mu)^4}, \tag{1.22}$$

where,

$$\mu = \frac{\sigma_{low}}{\sigma_{up}};\ \sigma_m = (\sigma_{low} + \sigma_{up})/2. \tag{1.23}$$

Adding earlier equations, E_i can be expressed as:

$$E_i = \frac{E_e}{1 + \frac{(\gamma l)^2}{12\sigma_m^3}\frac{(1+\mu)^4}{16\mu^2}}. \tag{1.24}$$

All presented cable-stay calculation methods depend on approximations, which affect the calculation's accuracy and do not consider the full effects of cable behaviour.

Various methods are available for calculating cable-stayed bridge systems. One such analytical approach is the method proposed by Starossek. This method involves dividing the entire structure into two parts, which are then connected by a conceptual bend, referred to as "M". Cuts labelled Rl and Rt are made at the end

supports. Conditional hinges are introduced at the ends of the elements (Fig. 1.11). This method transmits the axial forces acting on the cables directly to the deck (Starossek, 2002).

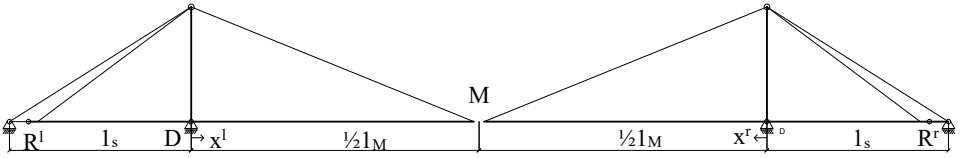

Fig. 1.11. Cable-stayed system (Staroseek, 2002)

This method can be used to assess the structure's general and local deformations under variable loads, assuming that the structures and supports in the model operate within an elastic range. In this analysis, the stiffening beam is considered a multi-supported beam. The subsequent step involves bisecting the structure into two equal parts, resulting in two elastic systems (L = ls + ½ lm), whose endpoints are free to move in the vertical plane. The pre-tensioning notches for the shingles are chosen to ensure no bending moments are induced in the stiffness beam.

Deformations for the analysed half of the bridge are calculated by measuring the deflection around the pylon support point. The system in focus includes a sheet, a pylon, a stiffening beam, a pylon support, and an edge support, which functions as an elastic spring (Fig. 1.12). To accurately gauge the local effects, the pylon and beam are treated as non-deformable, essentially forming a rigid body capable of rotating about a single point.

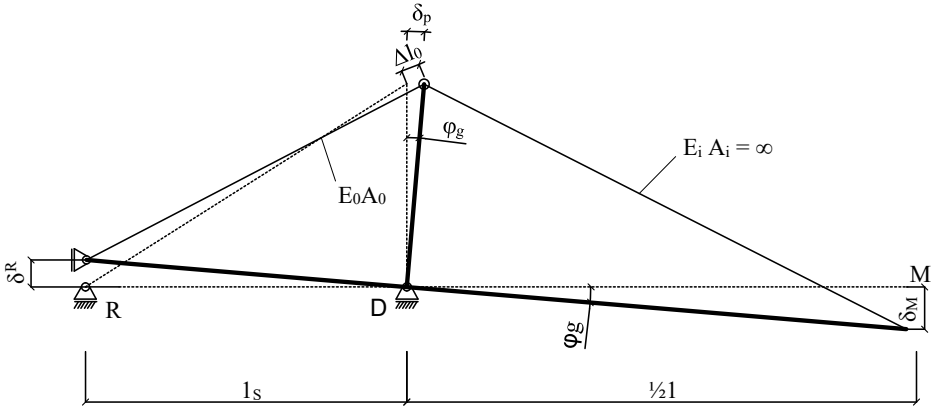

Fig. 1.12. Deflection scheme (Staroseek, 2002)

When subjected to a traffic load, the stiffening beam causes the movable support spring to elongate, resulting in the rotation of the structure. There is a direct relationship between the moment M^D, the operating point "D", and the displacement angle φ_g of the pylon. The resulting expression is as follows:

$$k_r = \frac{\varphi_g}{M^D}. \tag{1.25}$$

After substituting the distributed loads with concentrated loads, it becomes possible to calculate the stresses in the cable-stays (Fig. 1.1):

a)

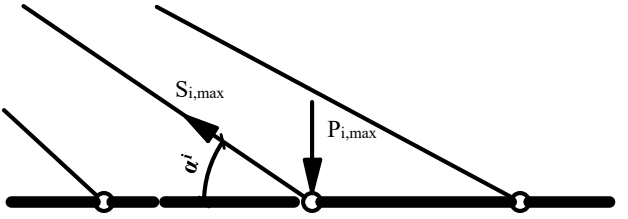

b)

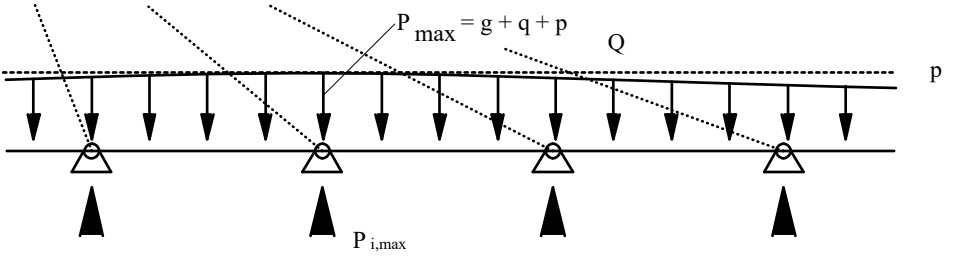

Fig. 1.13. Load evaluation: a) point and b) uniformly distributed (Staroseek, 2002)

The maximum load affecting the bridge is expressed as a component of the self-weight of the structure g, the variable load q and the cable-stay affect p_Q:

$$p_{max} = g + q + p_Q. \tag{1.26}$$

Peak load of cable stay depends on cable stay effect and inclination of the cable-stay:

$$s_{i,max} = \frac{P_{i,max}}{sin\alpha}. \tag{1.27}$$

It is possible to obtain the area of the cable stay from this expression while knowing its stress limit σ:

$$A \geq \frac{S_{t,max}}{\sigma \frac{p\left(h^2 + x_i^2\right)^{0.5}}{\sigma \cdot h}_{max}}. \tag{1.28}$$

Vertical beam displacement can be expressed as:

$$\delta(x_i) = \frac{P_i \cdot \left(h^2 + x_i^2\right)^{\frac{3}{2}}}{E_i \cdot A(x_i) \cdot h^2} = \frac{P_i \cdot \sigma \cdot h^2 + x_i^2}{E_i \cdot p_{max}}, \tag{1.29}$$

E_i, $A(x_i)$ – cable stay axial stiffness

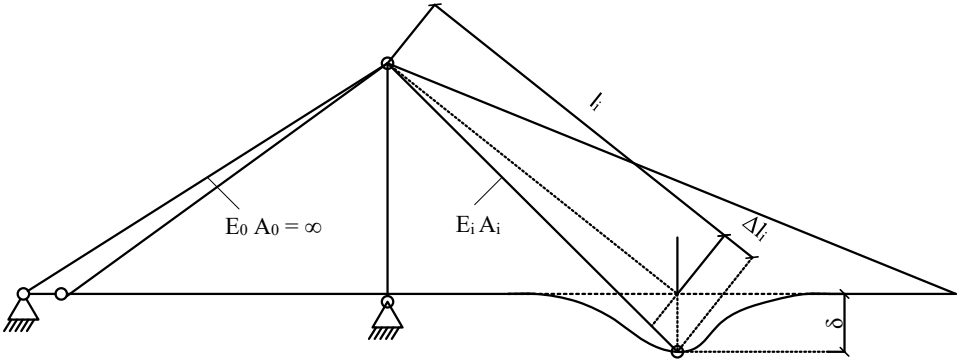

Fig. 1.14. Vertical beam displacement (Staroseek, 2002)

Svensson (2015) presents a similar method for the approximate calculation of the beam bending moments.

The system is approximated as a beam elastically supported at the cable anchor points, as shown in Figure 1.15. The cables are initially modelled as springs. In the subsequent step, these individual springs are approximated as continuous elastic support, illustrated in Figure 1.16. The key parameter for a beam on elastic foundations is the elastic length L, which is proportional to the fourth root of the ratio of beam stiffness to the elastic support, as detailed in Figure 1.17. The bedding factor is calculated by dividing the vertical displacement resulting from a unit load on the articulated system by the cable distance Δw.

For a concentrated load P, the bending moment of a beam on elastic foundations is given by $M^P = \frac{1}{4}PL$, shown in Figure 1.16a. For a uniformly distributed load p, the bending moment is $M^{UDL} = 0.161pL^2$, as depicted in Figure 1.16b.

These formulas can be used to estimate the governing bending moments along the length of the bridge.

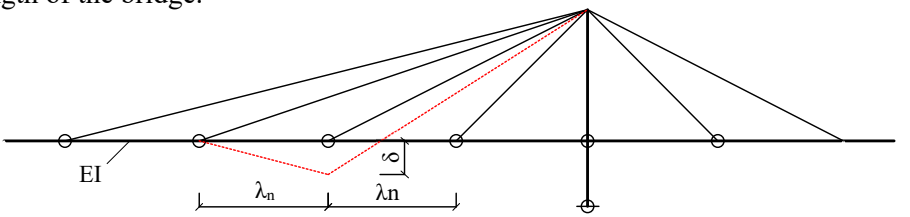

Fig. 1.15. Beam on elastic foundations (Svensson, 2015)

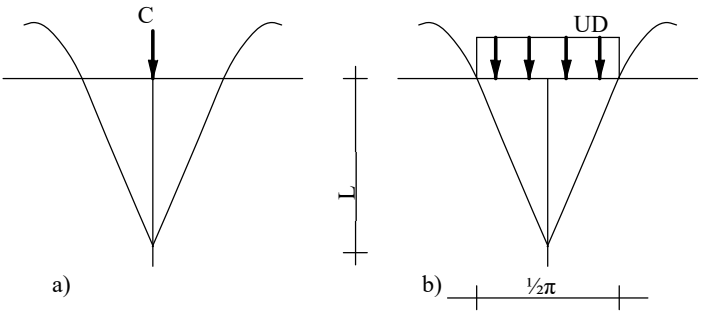

Fig. 1.16. Bending moments due to a) concentrated load and b) uniformly distributed load (Svensson, 2015)

A comparison between the positive moment influence line for a beam on an elastic foundation and the computer-calculated moment influence line for an actual bridge generally shows a good match, as illustrated in Figure 1.17. This approximation tends to be more accurate for slender beams. However, the match is less accurate for stiff beams like double-deck bridges. Conversely, the negative moment influence lines demonstrate poor accuracy.

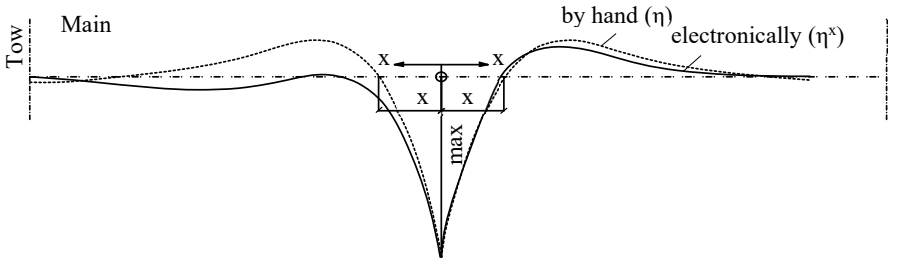

Fig. 1.17. Comparison of moment influence lines for beam on elastic foundations with the actual bridge (Svensson, 2015)

Although both discussed bridge calculation approaches are viable in traditional cable-stayed bridge systems, they do not include variables found in intersecting systems nor consider cross-cable effects on the redistribution of forces in the system.

1.3. Conclusions of the First Chapter and formulation of the tasks of the dissertation

1. Despite the complex behaviour, cable-stayed bridges are widely and successfully applied to pedestrian bridges. Scientists are actively exploring innovative solutions to increase the efficiency of such bridges. An example is the application of intersecting cable-stayed pedestrian bridges. The structural solution of intersecting cable-stays improves the behaviour of the bridge in case of asymmetric loading, as it effectively redistributes the asymmetric pedestrian loads, thus reducing the displacements and moments of the stiffening girder.
2. Intersecting cable systems are promising but still relatively new. When evaluating these cable-stayed bridges, it is necessary to note that, despite their possible advantages, they also have a drawback common to all cable-stayed bridges – a high-mass stiffness beam. This beam gains not only bending moments but also axial compressive forces.
3. Although several examples of intersecting cable-stay bridges have been built so far, their use and design are challenging, as no reliable analytical or calculation methods have been developed, and their research is in the early stages. Currently used FEM models describe individual structures and cannot be used to conclude the general behaviour of these structures.
4. No attempts have been made to detail the behaviour of the intersecting cable-string bridges, and it has yet to be detailed.

The following problems have to be solved to achieve the objective:

1. To compose the new structural system of the cable-stayed-string bridge and analyse its behaviour.
2. To develop a methodology for calculating the deformations of the load-bearing elements of the cable-stayed bridge.
3. To perform a numerical analysis of the behaviour of the newly built cable-stayed bridge structure under symmetrical and asymmetrical static loads.
4. To carry out experimental studies of the model of the cable-string steel bridge structure.

2

Innovative cable-stayed steel bridge

This chapter presents a numerical and analytical investigation of an intersecting cable bridge system. Two calculation methodologies are presented: for a system with a stiffening girder and a system with a string. This chapter includes the material presented in 2 journal publications (Dabrila, 2021; Dabrila & Juozapaitis, 2024a), and 2 conference proceedings (Dabrila & Juozapaitis, 2021; Dabrila & Juozapaitis, 2022).

2.1. Composition of the cable-stayed steel bridge with intersecting cable stays

The cable-stayed bridge system incorporates main pylons situated at the bridge supports and intermediate pylons mounted on the stiffness beam spanning the bridge's length. These intermediate pylons, spaced uniformly, create a truss-like grid. They can be connected to the stiffness beam either rigidly or flexibly. Pretensioned cables run from the top of these intermediate pylons to the attachment points of adjacent pylons on the stiffness beam. This design reduces pylon height compared to traditional cable-stayed bridges and enables better control of stiffness girder displacement under both symmetrical and asymmetrical loads. Two configurations with different heights need to be evaluated to assess the impact of

intermediate pylon heights on bridge stresses and displacements: equal pylons and varying pylons according to the parabolic curve.

2.2. Numerical analysis of the behaviour of cable-stayed steel bridge with intersecting cable stays under symmetric and asymmetric loads

To evaluate their behaviour, the considered bridge structure systems (numerical modelling) were analysed using the FEM program (Dlubal RFEM) and a geometrically nonlinear calculation procedure (Newton-Raphson). For the numerical analysis of the behaviour of cable-stayed bridges, bridge constructions with a main span length of 100 meters were selected (Fig. 2.1). This length was selected because the average span of already constructed intersecting cable-stayed footbridges is approximately 100 m (Table 1.1). The applied static loads are linearly distributed on the longitudinal beams. The considered dead load is 12.5 kN/m. Prestress for cables of the intersecting system is gained by shortening cables by 1/300 of their length. The variable (pedestrian) load (12.5 kN/m) is divided into two cases: symmetrically over the entire bridge length and asymmetrically over half of its length. The cross sections of the structural elements are given in Table 2.1.

Table 2.1. Sections of structural elements

Element	Steel type	Shape type	Parameters	Finite element type
Cables	S960		d=0.05m	Cable
Pylons	S355		d=0.508m, t=0.03m	Beam
Girder	S355		610×305mm, t=0.019m	Beam

The main load-bearing elements of the bridge (beam and pylons) are designed from structural steel S355. Cables are group A's heavy steel (HSS) round cross-section elements (EN 1993-1-11, 2006).

2.2.1. Equal pylons case

In the first case, the heights of all pylons are chosen to be the same 20 m (Fig. 2.1). The distance between the pylons would be constructed so that the inclination angle of the cross cables is 45°.

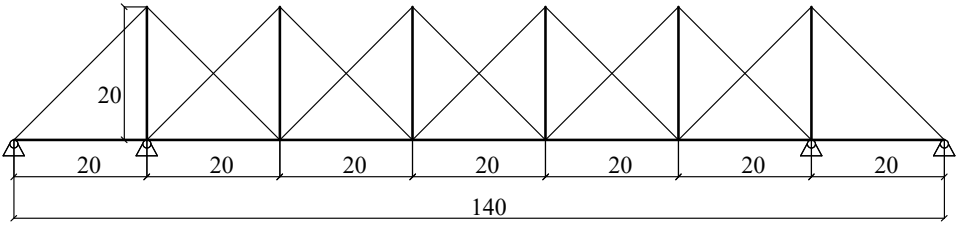

Fig. 2.1. Equal pylons bridge [m] (made by the author)

The summary results of the analysis of this bridge case are presented in Table 2.2.

Table 2.2. Equal pylons bridge elements stress

	Girder						Cable
	Maximum bending moment [kNm]		Minimum bending moment [kNm]		Axial forces [kN]	De-flec-tion [mm]	Maxi-mum/mi nimum axial stresses [MPa]
	M+	M-	M+	M-			
Symmetrical loading	894	728	639	244	-2463	754	332/3
Asymmet-rical loading	874	657	438	134	-2102	528	288/2

Figures 2.3–2.5 show the diagrams of stress distribution (axial forces and bending moments) and displacements in the bridge's structural elements under symmetrical and asymmetrical pedestrian loads. The presented data show that the values of bending moments in the stiffness girder in the case of asymmetrical loading are close to those of the moments caused by symmetrical loading. The same could be said for the distribution of axial forces in the cables and the stiffness girder under different load cases. These results demonstrate the structural advantages of the new design system because, in classic cable-stayed bridges, asymmetrical loading in most cases results in significant asymmetries in the stress distribution: higher bending moments in the main span of the stiffness beam and

lower axial forces in the cables and the stiffness beam. It was found that the maximum value of bending moment in the stiffness beam is formed under symmetrical loading and is equal to 1640 kNm at the main pylon and the lowest (244 kNm) in the beam span. This difference between the maximum and minimum values of bending moments in the stiffness girder is due to the accepted element scheme of the stiffness girder.

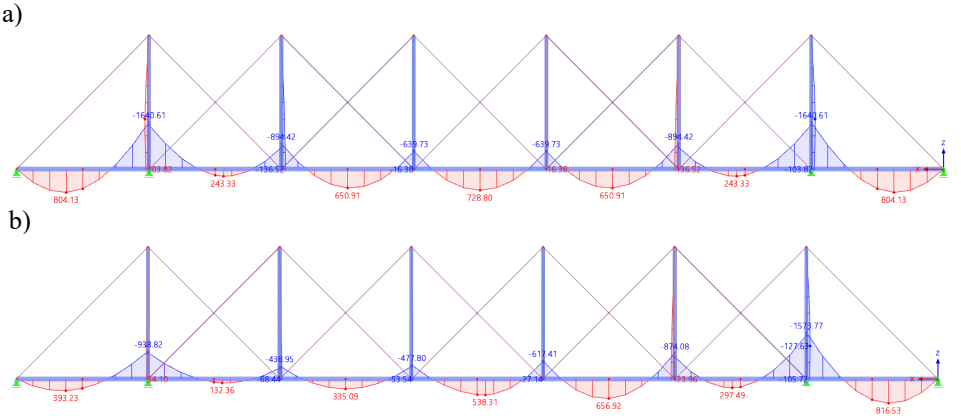

Fig. 2.3. Equal pylons bridge. Bending moments: a) under symmetrical loading and b) under asymmetrical loading (made by the author)

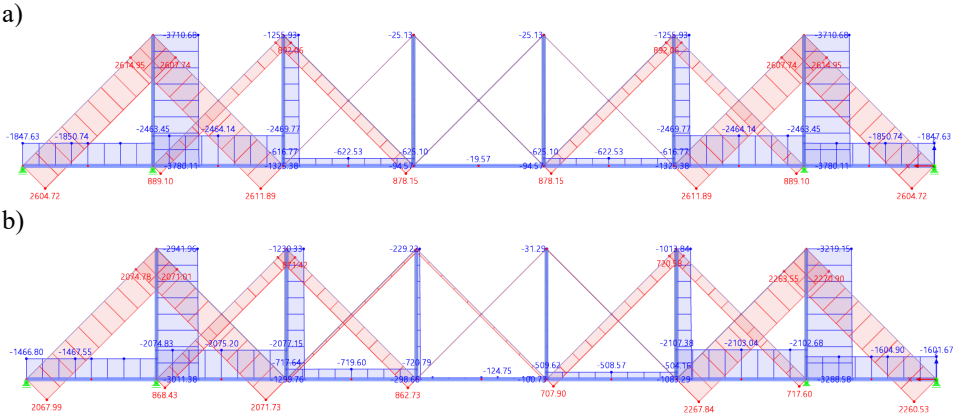

Fig. 2.4. Equal pylons bridge. Axial forces: a) under symmetrical loading and b) under asymmetrical loading (made by the author)

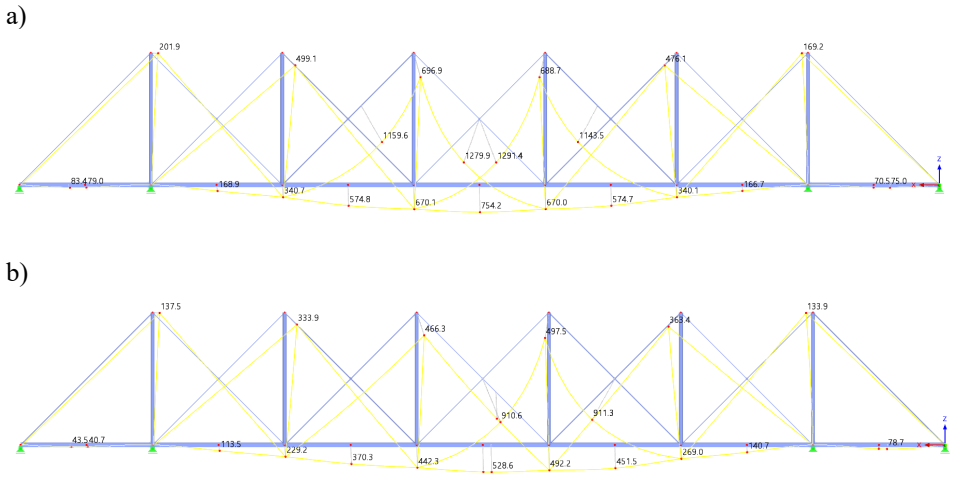

Fig. 2.5. Equal pylons bridge. Deflections: a) under symmetrical loading and b) under asymmetrical loading (made by the author)

When analysing the displacements of the bridge stiffness girder, in the case of asymmetric loading, the displacements are distributed practically symmetrically concerning the middle of the span, and their values are smaller (about 30%) than in the case of symmetrical loading.

2.2.2. Varying pylons case

As already mentioned, the challenges of the behaviour of cable-stayed bridges can be reduced by changing the standard (conventional) cable-staying scheme to the so-called cross-crossing (Fig. 2.3). It is proposed to improve the cross-hinge system by installing different pylon heights and varying them according to the parabolic curve (Fig. 2.6). The bridge of this structure is sometimes called the inverted truss of Fink (Robin et al., 2014).

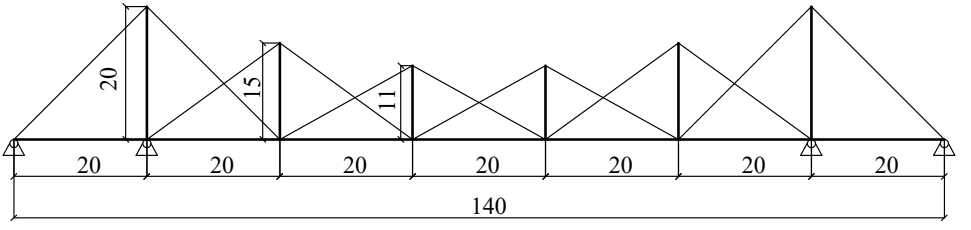

Fig. 2.6. Varying pylons bridge [m] (made by the author)

A visualisation of the obtained analysis results is provided in Figures 2.7–2.9, and the summarised results are presented in Table 2.3.

In the case of symmetrical and asymmetrical loading, the displacements and stresses of this bridge case differ by about seven per cent on average. This testifies to the ability of this cross-cable construction system to successfully "resist" asymmetrical loading.

a)

b)

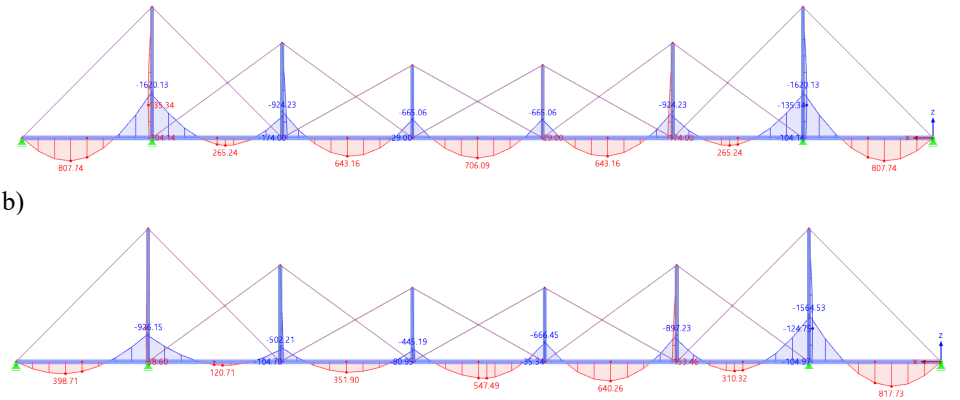

Fig. 2.7. Varying pylons bridge. Bending moments: a) under symmetrical loading and b) under asymmetrical loading (made by the author)

a)

b)

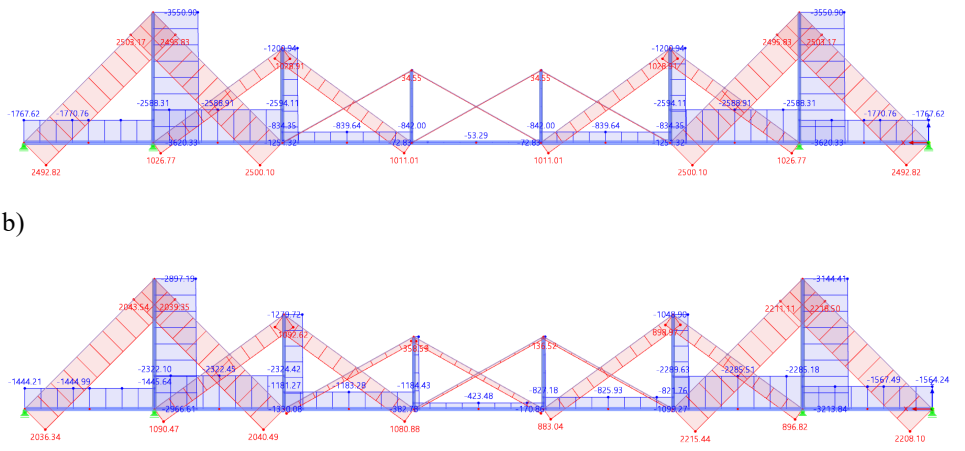

Fig. 2.8 Varying pylons bridge. Axial forces: a) under symmetrical loading and b) under asymmetrical loading (made by the author)

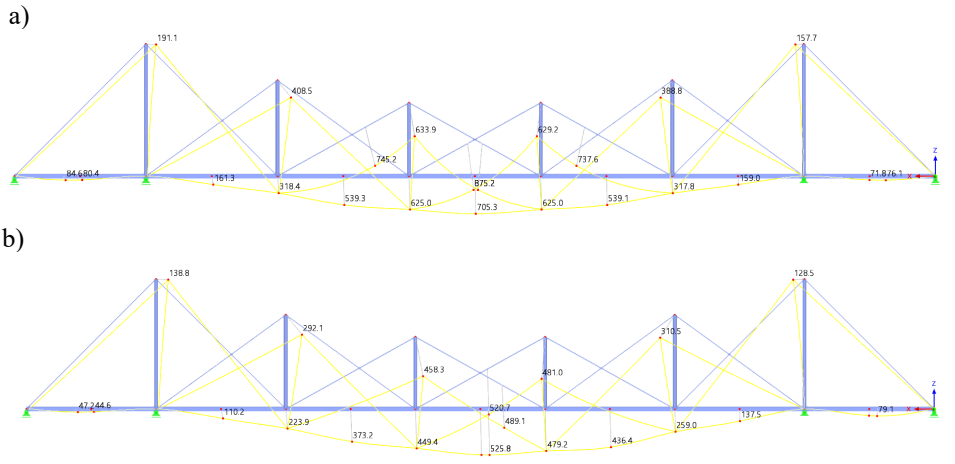

Fig. 2.9. Varying pylons bridge. Deflections: a) under symmetrical loading and b) under asymmetrical loading (made by the author)

Figure 2.7 shows that the maximum bending moments in the stiffness girder under asymmetrical loading are lower than the moments caused by symmetrical loading. The maximum axial forces in the cables and pylons under asymmetrical loads are also lower than under symmetrical loads.

Table 2.3. Varying pylons bridge elements stresses

Girder							Cable
	Maximum bending moment [kNm]		Minimum bending moment [kNm]		Axial forces [kN]	De-flec-tion [mm]	Maxi-mum/mi nimum axial stresses [MPa]
	M+	M–	M+	M–			
Symmetrical loading	924	–706	665	265	–2588	705	318/4
Asymmet-rical loading	897	–640	445	122	–2322	525	282/3

When comparing the two intersecting cable bridge cases, it should be noted that the bending moments in the stiffness beam are about four per cent lower than in the equal pylon height bridge case for both symmetrical and asymmetrical loading (Tables 2.2 and 2.3).

The previously discussed bridges are analysed by comparing them with a cable-stayed bridge (Figs. 2.10–2.13; Table 2.4). Cross-sections are kept the same, except for the pylons, which are CHS 610/30/H. The most pronounced difference in bending moments between classical land intersecting cable bridges can be observed by examining the relationship between asymmetrical and symmetrical loading results. In both cases, the asymmetrical loading on the stiffness beam caused higher forces than the symmetrical ones. However, asymmetrical loading at the central span at no point generates more significant bending stresses than symmetrical loading in a cross-type bridge. When the parabolic pylon-shaped bridge is operated under different load combinations, the moments are not higher than the discussed outline so that we can predict the behaviour of this system.
It should be noted that under symmetrical loads, the axial force in the stiffness beam of the bridge is significantly increased (compared to the classic bridge).

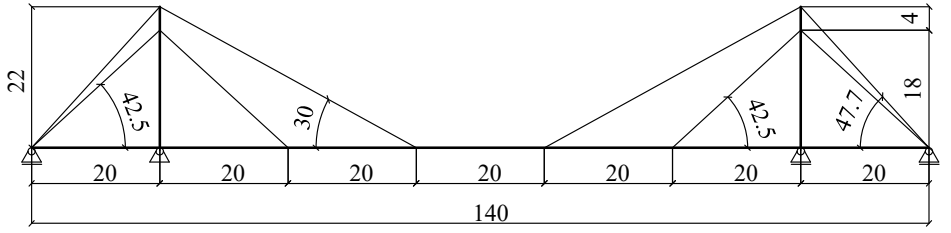

Fig. 2.10. Typical cable-stayed bridge[m] (made by the author)

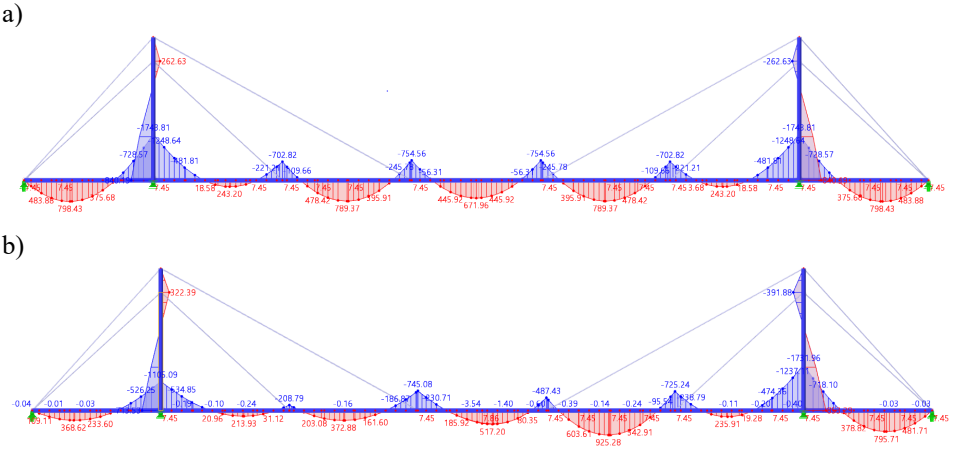

Fig. 2.11. Cable-stayed bridge. Bending moments: a) under symmetrical loading and b) under asymmetrical loading (made by the author)

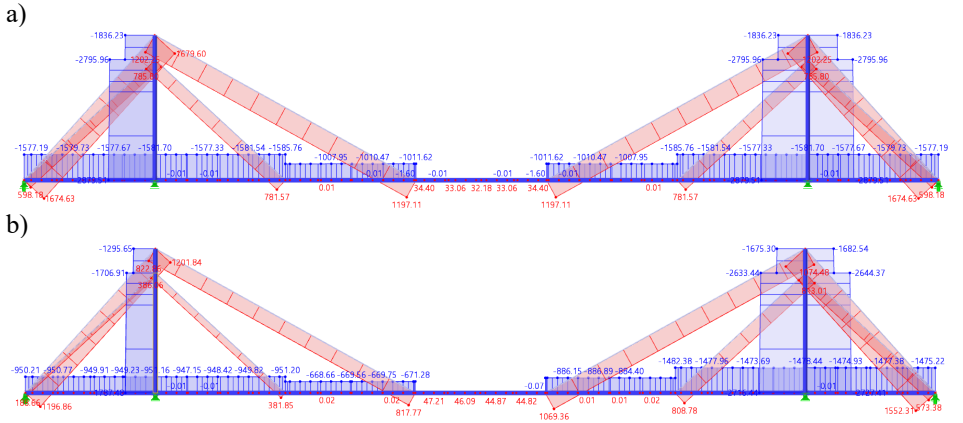

Fig. 2.12. Cable-stayed bridge. Axial forces: a) under symmetrical loading and b) under asymmetrical loading (made by the author)

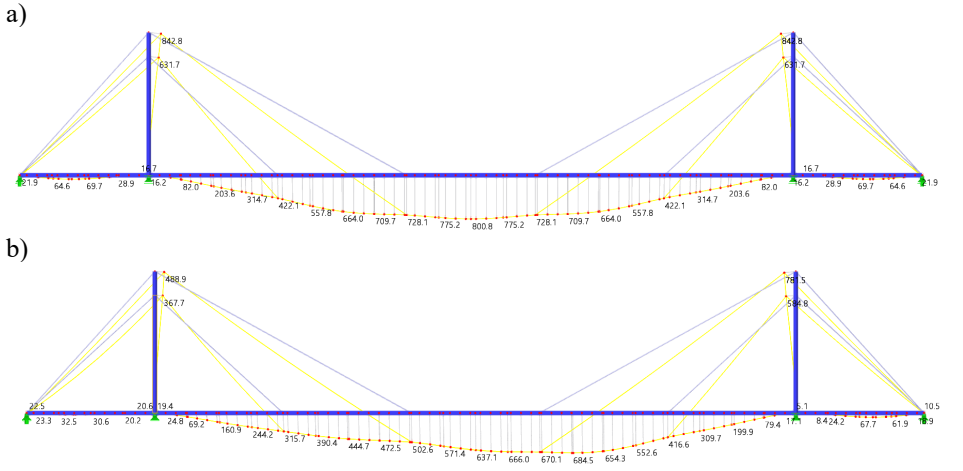

Fig. 2.13. Cable-stayed bridge. Deflections: a) under symmetrical loading and b) under asymmetrical loading (made by the author)

It should be noted that the design of an intersecting cable bridge requires higher prestressing values in the cables than in a typical bridge. This necessitates larger cross-section elements. However, it is worth noting that the extreme values of moments in the stiffness beam are reduced compared to the typical version of a cable-stayed bridge.

Table 2.4. Typical cable-stayed bridge elements stress

Girder							Cable
	Maximum bending moment [kNm]		Minimum bending moment [kNm]		Axial forces [kN]	De-flec-tion [mm]	Maxi-mum axial stresses [MPa]
	M+	M–	M+	M–			
Symmetrical loading	789	–754	243	–702	–1585	808	590
Asymmet-rical loading	925	–745	213	–208	–1473	800	548

FEM modelling showed that in intersecting cable bridge systems, it is possible to effectively stabilise the initial shape of this structural system under different loading with proper prestressing of its elements (strings and cross-cables). It should be noted that in the case of asymmetrical loading, the moments in the stiffening girder do not exceed the values of the symmetrical loading moments.

2.3. Calculation methodology of a cable-stayed steel bridge with intersecting cable stays and a stiffening girder

The analysed bridge system is composed of a stiffening girder, intersecting cable stays, and four intermediate pylons, as shown in Figure 2.14. The bridge's anchor cables are assumed to be anchored to fixed points, evaluating the horizontal deflection of the top supports. This approach is more universal, allowing for the evaluation of the system without a side pylon. The bridge's planar system. The bridge's planar system is analysed to define variables dependent on cable and beam interaction.

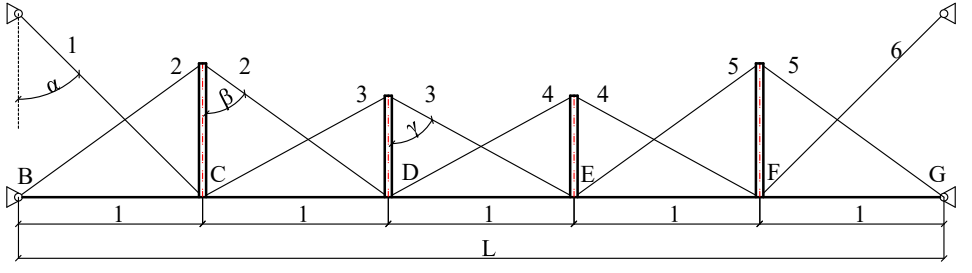

Fig. 2.14. Scheme of the innovative bridge with intersecting cable stays and intermediate pylons (made by the author)

Figure 2.15a shows the deformed scheme of the cable-stayed bridge under symmetrical load and 2.15b under asymmetrical load. The load considered is distributed linearly on the stiffness beam. The main unknowns, in this linear calculation case, are displacements at cable and beam connection (Δ_c, Δ_d, Δ_e, Δ_f) (Fig. 2.15), bending moments of the girder M, and axial forces of stay-cables N_i. Also, additional unknowns are beam support forces F_1, F_2, F_3, and F_4 (Figure 2.18).

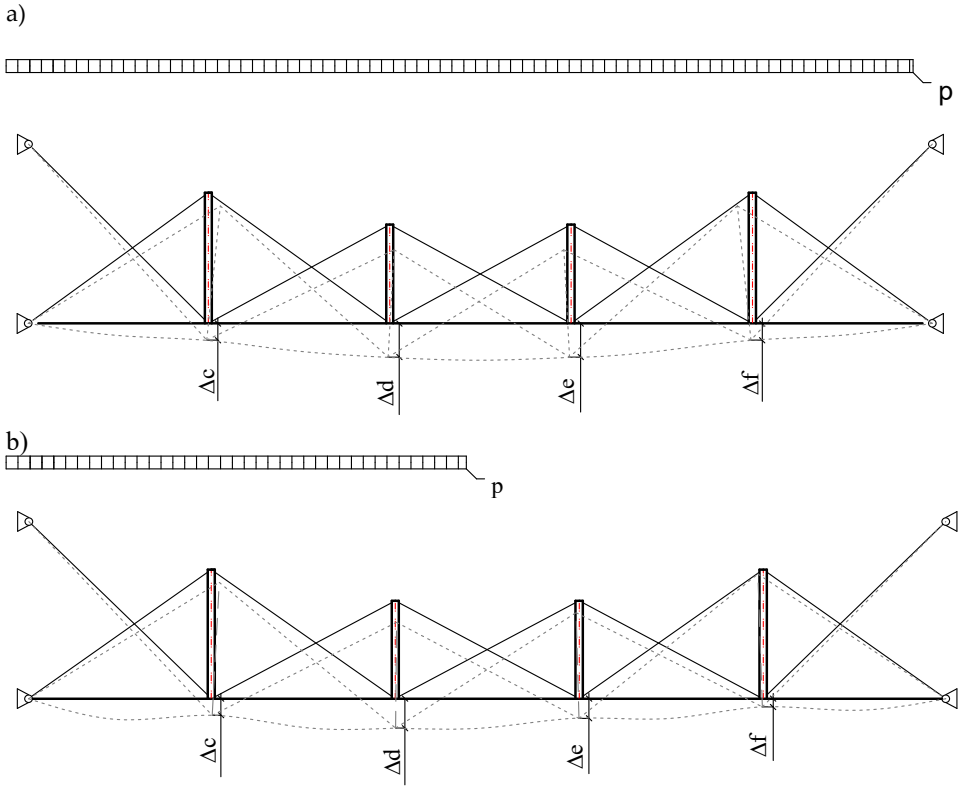

Fig. 2.15. Deformed bridge outline under a) symmetrical loading and b) asymmetrical loading (made by the author)

The cable-stayed bridge is calculated by considering the stiffness beam and the cross cables as two interacting systems. To define the beam's behaviour, actions influencing its deflections must be identified. These are the external distributed load and the supporting forces caused by the stay cables. From the equilibrium of a supported and uniformly loaded beam, a known expression (Kiusalaas, 2012) of the girder's deflections from symmetrical loading is obtained, as shown in Figure 2.16.

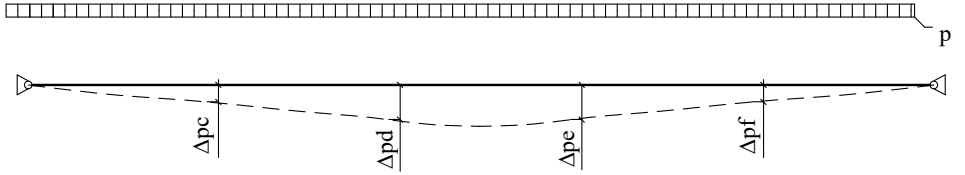

Fig. 2.16. Deformed beam under symmetrical loading (made by the author)

$$\Delta_{pc} = \frac{116pl^4}{24E_sI_s}; \tag{2.1}$$

$$\Delta_{pd} = \frac{186pl^4}{24E_sI_s}; \tag{2.2}$$

$$\Delta_{pe} = \frac{186pl^4}{24E_sI_s}; \tag{2.3}$$

$$\Delta_{pf} = \frac{116pl^4}{24E_sI_s}, \tag{2.4}$$

p – distributed load, l – the distance between intermediate pylons, E_s– – stiffening girder elastic modulus, I_s – stiffening girder cross-section area the second moment.

As shown in Figure 2.17, the same procedure can be used to obtain a known expression (Kiusalaas, 2012) of the girder's deflections from asymmetrical loading.

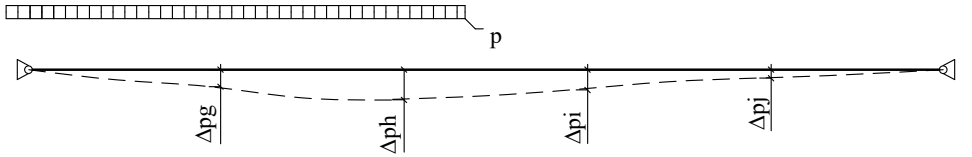

Fig. 2.17. Deformed beam deflections under asymmetrical loading (made by the author)

$$\Delta_{pg} = \frac{63.81pl^4}{24E_sI_s}; \tag{2.5}$$

$$\Delta_{ph} = \frac{96.625pl^4}{24E_sI_s}; \tag{2.6}$$

$$\Delta_{pi} = \frac{89.375pl^4}{24E_sI_s}; \tag{2.7}$$

$$\Delta_{pj} = \frac{52.1875pl^4}{24E_sI_s}. \tag{2.8}$$

To determine the effect of stay-cable support forces on the stiffening beam, first, the bending moments (M) those forces generate are defined. Figure 2.18 shows the beam's supporting force distribution.

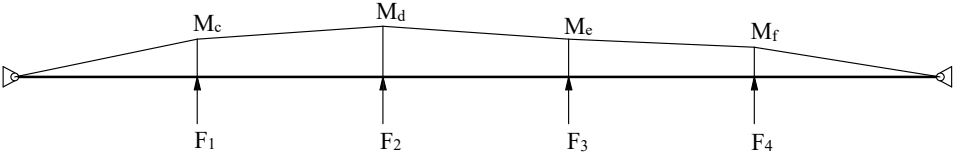

Fig. 2.18. Analogous beam support loads under asymmetrical loading (made by the author)

Bending moments in the stiffening girder that are generated by stay-cable supporting forces are determined according to the following equations:

$$M_C = \left(\frac{4F_1 + 3F_2 + 2F_3 + F_4}{5}\right) l; \tag{2.9}$$

$$M_D = \left(\frac{3F_1 + 6F_2 + 4F_3 + 2F_4}{5}\right) l; \tag{2.10}$$

$$M_E = \left(\frac{2F_1 + 4F_2 + 6F_3 + 3F_4}{5}\right) l; \tag{2.11}$$

$$M_F = \left(\frac{F_1 + 2F_2 + 3F_3 + 4F_4}{5}\right) l. \tag{2.12}$$

Knowing the girder's bending moments, the displacement of intermediate nodes generated solely by cable stays is determined according to the following equations (2.13–2.16), which were obtained using the moment-area expression (Kiusalaas, 2012).

$$\delta_c = \frac{\big((0{,}634M_c) + (0{,}6M_d) + (0{,}4M_e) + (0{,}2M_f)\big)l^2}{E_S \cdot I_S}; \tag{2.13}$$

$$\delta_d = \frac{\left((0{,}6M_c) + (1{,}034M_d) + (0{,}8M_e) + (0{,}4M_f)\right)l^2}{E_S \cdot I_S}; \quad (2.14)$$

$$\delta_e = \frac{\left((0{,}4M_c) + (0{,}8M_d) + (1{,}034M_e) + (0{,}6M_f)\right)l^2}{E_S \cdot I_S}; \quad (2.15)$$

$$\delta_f = \frac{\left((0{,}634M_c) + (0{,}6M_d) + (0{,}4M_e) + (0{,}2M_f)\right)l^2}{E_S \cdot I_S}. \quad (2.16)$$

When the expressions of beam deflections from the uniform load (2.1–2.8) and cable stay support forces (2.13–2.16) are known, girder deflection can be expressed from both actions by subtracting cable support force deflection from uniform load deflection.

$$\Delta_c = \Delta_{pc} - \delta_C; \quad (2.17)$$

$$\Delta_d = \Delta_{pd} - \delta_d; \quad (2.18)$$

$$\Delta_e = \Delta_{pe} - \delta_e; \quad (2.19)$$

$$\Delta_f = \Delta_{pf} - \delta_f. \quad (2.20)$$

To determine cable stay generated uplifting forces Fi on stiffness beam, the state of forces shown in Figure 2.19 will be used in cable attachment points:

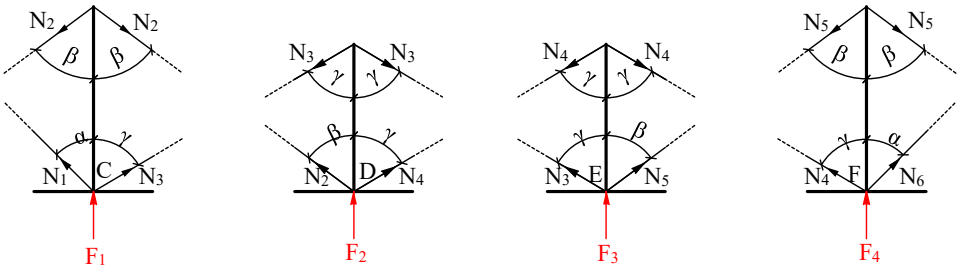

Fig. 2.19. Cable stay forces generating uplifting force F (made by the author)

The vertical projection of cable N_i forces can be used to define the overall supporting force Fi generated by cable stays on the stiffening girder. It is worth mentioning that the compression of the pylon is not considered, which allows for expressing Fi only through cable tension forces and their respective angles at the initial state of the structure.

$$F_1 = N_1 cos\alpha + N_3 cos\gamma - 2N_2 cos\beta; \quad (2.21)$$

$$F_2 = N_2 cos\beta + N_4 cos\gamma - 2N_3 cos\gamma; \quad (2.22)$$

$$F_3 = N_5 cos\beta + N_3 cos\gamma - 2N_4 cos\gamma; \quad (2.23)$$

$$F_4 = N_6 cos\alpha + N_4 cos\gamma - 2N_5 cos\beta. \quad (2.24)$$

To define cable-stay axial forces, it is necessary to divide cable stays into triangular systems, with pylons and cables that connect at their top. Cable elongation in this system is dependent on deflections at the cable ends and pylon vertical deflection. By recognising this relationship, the behaviour of these connected members can be analysed separately. This is especially important considering asymmetrical loading. This assumption can be utilised by noting that cables connected to the same pylon with the same angle should have the same tensile forces from equilibrium. These expressions are provided as equations (2.25–2.30). On the other hand, it helps to simplify systems calculation by decreasing the number of variables and providing a way to connect systems' deflections and cable stays internal forces. Additionally, prestress forces are noted as N_{p1}.

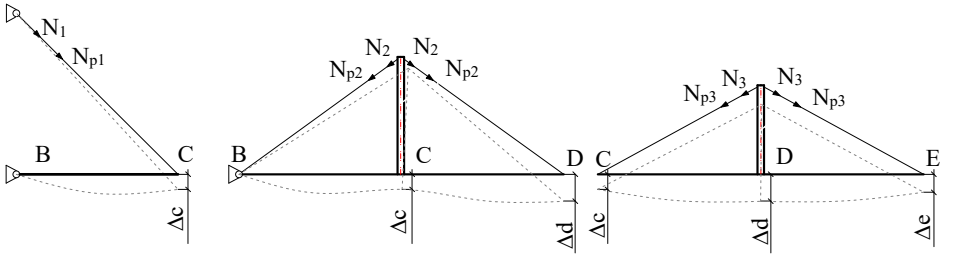

Fig. 2.20. Cable stays and pylons, divided into triangular systems (made by the author)

$$N_1 = \frac{E_{v1}A_v(cos\alpha \cdot (\Delta_c) - sin\alpha \cdot (\Delta_{sl}))}{l_1} + N_{p1}; \quad (2.25)$$

$$N_2 = \frac{E_{v2}A_v cos\beta \cdot (\Delta_d - 2\Delta_c)}{2l_2} + N_{p2}; \quad (2.26)$$

$$N_3 = \frac{E_{v3}A_v cos\gamma \cdot (\Delta_c - 2\Delta_d + \Delta_e)}{2l_3} + N_{p3}; \quad (2.27)$$

$$N_4 = \frac{E_{v4}A_v cos\gamma \cdot (\Delta_f - 2\Delta_e + \Delta_d)}{2l_4} + N_{p4}; \quad (2.28)$$

$$N_5 = \frac{E_{v5}A_v cos\beta \cdot (\Delta_e - 2\Delta_f)}{2l_5} + N_{p5}; \quad (2.29)$$

$$N_6 = \frac{E_{v6}A_v(cos\alpha \cdot (\Delta_f) - sin\alpha \cdot (\Delta_{sr}))}{l_6} + N_{p6}, \quad (2.30)$$

E_{vi} – cables elastic modulus, A_v – cable cross-section area, N_{pi} – prestress force, Δ_{sl} – horizontal deflection of top left support, Δ_{sr} – horizontal deflection of the top right support.

This method can be selected to consider cable stays behaviour while keeping the linear calculation method. The scheme of this calculation approach is provided in Figure 2.21.

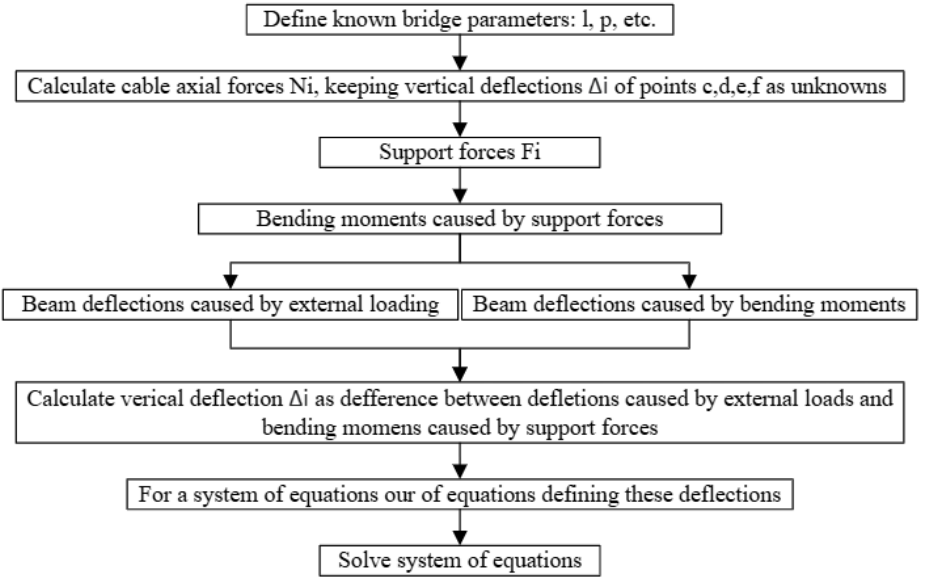

Fig. 2.21. Calculation sequence for cable-beam system (made by the author)

An intersecting cable bridge (Fig. 2.22) with cross-sections listed in Table 2.1 was calculated using the method defined in Figure 2.18 and compared with Dlubal RFEM numerical modelling results. Results of this comparison are provided in Tables 2.5 and 2.6.

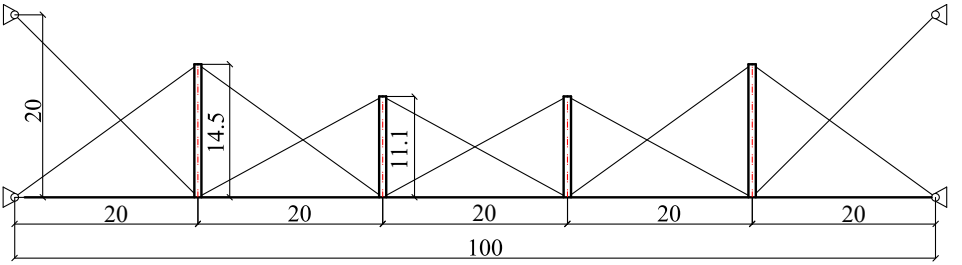

Fig. 2.22. Analysed systems measurements [m] (made by the author)

Table 2.5. Forces and displacements under symmetrical loading

Girder							Cable stays
	Maximum bending moment [kNm]		Deflection [m]				Maximum axial force [kN]
	M+	M-	Δ_c	Δ_d	Δ_e	Δ_f	
FEM Model	772	1214	0.142	0.306	0.306	0.142	2225
Analytical solution	802	1258	0.144	0.318	0.318	0.144	2285
Difference [%]	3.74	3.50	1.39	3.77	3.77	1.39	2.63

Table 2.6. Forces and displacements under asymmetrical loading

Girder							Cable stays
	Maximum bending moment [kNm]		Deflection [m]				Maximum axial force [kN]
	M+	M-	Δ_c	Δ_d	Δ_e	Δ_f	
FEM Model	773	1181	0.116	0.231	0.206	0.087	1966
Analytical solution	796	1224	0.115	0.229	0.203	0.087	1983
Difference [%]	2.89	3.51	0.862	0.866	1.46	0	0.86

To evaluate the nonlinear behaviour of cable stays, their sag must be considered (Juozapaitis, 2008). It is assumed that the cable is not pre-tensioned in the first stage of the analysis. The main unknowns are the cable-stay displacements at the joints Δl, and the cables Δf, and its axial force S. Also, the additional unknowns are the axial force N and elongation s_g (Fig. 2.23).

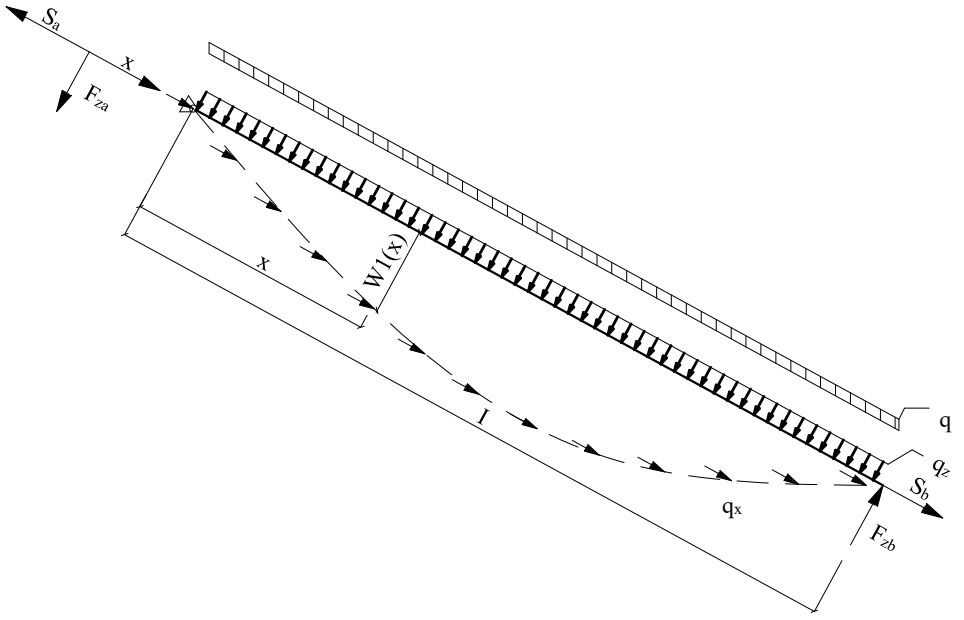

Fig. 2.23. Forces affecting a cable (made by the author)

First, supportive reactions at the cable's ends are determined (in local coordinates).

$$F_{za} \cong \frac{q_z \cdot l}{2} + \frac{2}{3} q_x f; \tag{2.31}$$

$$F_{za} \cong \frac{q_z \cdot l}{2} + \frac{2}{3} q_x f, \tag{2.32}$$

q_z and q_x – cables weight load in z and x-axis.

The axial (tension) load on the cable can be determined throughout its length thusly:

$$S(x) \cong S_m + \frac{q_x \cdot l}{2} + \left(1 - \frac{2x}{l}\right), \tag{2.33}$$

S_m – average axial force at the middle of the cable.

The curve shape of the cable is determined by the ratio between the sum of moments caused by the cable's weight and axial tension force.

$$z(x) \cong \frac{M_z(x) + M_x(x)}{S(x)}; \tag{2.34}$$

$$M_z(x) \cong \frac{q_z \cdot l}{8}\left(\frac{4x}{l} - \frac{4x^2}{l^2}\right); \tag{2.35}$$

$$M_x(x) \cong \frac{2}{3} q_x l f \left(\frac{2x^3}{l^3} - \frac{3x^2}{l^2} + \frac{x}{l}\right). \tag{2.36}$$

The cable length difference after deformation can be described as follows.

$$S \cong l + \frac{8}{3}\frac{f^2}{l}. \tag{2.37}$$

Knowing this expression, the geometrical elongation of the cable after its deformation and loading can be obtained.

$$\Delta S_g = S - S_0 \cong \frac{8}{3}\frac{(f^2 - f_0^2)}{l}. \tag{2.38}$$

These expressions can be added to the methodology mentioned by evaluating the nonlinear behaviour of cable-stays. The start can be defining axial cable forces through the change in cable-stay deflection:

$$N_{in} = \frac{p_l \cdot {l_i}^2}{8(f_i - f_{vi})}, \tag{2.39}$$

p_l – cables own weight.

The discussed deflection change can be obtained by comparing the geometrical cable length change with elastic elongation:

$$s_{0i} - s_{1i} = \frac{N_{1i} \cdot l_i}{E_v A_v}, \tag{2.40}$$

where

$$s_{1i} = \left(l_i + \Delta l_i + \frac{8}{3}\frac{(\Delta f_{0i} - \Delta f_{v1})^2}{l_i + \Delta l_i}\right); \tag{2.41}$$

$$s_{0i} = \left(l_i + \frac{8}{3}\frac{{\Delta f_{0i}}^2}{l_i}\right); \tag{2.42}$$

$$\Delta l_1 = cos\alpha \cdot \delta_C; \tag{2.43}$$

$$\Delta l_2 = \frac{cos\beta \cdot (\delta_D - 2\delta_C)}{2}; \tag{2.44}$$

$$\Delta l_3 = \frac{cos\gamma \cdot (\delta_C - 2\delta_D + \delta_E)}{2}; \tag{2.45}$$

$$\Delta l_4 = \frac{cos\gamma \cdot (\delta_F - 2\delta_E + \delta_D)}{2}; \tag{2.46}$$

$$\Delta l_5 = \frac{cos\beta \cdot (\delta_E - 2\delta_F)}{2}; \tag{2.47}$$

$$\Delta l_6 = cos\alpha \cdot \delta_F. \tag{2.48}$$

Axial forces can be obtained from the defined cable forces, which affect the stiffening girder's internodes C, E, D, and E (Fig. 2.14).

Second, it is important to evaluate the nonlinear behaviour of the bridge beam under bending and affected by axial load. Cable stays generate supportive actions and transfer part of their axial forces to the girder as compression due to intersecting arrangement.

The effect of axial girder force on its deflections and bending moments can be described through the compliance ratio α (LST EN 1993-1-1+AC). α is described through the ratio between the girders' axial force P and girder critical buckling load (Laumann, 2022):

$$\alpha_{cr} = \frac{1}{1-\rho} = \frac{1}{1-\frac{P}{P_E}}; \tag{2.49}$$

$$P_E = \frac{\pi^2 EI}{L^2}. \tag{2.50}$$

Then girder deflections and bending moments can be described thusly:

$$w_n = w_l \cdot \alpha; \tag{2.51}$$

$$M_n = M_l \cdot \alpha, \tag{2.52}$$

w_l, M_l– deflections and bending moments obtained with linear calculation and w_n, M_n– deflections and bending moments, considering nonlinear effects.

With all the parameters defined, equations 2.17–2.20 form a system of equations, with Δ_c, Δ_d, Δ_e, Δ_f as unknowns, which, when solved, define these deflections. With this calculation methodology, we can determine the bridge system's deflections and other unknowns. Furthermore, expressed relations between structural parameters allow for determining their influence on the system's behaviour.

In the case of asymmetrical loading, the main difference in calculation is the effect of a linearly distributed load on the bridge deck. Consider the loading case when half of the bridge is loaded, as shown in Figure 2.18.

2.4. Calculation methodology of a cable-stayed steel bridge with intersecting cable stays and a string

The earlier discussed structural system has a typical drawback to cable-stay bridges, i.e., a high-mass stiffness beam. This beam must withstand bending moments and relatively high axial compressive forces, which create stability problems. As mentioned in the previous chapter, solutions exist where flexible hanging ropes or strings can be applied instead of rigid bending elements. Such elements are usually pretensioned and anchored to the foundation/soil. Therefore, only tensile stresses appear in bridge elements when external loads are applied. Although no such structures have been built, an alternative solution for bridge deck load-bearing element in the discussed bridge system could be a string. Its behaviour can be defined by starting with its single-string internode.

A general expression can be acquired from the deformation consistency principle (Fig. 2.24) (Sandovič, 2011):

$$s_0 + \Delta s_{el} = s_1, \tag{2.53}$$

here,

$$s_0 = a; \tag{2.54}$$

$$\Delta s_{el} = \frac{H\ a}{EA}; \tag{2.55}$$

$$s_1 = a - \Delta h + \frac{8\Delta f^2}{3\ (a - \Delta h)} + \frac{\Delta v^2}{2(a - \Delta h)}. \tag{2.56}$$

Then, after rearrangement, we can describe the displacement of the string node in the middle when one of its ends has a vertical deflection (Fig. 2.23) Δv and horizontal deflection Δh as this:

$$\Delta f = \sqrt[3]{\frac{3\ p\ a^4}{64\ EA\ \ d}}; \tag{2.57}$$

$$d = 1 + \frac{3\ \ \Delta v^2}{16\ \Delta\ f^2} \pm \frac{3\ \ \Delta h \cdot l}{8\ \Delta\ f^2}. \tag{2.58}$$

Here, d – member evaluates strings internode end displacement, sag, and horizontal shift.

Then, string tension force:

$$H = \sqrt[3]{\frac{p^2\ a^2\ EA\ d}{24}}. \tag{2.59}$$

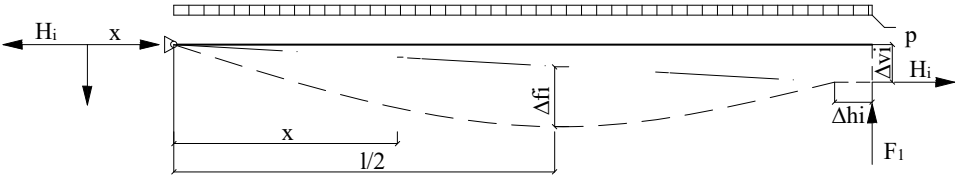

Fig. 2.24. Loaded string (made by the author)

The problem is that formulas (2.57–2.59) include both H and d, making the calculation iterative.

The iterative calculation could proceed as follows (main unknown Δf):

1. Calculate the displacement value Δf when $\Delta v = 0$;
2. Assume $\Delta v \neq 0$;
3. Calculate the parameter d according to formula (2.58);
4. Calculate the displacement value Δf according to formula (2.58) when $\Delta v \neq 0$;
5. Check the difference between Δf values;
6. If they do not match (within a certain accuracy), return to step 2 and adjust Δv .

The iterative calculation can also be performed with the tension force H (as the other primary unknown value). The number of iterations in this approach is smaller, but the accuracy is lower. This iterative path can be chosen:

1. The value of the tension H is calculated when $\Delta v = 0$ (with d = 1);
2. Assume $\Delta v \neq 0$;
3. Calculate the value of Δf using the expression:

$$\Delta f = \frac{pa^2}{8\,H}. \tag{2.60}$$

4. Calculate the value of the parameter d according to formula (2.58);
5. Calculate the value of the tension force H according to formula (2.59);
6. Compare the values of H. If they do not match (within a certain accuracy), return to step 2 and adjust Δv .

Both iterative processes mentioned have one drawback: no well-defined choice of values.

An additional equation can be obtained from the equilibrium condition of the node (node at the movable support):

$$F_v = \frac{p\ a}{2}\left(1 - \frac{\Delta v}{4\ \Delta f}\right). \tag{2.61}$$

To evaluate the multi-span system with nodal loads in place of supports (Fig. 2.15), the bending moment outline of the string must be acquired. Acquiring moments generated by nodal loads $M(x)_{nodal}$, from the previous chapter (2.9 2.12), and moments generated by the distributed load $M(x)_{dist}$, bending moments can be described:

$$M(x) = M(x)_{dist} - M(x)_{nodal}. \tag{2.62}$$

Then, string deflection from a known expression can be obtained:

$$\Delta f = \frac{M(x)}{H(x)}. \tag{2.63}$$

Having string and cable stays defined nonlinear behaviour, it is possible to propose a calculation sequence for an entire bridge system. As discussed earlier, the iterative solution will be needed with unknowns dependent on each other's value. This iterative path for symmetrical loading can be chosen. First, select guess values Δc and Δd of string and cable connection points (Δe and Δf will be equal). Having them, the axial force of the cable stays N_i can be acquired according to earlier equations (2.25–2.28) and their horizontal actions N_{i-hor}:

$$N_{1-hor} = sin\alpha \cdot N_1; \tag{2.64}$$

$$N_{2-hor} = sin\beta \cdot N_2; \tag{2.65}$$

$$N_{3-hor} = sin\gamma \cdot N_3. \tag{2.66}$$

Then, support forces F_i value (2.21–2.24) and bending moments at points c and d (2.63) can be calculated. Having these values, it is possible to define fictional horizontal forces H_c and H_d:

$$H_i = \frac{M(x)}{F_i}. \tag{2.67}$$

The next step is calculating the axial force H_{cd}, as an average between H_c and H_d. This step evaluates axial force affecting the string internode between two points, c and d, and their fictional force values.

$$H_{cd} = \frac{H_c + H_d}{2}. \tag{2.68}$$

Having H_{cd}, H_{bc} and H_{de} can be defined:

$$H_{bc} = H_{cd} - H_{\Delta c}; \tag{2.69}$$

$$H_{de} = H_{cd} + H_{\Delta d}, \tag{2.70}$$

here:

$$H_{\Delta c} = N_{1-hor} - N_{3-hor}; \tag{2.71}$$

$$H_{\Delta d} = N_{2-hor} - N_{4-hor}. \tag{2.72}$$

Having defined axial forces and their vertical deflections, these results can be checked with (2.58–2.60) equations. The cycle is repeated until specified accuracy is achieved. The scheme of this calculation approach is provided in Figure 2.23.

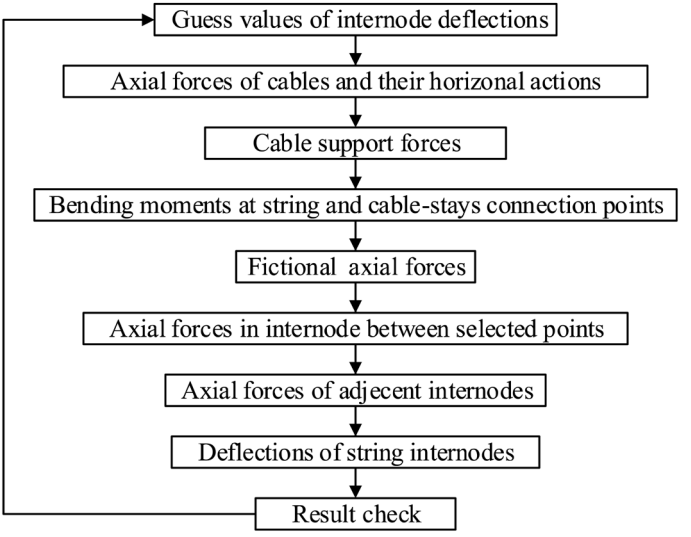

Fig. 2.25. Calculation sequence for cable-string system (made by the author)

A string-cable system (Fig. 2.22) with cable and pylon profiles listed in Table 2.1 was calculated using the method defined in Figure 2.25 and compared

with Dlubal RFEM numerical modelling results. String cross-section was selected as $A_{string} = 78.5\ cm^2$. The results of this comparison are provided in Table 2.7.

Table 2.7. Cable-string systems forces and displacements under symmetrical loading

String						Cable stays
	Maximum axial force [kN]	Deflection [m]				Maximum axial force [kN]
		Δ_c	Δ_d	Δ_e	Δ_f	
FEM Model	6683	0.423	1.134	1.134	0.423	3761
Analytical solution	6475	0.415	1.120	1.120	0.415	3741
Difference [%]	3.11	1.92	1.25	1.25	1.92	0.53

Deflection differences are under 2%, and strain differences are under 4%, highlighting the accuracy of this calculation methodology.

2.5. Rational parameters of the cable-string system

Having defined calculation methodologies for two cases of intersecting cable-stayed bridges, it is possible to examine an innovative cable-string bridge's design and rational parameters. An algorithm is applied to define an effective pylon outline, accounting for changes in internode length and prestressing forces. The rational internode number is determined. Prestress values are calculated to ensure selected limits. Lastly, system stresses during the installation phase are analyzed to maintain structural integrity throughout construction.

2.5.1. Pylon outline

Intersecting cable-stay bridges generally follow two pylon arrangement types (Fig. 2.26): equal pylons (Olstgracht bridge) and the most usual – parabolic pylons (Frank Gehry bridge, Forthside bridge, etc.).

The most striking distinction between the systems under comparison lies in the bending moments generated on the pylons. Compared to a bridge with flat pylons, the bending moment value decreases by more than ten times. Given the substantial difference between the axial and bending stresses, these pylons appear primarily in compression and are subject to axial forces (Fig. 2.7). This helps the bridge to maintain its initial shape, allowing for the selection of more economical cross-sections. Such a significant difference alters the bridge behaviour, where the entire system deforms. The cable stays do not transfer bending to the pylon from

the stiffness beam, and pylons can deform in unison with it. This affects not only stresses but also system deformations. The system deforms less by rearranging pylons (of the same total length) in a curve pattern (Fig. 2.27).

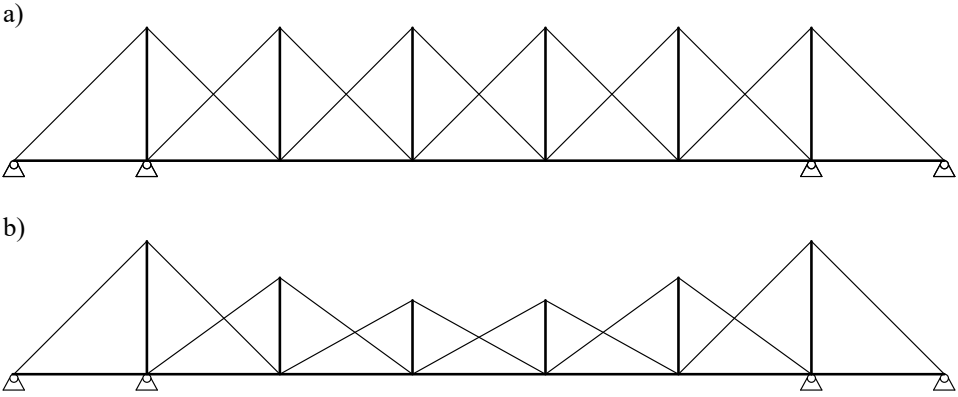

Fig. 2.26. Pylon arrangement: a) equal and b) parabolic (made by the author)

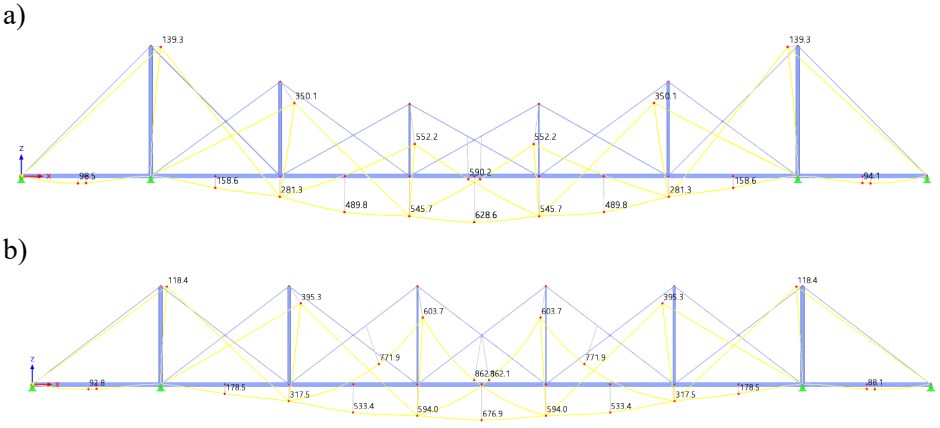

Fig. 2.27. Same total length pylon arrangement: a) equal and b) parabolic (made by the author)

The linear calculation methodology for cable-beam systems can be a tool for searching for rational pylon heights. Equations 2.1–2.30 can be used to define an algorithm describing the relations between bridge characteristics, deflections, and internal forces. Analysing the system, the sum of the pylon heights can be defined as a constant $h_1 + h_2 + h_3 + h_4 + h_5 + h_6 = const$. Then, the program varies the heights of bridge pylons in defined constraints until the lowest deflection sum

is found $\Delta_c + \Delta_d + \Delta_e + \Delta_f \rightarrow min$. This allows for obtaining the distribution of those lengths in different pylons, revealing the rational heights. This approach helps to obtain the pylon configuration and identify the overall influence of the bridge on it.

The defined algorithm was solved using Python programming language and the open-source SciPy library (Virtanen, 2020). It used the limited memory variant of BFGS (Broyden–Fletcher–Goldfarb–Shanno) (known as L-BFGS) to solve the problem. This type of quasi-Newton method is often used in algorithms to solve nonlinear objective functions. It works by computing search directions using (inverse) Hessian approximations that are set using iterate and gradient displacement information from one iteration to the next (Berahas, 2019).

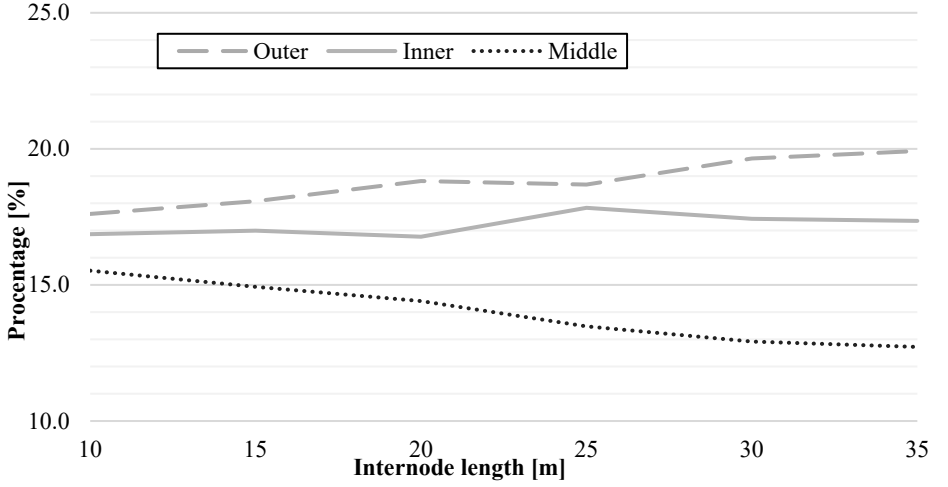

Fig. 2.28. Pylon height percentage from the sum of pylon height

The presented data show that widening internodes between pylons change their outline (Fig. 2.28). While outer pylons gain height, middle pylons shorten. This trend remains consistent throughout the internode length from 10 to 35 meters. It should be noted that the positioning and height of the pylons after the calculation roughly follow a known geometric principle. Pylons align according to the following principle: the intersection points of the cables between two adjacent pylons form a parabola, similar to a beam's bending moment diagram. The shape of that parabola changes according to internode width; a broader internode structure has a more expressed shape (Fig. 2.29). This can be attributed to higher forces in the system and the need for more expressed outer pylons.

Additionally, the influence of cable stays prestress on pylon configuration was evaluated (Fig. 2.30).

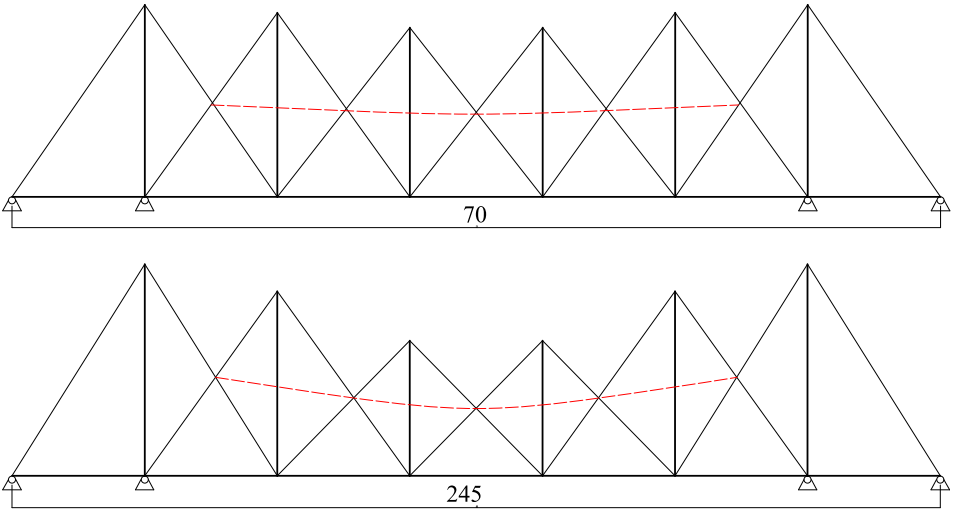

Fig. 2.29. Rational pylon outline according to bridge length [m] (made by the author)

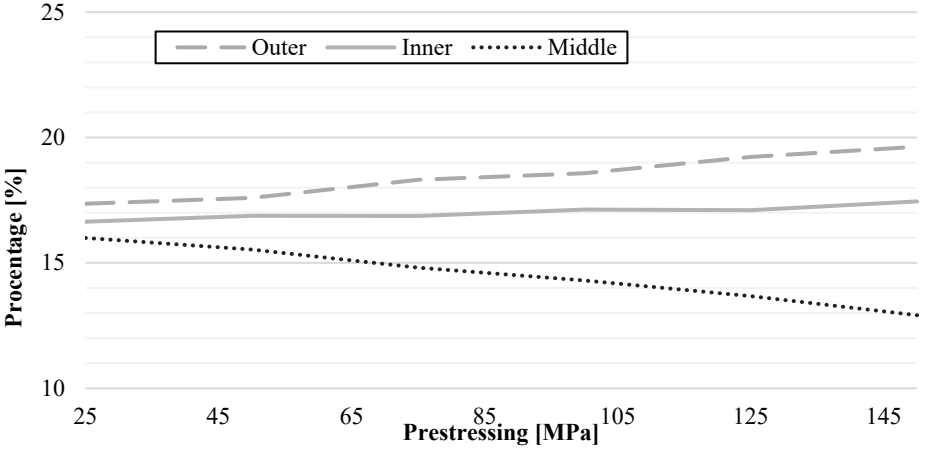

Fig. 2.30. Pylon height percentage from the sum of pylon height during cable prestressing change

An equal prestressing force was applied to all cable stays. The data shows that changing the prestressing force similarly affects pylon configuration as the internode widens.

2.5.2. Internode number

One of the main differences between typical cable-stayed bridges and intersecting cables is the limitations and influence of internode numbers. While this number has a minimal influence on the classical type, for intersecting cable type, the number and even its parity are important. Usually, intersecting cable-stayed bridges have 5 or 7 internodes (Table 2.8).

Table 2.8. Internode number of intersecting cable-stayed bridges

Bridge	Number of deck internodes
Olstgracht	4
Zhangjiatang	5
Royal Victoria	5
Passerelle du Grand Large	7
Forthside	7
Frank Gehry	7
Grand Canal	9

The vast majority of existing intersecting cable bridges have odd number deck internodes. This number of internodes is favoured due to middle pylon behaviour in a system with an even number of internodes. In general, axial force change of cable-stay can be described in connection to a specific pylon top due to systems deformation like this:

$$N_i \cong \frac{E_{vi}A_{vi}cos\alpha_i \cdot (\Delta_{i-1} - 2\Delta_i + \Delta_{i+1})}{2l_i} + N_{pi}, \tag{2.73}$$

E_{vi} – cables elastic modulus, A_{vi} – cable cross-section area, N_{pi} – prestress force; α_i– the angle between pylon and its top cable-stay, Δ_i – deflections of the pylon, $i-1$ – deflections of the pylon to the left, Δ_{i+1} – deflections of the pylon to the left.

In the case of symmetrical loading, due to the deformation outline, for the middle pylon $2\Delta_i$ will be much greater than $\Delta_l + \Delta_r$ and turning member $(\Delta_l - 2\Delta_i + \Delta_r)$ negative. This causes the cables to lose tension and has a support effect on the deck. Furthermore, the parabolic outline will dictate short pylon height, lowering the effectiveness of the cables due to the angle. This means that there will be a need for higher prestressing force N_{pi} and a broader section of the cable. This renders the middle pylon much less effective.

Geometrical limitations define the maximum efficient number of internodes. When connected to the pylon and deck, every cable axial force is divided into two effects (Fig. 2.16). Part of it affects the beam (or string) as compression (or tension), and the other affects the pylon, generating a support effect and enabling tension in cable stays further on the deck. As described in 2.21–2.24:

$$F_{support} \cong N_{i-1}cos\alpha_{i-1} + N_{i+1}cos\alpha_{i+1} - 2N_i cos\alpha_i. \quad (2.74)$$

With more pylons, this effect waning is more prominent, and a larger number of pylons can be counterproductive compared to a bridge system with fewer pylons (Fig. 2.31). The system may lose the support effect at the middle of the bridge at a higher rate, causing higher deformation in the middle of the span.

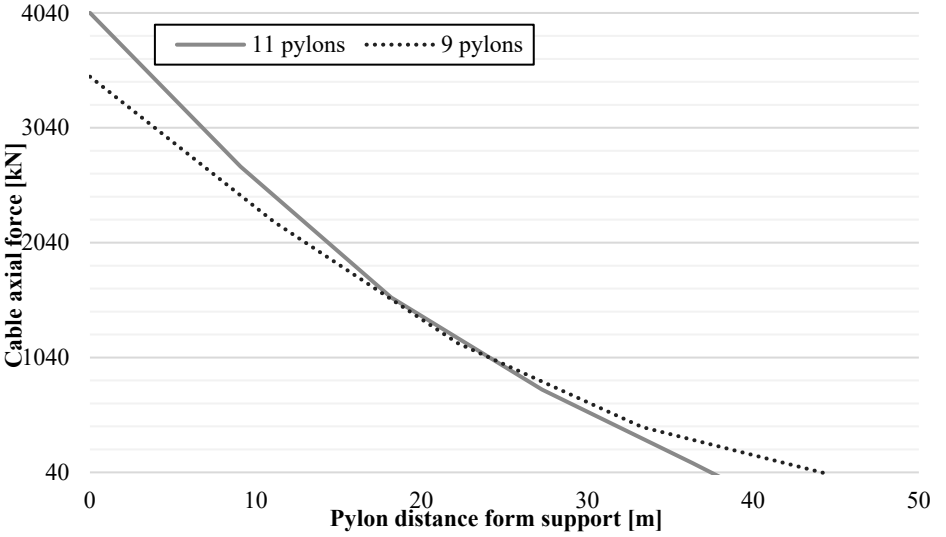

Fig. 2.31. Cable axial forces distribution along bridge length

This, combined with the maximum rational spans of unsupported beams or strings, limits the total span length of intersecting cable systems.

2.5.3. Minimal prestress value

The key regulatory condition for cross-cables and strings is their propensity to loosen. As outlined in Section 2.1, as the bridge undergoes deformation, the cross cable experiences a reduction in tension, compromising the supportive effect of

the cables. This is particularly evident during the symmetrical loading of an experiment that impacts the central cross-cables. During asymmetric loading, cables that connect the intermediate pylons of the adjacent section are under exceedingly low tension. Initially, the tensile force of these cross-cables is merely 0.01 kN, increasing slightly to 0.02 kN in the second loading stage. Given the disparity between asymmetric and symmetric loads, the cross-cables' prestressing forces (strains) must be meticulously calibrated. The greater the asymmetric load, the higher the required tension force of these cables. Ultimately, it is evident that the axial forces between string nodes are directly influenced by the cross-cable forces under both symmetric and asymmetric loading scenarios.

Considering the serviceability ultimate limit, limit values for bridge deflections Δc, Δd, Δe, Δf at symmetrical loading can be described. Then, knowing deflections in the stiffening girder, which are caused by external loads (Δpc, Δpd, Δpe, Δpf) (2.1–2.4), needed values can be expressed for deflections that cable support forces should cause in the stiffening girder (δC, δd, δe, δf) (2.5–2.8). Knowing those values, we can calculate bending moments in the girder (MC, MD, ME, MF) (2.9–2.12) and supporting forces that cause them (F1, F2, F3, F4) (2.21–2.24). This allows for the expression of cable stay forces N_i (2.25–2.29) and with them – prestress values for each cable stay N_{pi}. However, this approach does not grant optimal bending moment outlines in the beam, which is instrumental when considering the ultimate limit state.

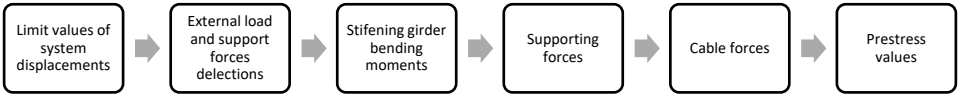

Fig. 2.32. Prestress definition process

The string's prestressing is based on two factors. First, a minimal prestress is necessary to mitigate stress changes during the system's installation. During cable-stay prestressing, the internal forces of the strings change, which creates a possibility that the string could be compressed during installation. Thus, a minimal prestress is necessary to ensure stability in this stage. Second, prestress is necessary to constrain the system's deflections.

2.5.4. Stress and deformation state of the string-cable bridge structure concerning the installation sequence

Given the complex stress state, it is essential to plan the installation sequence of this bridge system carefully. Due to the potential for significant deflections and redistribution of forces, the cross-cables cannot be pre-tensioned to their design values before the deck is installed. The support effect generated by the cross-cables causes the entire structure to lift (relative to an unloaded, pre-installed system). However, tensioning the cross-cables after the deck is in place is also not feasible, as the system may experience excessive deflections (relative to an unloaded, installed system), potentially damaging the deck structure and inducing additional stresses in the deck components.

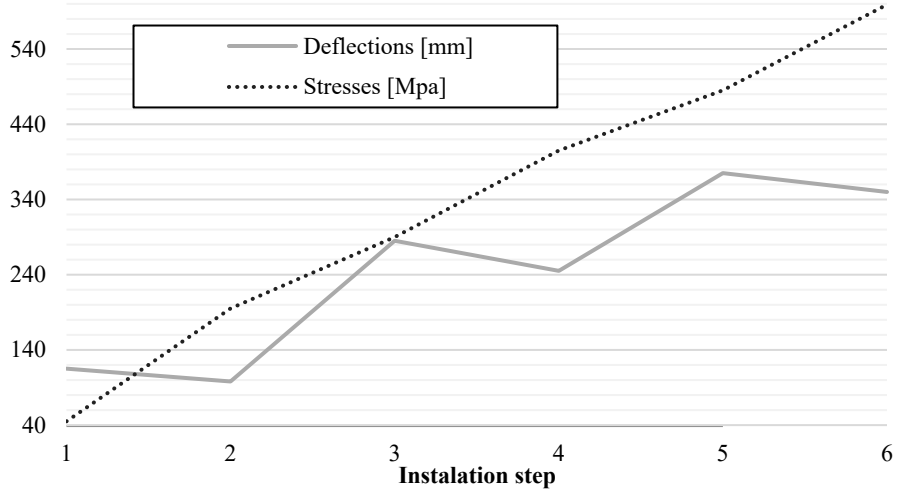

Fig. 2.33. Stress-deflection outline during installation

Due to these considerations, it is essential to implement a phased installation and tensioning approach for the structure in question. Here is a possible sequence:

1. Prestress the string to 100% of the designed tension force and tension the cables to 33% of the designed tension force.
2. Load half of the deck's weight onto the string (this can be achieved by completing half of the concrete or assembling every alternate deck slab, utilising residual concrete formwork).
3. Increase the tension of the cables to 66% of the designed tension force.
4. Load the remaining half of the weight onto the string.
5. Finally, tension the shingles to 100% of the designed tension forces.

2.6. Conclusions of the Second Chapter

1. Proper prestressing of elements (strings and cross-cables) in intersecting cable bridges can effectively stabilise the initial shape under various load conditions, ensuring that moments in the stiffness beam under asymmetrical loading do not exceed those under symmetrical loading.
2. The calculation methodology for both types of bridge structures was validated against numerical analysis, showing a discrepancy margin of less than 5% for axial forces and displacements. Under asymmetrical loading, the internal forces and displacements do not exceed those of symmetrical loading due to the interconnectedness of cable stays and pylons.
3. The presented methodology can be applied to system composition, cross-section selection, and defining the prestressing of elements. The provided equations serve as the calculation basis of this structural system under different loading.
4. Parabolic pylon arrangements reduce bending moments compared to equal pylon configurations. The L-BFGS algorithm determined rational pylon heights to minimise deflections. It revealed that outer pylons gain height while middle pylons shorten, following a parabolic distribution influenced by internode length width or prestress amount. Wider internodes result in more pronounced parabolic shapes, affecting the distribution of forces and the configuration of pylons.
5. The cable-string bridge design may lead to lighter and more cost-effective than traditional designs and reduced material usage. Despite the benefits, the cable-string bridge generates higher support reactions.

3

Experimental study of the cable-string steel bridge model

The primary goal of the experimental study was to examine how the new bridge structure responds to static symmetric and asymmetric loads. The study also sought to measure the stress levels and deformations gained by the bridge components and assess how cross-cables affect the bridge's deformability. Additionally, within the same experiment, the impact of pretensioning the string and cross-cables on the displacements and stresses of the bridge model was evaluated. This chapter includes the material presented in 1 journal publication (Dabrila & Juozapaitis, 2024b).

3.1. Experiment model

The new cable-stayed string steel bridge model was constructed to meet the experiment's objectives. This model features four intermediate pylons of varying heights, each supported by a pre-tensioned steel string that functions similarly to a conventional stiffness beam, as previously mentioned. The intermediate pylons are attached to the string using cross cables.

3.1.1. Test model design

Instead of traditional supporting (side) pylons, the model employed rigid supports designed to restrict potential horizontal displacements of these pylons during the experiment (Fig. 3.1). This was done to adapt to testing environment limitations but still keep the shape of a bridge with six pylons. The ends of the pretensioned string were also anchored to the same rigid supports. The bridge model, measuring 4995 mm in length, features spans between pylons of 1000 mm, each flanked by 997.5 mm outer spans. These measurements were selected considering the constraints of manufacturing and the lab environment. The outer pylons' height is 731 mm, and the inner pylons are 556 mm. The top ends of the intermediate pylons follow a parabolic curve. The vertical distance between fixed supports and support bearings is 1000 mm (Fig. 3.2). The width between strings is 320 mm. Strings and side (support) cable supports are installed in support blocks that can rotate around the horizontal axis fixed through tapered bearings (Fig. 3.3a). The string was designed as a continuous steel bar to ensure uniform prestressing in this element. All the bar ends with a thread for assembly and prestressing. Prestressing of the string is achieved with anchor bolts fixed in blocks on hinged supports. Cable stays were prestressed with their threading. Intersecting cables-stays are connected to pylons through coupling nuts on their threaded endings. This type of connection only restricts cable stay tension forces, preventing bars from losing tension. A string supports pylons threaded through bushings and anchored with U-shaped bolts to the string, thus avoiding the slip of pylons across the length of the string (Fig. 3.3b).

Fig. 3.1. Model of cable-stayed string bridge

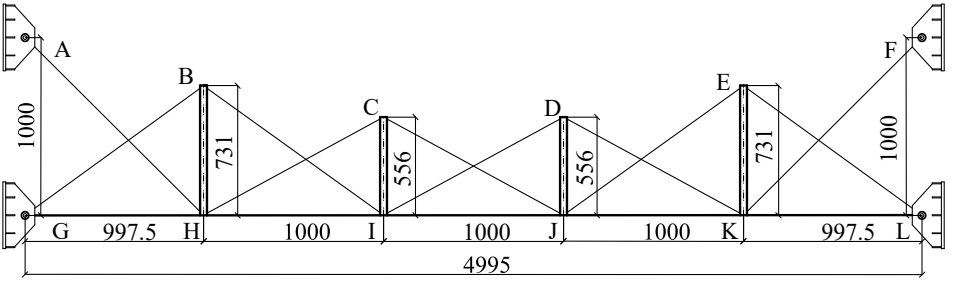

Fig. 3.2. Model scheme and geometrical parameters [mm] (made by the author)

a)

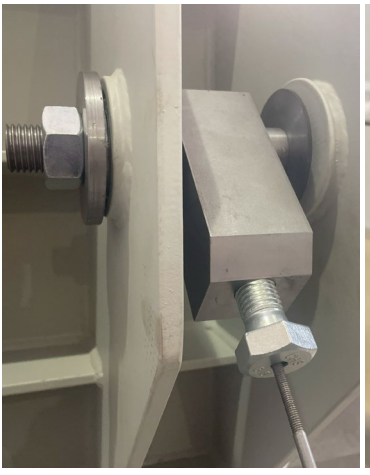

b)

c)

Fig. 3.3. a) Anchor cable support “A”; b) Pylon bottom joint “I”; and c) Support “L”

The string and cross-cables are designed from a round rod with a diameter of d = 6 mm. This type of element was selected according to existing laboratory testing equipment and conditions to ensure accurate measurements of deflections and stresses. The elements of the pylon are designed from a rectangular tube 40×40×3 mm. These dimensions were selected to eliminate possible axial deformations of the pylon and, at the same time, their effect on the behaviour of the bridge. Anchor cable supports (Figure 3.3a) are designed so that it is possible to tension the anchor cable and string without causing additional (mainly torsional) stresses in them.

3.1.2. Materials of experimental model

30 cm long specimens were selected to determine the material properties of the string and cable-stays of the bridge model. This test used drawn calibrated round steel (J2C+C) (EN 10278).

a) b)

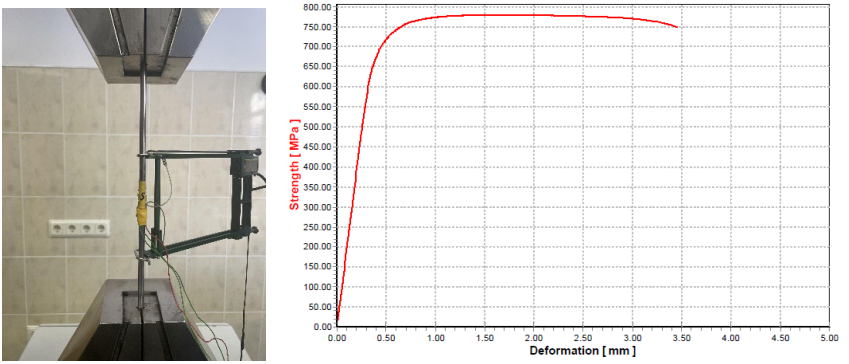

Fig. 3.4. Tension test of string and cable-stay steel a) and strength-deformation curve b)

The test used a tensile machine, CH-8224. A 352-050M-100-ST extensometer was attached to the specimen to measure the relative deformations. The samples' modulus of elasticity was within the expected boundaries. The mechanical characteristics of the samples are presented in Table 3.1.

Table 3.1. Properties of bar elements

Bar diameter (mm)	Modulus of elasticity (N/mm^2)	Tensile strength R_m (MPa)	Offset yield strength $R_{P0,2}$ (MPa)
6	196 000	778	737

Tests were conducted according to ISO 6892-1:2019 A223 in the Applied Laboratory of Buildings, Constructions and Materials of the Faculty of Construction, Vilnius Gediminas University of Technology.

3.1.2. Arrangement of measuring points

Two types of measuring tools were selected for this test (Fig. 3.5): strain gauges (marked red) and displacement meters (marked blue).

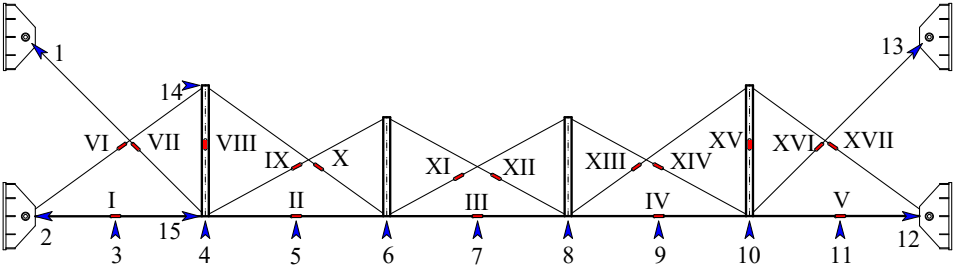

Fig. 3.5. Strain gauges and displacement meters arrangement (red-strain gauges; blue – displacement meters) (made by the author)

Almemo data logger 5990-2 was used to record data from gauges and meters. The FLAB-6-1, by TMI, was used for strain gauges with a gauge length of 6 mm and a gauge resistance of 120±0,3 Ω. For displacement meters, Almemo displacement potentiometric FWA sensors were selected. Strain gauges were placed on every cable-stay bar as close as possible to the middle of its span and on each span of string. Four additional gauges were put on the string to evaluate possible bending moments in the string. Two strain gauges were put on exterior pylons. Displacement meters were used for three purposes. First, they measured string displacements arranged under pylons at junctions with the string and internodes. Second, support deflections (meters 1, 2, 12, 13) were measured. Third, they monitored the horizontal movements of pylons (meters 14, 15).

3.2. Experimental testing

The cable-stayed bridge model was tested under quasi-static loads. Dead load is described as the weight of string, stay-cables, and pylons. For stay-cables and pylons, it is marked as F1 for outer pylon joints and F2 for inner joints. The values of these concentrated loads are presented in Table 3.2. The uniformly distributed

load of the cable-stayed bridge model was formed from steel square bars (24×24×500 mm).

3.2.1. Loading and prestress

Two loading scenarios were considered: symmetrical and asymmetrical. An incremental loading was adopted throughout the test, with a load of 0.12 kN for every loading step. After a specific load on the bridge was reached, the load was held for a period of time to observe behaviour and record meter data. Due to the installation of measuring devices and the dimensions of the supports, the string was loaded with static loads q1 and q2 of different magnitudes with different distribution lengths (Fig. 3.6). However, the effect of these loads on each internode in the string was equivalent. Load q1 marks load for G–H and K–L string internodes and q2 for H–F (Table 3.2).

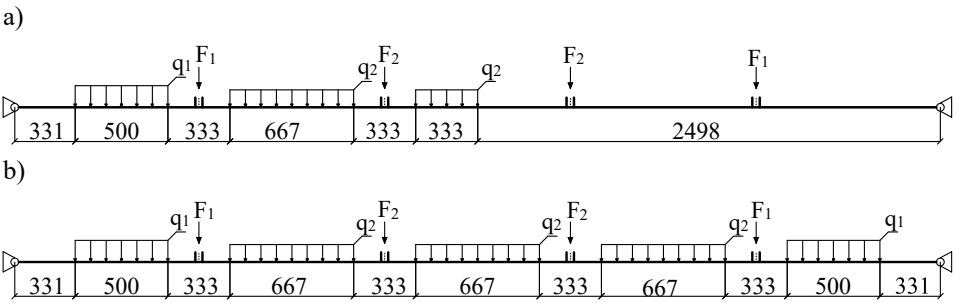

Fig. 3.6. Loading placement scenarios: a) asymmetrical and b) symmetrical [mm] (made by the author)

Table 3.2. Loading steps

Loading step	q_1 (kN/m)	q_2 (kN/m)	F_1 (kN)	F_2 (kN)
1	0.8	0.6	0.1	0.09
2	1	0.75	0.1	0.09

As already mentioned, a cable-stayed bridge is a prestressed steel system. Prestressing is crucial to this bridge model to prevent cable stays and the string from compression. Under specific loading, the outer spans of the string and middle cable stay loose tension. The pre-tensioning of the model elements was carried out gradually. First, the string was prestressed before the pylons and cable-stays were installed. After that, pylons were fixed on the string after reaching the prestress value of 2.38 kN. After that, cable-stays were prestressed by tightening the fastening nuts on the end of the threaded rods.

Table 3.3. Elements axial forces after prestressing steps [kN]

Prestressing element	Outer string internode (G–H and K–L)	Middle string internode (I–J)	Anchor cable-stay (A–H and F–K)	Middle cable-stays (C–J and I–D)
	Strain gauge 1	Strain gauge 3	Strain gauge 7	Strain gauge 11&12
1. String pre-stressing	2.38	2.38	0	0
2. Cable stays prestressing	2.81	1.51	0.38	1.13

The prestress value in the middle cable stays (C–J and D–I) at 1.13 kN, and the outer pylon cable stays at 0.38 kN (Fig. 3.2). The prestress was monitored continuously through strain gauges (meters 11 and 12). As mentioned earlier, the string gains an axial force value of 2.38 kN during prestressing. However, as the cable stays are prestressed, string internal forces change, as shown in Table 3.3. The tension forces in internodes H–I, I–J, and J–K decreased, especially in the middle of the string (1.51 kN), I–J, while increasing in the outer internodes G–H, K–L (2.81 kN).

3.2.2. Results

Table 3.4 and Figure 3.7 present the displacement values of the symmetrically loaded cable-stayed bridge model and its deformation outline, respectively. Table 3.5 shows the axial forces of the bridge model elements in cable stays and string under symmetrical loading. It should be noted that the experiment was carried out within the elastic stage, with each loading scenario repeated four times for accuracy, and averages are presented.

Table 3.4. String deflections under symmetrical loading [mm]

	Exterior internode	Inner internode	Middle internode
Load step	Disp. meter 3 (G–H, K–L)	Disp. meter 5 (H–I, J–K)	Disp. meter 7 (I–J)
1	16.05	14.96	15.95
2	20.97	15.30	17.50

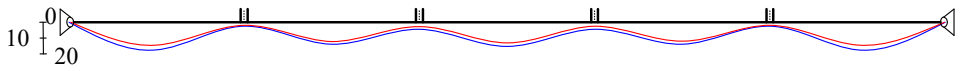

Fig. 3.7. Symmetrical loading deflections [mm]. Loading 1 – red and 2 – blue [mm] (made by the author)

As can be seen from the data presented, the highest string deflections, during symmetrical loading, occur in outer string internodes (G–H and K–L). At the first stage of loading, smaller displacements appeared in the internal internodes of the string (H–I, I–J, and J–K). The difference between these displacements is about 7%. The displacements of the mid-string internode were only 0.6% smaller than the outer ones. When the load was increased by 25% (Step 2), the displacements in the string internodes increased disproportionately. The displacements of the outer internode (G–H) increased by over 30%, the inner (H–I) only about 2.3%, and the middle internode by about 10% (Table 3.4). This can be explained by the rotation of outer pylons and their connection point with the horizontal shift of the string due to string deformation.

Upon symmetrical load (step one) application, the string outer internode's axial force increased to 4.01 kN, while the middle internode reached 5.03 kN (Table 3.5). Simultaneously, the anchor cable forces (A–H and F–K) increase to 2.26 kN, whereas the force in the middle cables decreases to 0.68 kN. In the case of load Step 2 string internode (G–H and K–L), the axial force increased to 4.53 kN (about 12.9%), and the middle string internode tensile force increased to 6.33 kN (about 25.8%).

Table 3.5. Element axial forces under symmetrical loading [kN]

Load step	Outer string internode (G–H, K–L)	Inner internode (H–I, J–K)	Middle string internode (I–J)	Anchor cable-stay (A–H)	Middle cable-stays (C–J, I–D)
	Strain gauge 1	Strain gauge 2	Strain gauge 3	Strain gauge 7	Strain gauge 11&12
After prestress	2.81	2.35	1.51	0.38	1.13
1	4.013	4.76	5.03	2.26	0.68
2	4.53	5.35	6.67	2.63	0.51

These data show that the load is distributed unevenly between the points of the string during loading. This underscores the intricate relationship between string and cable stays, particularly the balance of axial forces within the bridge's middle elements: cable stays (C–J and D–I) and string internodes I–J. It becomes evident that the middle string's internode would endure excessive stress without prestressing, and the middle cables may be compressed, thus, guaranteeing the initial shape by keeping string and cable elements under tension.

The data in Table 3.5 show that at a certain level (intensity) of symmetrical loading, the prestress of the middle cable stays can decrease to a minimum value. Therefore, when designing a bridge with cross cables, it is necessary to combine the values of the pre-tensioning force of these cables with the size (values) of the external symmetrical load.

As mentioned in the introduction, one of the disadvantageous loads of cable-stayed steel bridges in terms of displacements is asymmetric, and usually when the temporary load is distributed over half of its span. Therefore, the new cross-cable bridge model was loaded, as shown in Figure 3.7b. The displacement values of the cable-stayed bridge model loaded in this way and its deformation scheme are shown in Table 3.7 and Figure 3.8.

Table 3.6. String deflections under asymmetrical loading [mm]

Load step	Exterior internode	Inner internode	Middle internode	Inner internode	Exterior internode
	Disp. meter 3 (G–H)	Disp. meter 5 (H–I)	Disp. meter 7 (I–J)	Disp. meter 9 (J–K)	Disp. meter 11 (K–L)
1	16.00	16.20	10.04	3.2	0.3
2	20.40	18.00	12.26	4.3	0.4

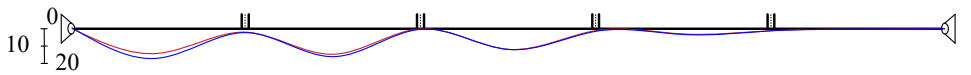

Fig. 3.8. Asymmetrical loading deflections. Loading: 1 – red and 2 -blue [mm] (made by the author)

From the presented data, in the case of asymmetric loading of the 1st stage, the maximum displacements of the string occur at the exterior internode and inner internode of 16.0 and 16.2 mm, respectively. The displacement of the middle node is 61% less and amounts to 10.04 mm. During the asymmetric load of the 2nd stage, the maximum string displacement value at the exterior internode was 20.4 mm. The inner internode of the string increased displacements by about 11%

and the middle internode by about 22%. It is necessary to note that, under asymmetric loads, the displacements of the max string at the exterior internode and middle internode are not more significant than the displacements caused by symmetric loads. This indicates the effectiveness of this structural system under asymmetric loading. It is necessary to notice that the displacements of the inner internode of the string become larger by about 18% when compared with symmetrical loading.

However, considering the nature of the string's internodal deformation, these displacements from the first internode gradually decrease in the case of asymmetric loading.

In the case of asymmetric loading, the axial forces of the elements of the cable-stayed bridge model do not exceed symmetrical loading values. The axial force strings in the outer string internode in load cases 1 and 2 are practically equal (the maximum difference is about 6%). Compared to symmetrical loading, axial forces in both the string and the anchor and cross cables are smaller in this loading case (Table 3.7). In the outer string internode, they changed little (decreased by about 5%); in the middle string internode, they decreased by about 40%. Anchor cable A–H tension also decreased from 2.63 kN to 1.66 kN. The tension of the middle cross cable C–J practically did not change, but it increased from 0.51 to 0.93 kN in the cross cable I–D.

Table 3.7. Element axial forces under asymmetrical loading [kN]

Load step	Outer string internode (G–H)	Inner internode (H–I)	Middle string internode (I–J)	Inner internode (J–K)	Outer string internode (K–L)	Anchor cable-stay (A–H)	Middle cable-stays (C–J, I–D)	
	Strain gauge 1	Strain gauge 2	Strain gauge 3	Strain gauge 4	Strain gauge 5	Strain gauge 7	Strain gauge 11	Strain gauge 12
1	3.88	4.06	3.67	3.48	2.73	1.24	1.01	0.72
2	4.32	4.61	4.53	4.32	3.18	1.66	0.93	0.52

Figure 3.9 compares string displacements between symmetrically and asymmetrically loaded models. It demonstrates that the displacements of an asymmetrically loaded string are smaller across nearly all its internodes compared to those observed under symmetrical loading. To ascertain the behavioural characteristics of the new cable-stay bridge system, the experiment also included measurements of horizontal displacements of the bridge model's anchor nodes and pylons. These measurements are detailed in Table 3.8. Symmetric loading showed relatively uniform displacements, with minimal deviations (5%) between.

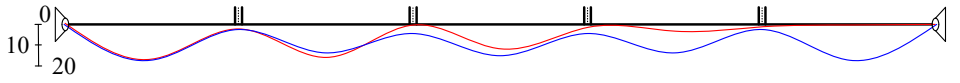

Fig. 3.9. Loading deflections. Symmetrical blue, asymmetrical – red [mm] (made by the author)

Asymmetrical loading conditions yielded similar trends. It is necessary to note that the horizontal displacements of the anchor cable support were directed to the middle of the span, practically did not change in both loading cases, and amounted to only 0.07 mm. An analogous situation can be observed in the string support nodes, where only the values of these horizontal displacements were higher (on average, from 0.90 mm to 0.95 mm). The horizontal displacements of the upper and lower nodes of the intermediate pylons had opposite signs. The top of the pylons moved towards the middle of the span under both symmetric and asymmetric loading, while the lower nodes of the pylons moved towards the string supports. In all cases of symmetrical loading, the displacements of the pylon's lower node were smaller in absolute magnitude than those of the upper node (about 20%). In the case of asymmetric loading, the top of the pylon horizontal displacements are close in their absolute magnitude to the horizontal displacements of the top node of the pylon (the most significant difference was about 10–12%). It should be noted that the horizontal displacements of the pylons were slightly more significant in the case of symmetrical loading (Table 9).

Table 3.8. Support and pylon deflections under symmetrical and asymmetrical loading

Loading	Load step	Deflection	Measurement	Value (mm)
Symmetrical	1	Anchor cable support	Disp. meter 1	0.07
		String support	Disp. meter 2	0.76
		Top of pylon horizontal	Disp. meter 14	–1.86
		Bottom of pylon horizontal	Disp. meter 15	1.35
	2	Anchor cable support	Disp. meter 1	0.08
		String support	Disp. meter 2	0.90
		Top of pylon horizontal	Disp. meter 14	–2.11
		Bottom of pylon horizontal	Disp. meter 15	1.78
Asymmetrical	1	Anchor cable support	Disp. meter 1	0.07
		String support	Disp. meter 2	0.83
		Top of pylon horizontal	Disp. meter 14	–1.28

End of Table 3.8

Loading	Load step	Deflection	Measurement	Value (mm)
		Bottom of pylon horizontal	Disp. meter 15	1.47
	2	Anchor cable support	Disp. meter 1	0.07
		String support	Disp. meter 2	0.95
		Top of pylon horizontal	Disp. meter 14	–1.53
		Bottom of pylon horizontal	Disp. meter 15	1.44

It should be noted that the horizontal displacements of the pylons affect the stress and deformation state of the entire bridge structure. The beam's support changes as the pylons move, affecting deflections and stresses.

3.3. Numerical modelling

The analysis of the bridge structure (numeric modelling) was performed using a FEM program (Dlubal RFEM). Its spatial view is presented in Figure 3.10. The cross-sections of the FE model were selected according to the geometrical and physical parameters of the experimental model (Section 3.2). Cross cables and strings are modelled as cable-type elements, subjected to pretension by initial prestress force application. Pylons (BH, CI, DJ, EK) are modelled as beam-type elements, withstanding bending moments and axial forces. Cable-stay and string supports are modelled according to experiment – hinged, allowing rotation around one support axis. Static calculations of the bridge model are nonlinear.

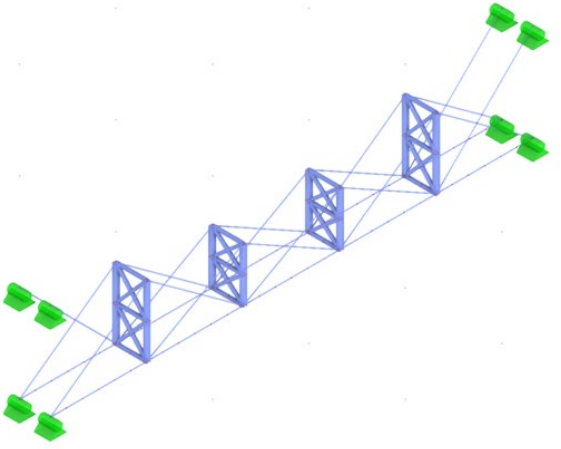

Fig. 3.10. Model of cable-stayed string bridge in a FEM program (made by the author)

The numerical analysis results are presented graphically in Figures 3.11–3.14. The displacements and axial force values under symmetrical load are shown in Figures 3.11 and 3.12. It can be seen from the presented data that both at the first stage of loading and the second stage of loading, the displacements of the string reach the highest values in its first (outer) internode (17.7 mm and 20.1 mm). It is necessary to note that the displacements of the other internodes of the string have the same values (14.4 mm and 16.0 mm) and are about 23–25% smaller than the first (outer) internode. Axial forces in the string in the first and second stages of symmetrical loading acquire maximum values in the middle internode of the string: 6.02 kN and 6.94 kN, respectively. The minimum axial force in this loading case is at the first (outer) intermediate node of the string and amounts to 4.25 kN and 4.69 kN, according to the described load steps. In the case of symmetrical loading, the anchor cable gains the most significant axial force. The most minor axial force is generated in the middle cable-stays. It is necessary to note that the axial forces of the cables coming out from the top of the intermediate pylons are mutually equal (Figs. 3.11 and 3.12).

a)

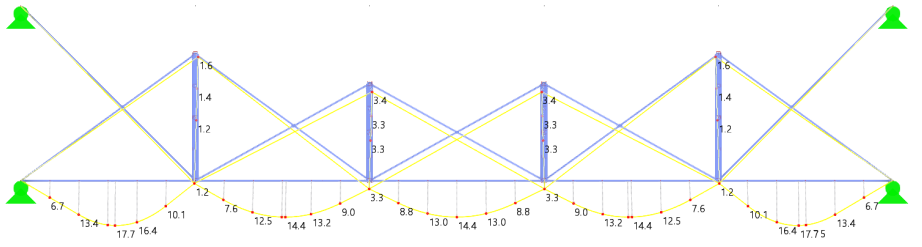

b)

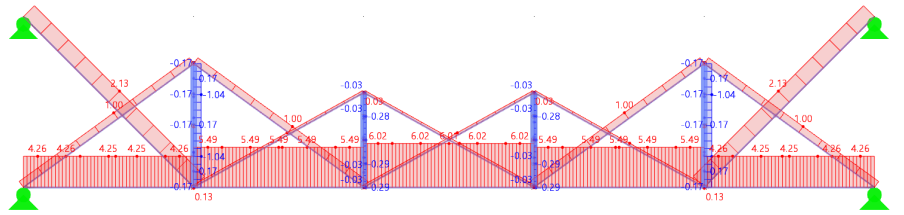

Fig. 3.11. FEM results of the first loading step of symmetrical loading: a) deflections and b) axial forces (made by the author)

a)

b)

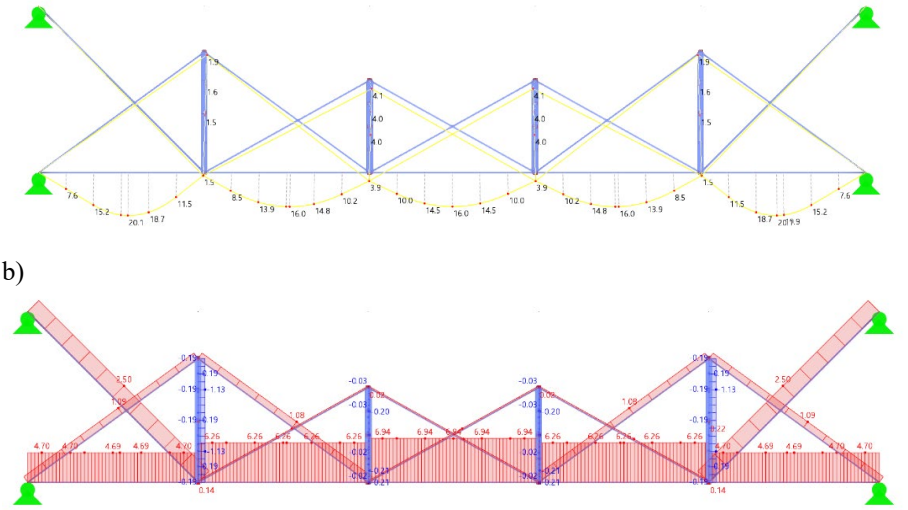

Fig. 3.12. FEM results of the second loading step of symmetrical loading: a) deflections and b) axial forces (made by the author)

The asymmetrically loaded bridge model's string displacements (their distribution) are not symmetrical about the middle of its span. They acquire the highest values of the first (outer) internode of the string loaded with asymmetric load (Figs. 3.13 b) and 3.14 b)). It should be noted that the values of the internodal displacements of this string are practically equal to the displacements caused in the case of symmetrical loading. The difference between these shifts is only about 2%. This means there is no dangerous asymmetric loading for this structural cross-cable system.

As for the forces in the string caused by asymmetric loading, it is necessary to note that the highest values occur in the second internode of the string both at the first and second loading stages. However, the difference between adjacent string internodal pitch values is not significant and is about 13% on average (Figs. 3.13 and 3.14). In the remaining two internodes of the string, not loaded with asymmetric load, the values of the axial forces are significantly lower and amount to 3.52 kN and 2.77 kN, respectively. As for the forces in the cable stays, the unloaded asymmetric load part cables are the most tensioned. The maximum tensile strength of the anchor cables is 2.15 kN, and that of the adjacent cross cables is 1.61 kN (Fig. 3.13).

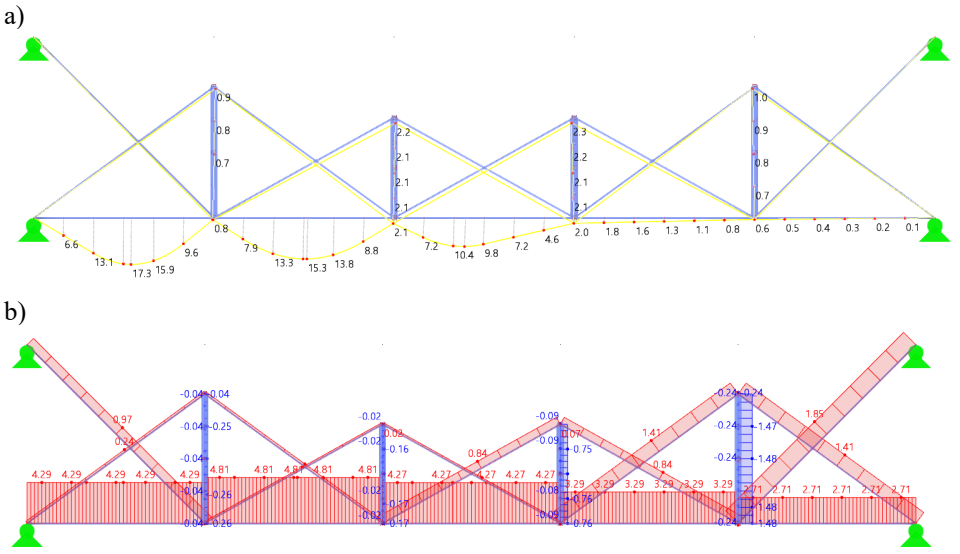

Fig. 3.13. FEM results of the first loading step of asymmetrical loading: a) deflections and b) axial forces (made by the author)

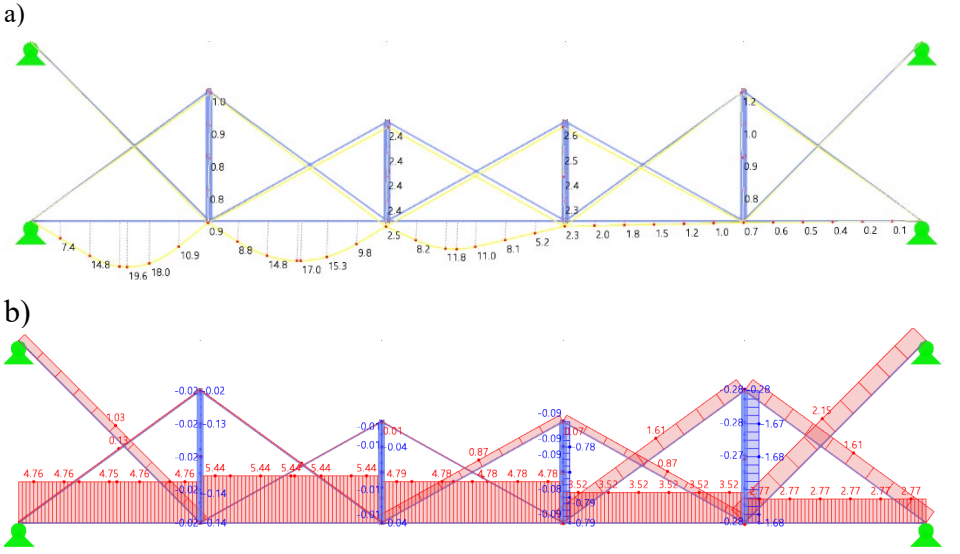

Fig. 3.14. FEM results of the second loading step of asymmetrical loading: a) deflections and b) axial forces (made by the author)

Meanwhile, the force of the anchor cable of the string part loaded with asymmetric load reaches only 0.02 kN. It is necessary to notice that the cables connecting the intermediate pylons of the adjacent part of the asymmetric load are under extremely low tension. In the first stage of loading, the tensile force of these cross-cables is only 0.01 kN, and in the second stage of loading, it is just 0.02 kN. Considering the asymmetric and symmetric load ratio, the cross-cable prestressing forces (strains) must be carefully selected. The larger the asymmetric load, the higher the tension force of this cable must be. In conclusion, it can be said that the axial forces between string nodes directly depend on the cross-cable forces, both in symmetric and asymmetric loading cases.

3.4. Result comparison

The data of the string displacement values obtained experimentally and by applying FEA are presented in Table 3.9. From it, the most significant differences between the string displacement values obtained experimentally and by applying FEA are about 9–10%, regardless of whether symmetric or asymmetric loads. The mismatch between the actual and calculated schemes of the bridge model could explain the differences. In the experimental and experimental model, the string and the cable stays have a specific bending stiffness, as they were designed from round bars with a diameter of 6 mm. In the actual model, the pylon support to the string connection was not flexible because the string was pierced through the bushings at the bottom of the pylons. These connections were not modelled in detail because this experiment's main focus was the structure's behaviour. It is necessary to notice that only the displacements obtained by the experiment of the outer internode of the string are greater than those calculated by FEA. In all other cases, FEA gave larger displacement values.

The values of string and cross-cable axial forces obtained experimentally and using FEA are presented in Table 3.10. From the data in the table, string internodal forces in both cases of load stages, calculated by FEA, have higher values than those obtained experimentally. The difference in maximum values in the outer string internode does not exceed 7%, and the difference in maximum displacements in the middle string internode reaches 19% only at the first loading stage. As the load intensity increases (Stage 2), the difference decreases to 7%. Examining the values of the cable stays, only the middle cable stays, calculated by FEA, have lower values than those obtained by the experiment. Their most significant difference occurs at the second load stage (Table 3.10).

Table 3.9. Deflection comparison between FEA and test

Loading	Load step	Deflection data	Outer span (G–H)	Inner span (H–I)	Middle span (I–J)
			Disp. meter 3	Disp. meter 5	Disp. meter 7
Symmetrical	1	Test [mm]	16.05	14.96	15.95
		FEA [mm]	17.70	14.40	14.40
		Difference [%]	9.3	3.7	9.7
	2	Test [mm]	20.97	15.30	17.50
		FEA [mm]	20.20	16.00	18.00
		Difference [%]	2.7	4.4	8.6
Asymmetrical	1	Test [mm]	16.00	16.20	10.04
		FEA [mm]	17.30	15.30	10.40
		Difference [%]	7.5	5.6	3.5
	2	Test [mm]	20.40	18.00	12.26
		FEA [mm]	19.60	17.00	11.80
		Difference [%]	3.9	5.6	3.7

Table 3.10. Axial forces comparison between FEA and test

Loading	Load step	Axial force data	Outer string internode (G–H)	Inner internode (H–I)	Middle string internode (I–J)	Anchor cable stay (A–H)	Middle cable-stays (C–J, I–D)	
			Strain gauge 1	Strain gauge 2	Strain gauge 3	Strain gauge 7	Strain gauge 11	Strain gauge 12
1	2	3	4	5	6	7	8	9
After prestress		Test [kN]	2.93	2.35	1.68	0.49	1.02	
		FEA [kN]	2.81	2.13	1.51	0.38	1.13	
Symmetrical	1	Test [kN]	4.013	4.76	5.03	2.26	0.68	
		FEA [kN]	4.26	5.49	6.02	2.13	0.03	

End of Table 3.10

1	2	3	4	5	6	7	8	
	2	Test [kN]	4.53	5.35	6.67	2.63	0.51	
		FEA [kN]	4.69	6.26	6.94	2.50	0.02	
Asym-metrical	1	Test [kN]	3.88	4.06	3.67	1.24	1.01	0.72
		FEA [kN]	4.29	4.81	4.27	1.85	0.84	0.08
	2	Test [kN]	4.32	4.61	4.53	1.66	0.93	0.52
		FEA [kN]	4.76	5.44	5.78	2.15	0.87	0.01

It should be noted here that according to FEA data, the middle cable-stay strain is practically close to zero, but according to experimental data, it is significantly higher. Such a difference in results is explained by the previously mentioned differences between the calculated and actual bridge models. It is also necessary to note that during the experiment, both in the string and in the anchor cable, the values of the prestressing forces, as obtained by FEA, were not reached, except for the middle cross-cables (Table 3.10).

3.5. Conclusions of the Third Chapter

After conducting experimental studies and numerical analysis of the new cable-stay bridge model, the following conclusions can be drawn:

1. Experimental studies of the innovative cable-stayed bridge model have shown that string displacements are unevenly distributed under symmetric loads, highlighting atypical behaviour for these cable-stayed bridges.
2. Under asymmetric loads, the distribution of the values of displacements between the string nodes is uneven. However, the values of maximum string displacements in the exterior and middle internode did not exceed the corresponding inter-nodal displacement values of a symmetrically loaded bridge, which describes the effectiveness of this structural system under asymmetric loads.
3. String forces under symmetrical loads were equally distributed, but moving towards the middle of the span, the forces in the cross-cables

decreased evenly. At a certain intensity of symmetric loading, the tension of the middle cables may decrease to an unacceptable minimum value.

4. When asymmetric loads are applied, it is determined that the axial forces of the elements of the cable-stayed bridge model do not exceed symmetrical loading values.
5. The FEA analysis of the cable-stayed bridge model showed a reasonable agreement between the values of forces and displacements and the experimentally obtained values under symmetric and asymmetric loads. The difference in the values of forces in the internodes of the string does not exceed 9%, and the difference in the values of the displacements is about 10%. These differences may occur due to differences of connections between pylons and cable-stays in the FEM model and experiment.

General conclusions

This study investigated a new cable-stayed bridge behaviour with intersecting cable stays. Here are the key findings:

1. A new cable-stayed bridge structure with intersecting cable-stays and a string was presented. A calculation method was developed to analyse this structure's behaviour. The presented calculation methodology can be used to define rational structure parameters. Using suggested expressions, rational pylon height configuration, and elements' prestress can be defined.
2. Intersecting cable-stayed bridge exhibit outstanding performance when subjected to asymmetrical loading. Experimental, numerical, and analytical analyses have shown that these bridges effectively redistribute asymmetrical pedestrian loads. This redistribution mitigates displacements and internal forces in the stiffening beam, maintaining them at or below the levels observed during symmetrical loading scenarios.
3. The uneven distribution of displacements in the cable-string bridge with intersecting cable-stays emphasises the need for accurate prestressing. Tests showed that, under both symmetrical and asymmetrical loads, displacements are most significant in the outer internodes of the string (for example, G–H and K–L) and lower in the middle internodes (such as I–J). Therefore, selecting appropriate prestressing levels in the anchor and

intersecting cable-stays is essential to prevent excessive deformation and ensure overall structural stability.

4. Experimental results and finite element analysis validate the feasibility of the new cable-stayed-string bridge system. Comparisons between experiment and FEA under symmetrical and asymmetrical loads show less than 9% discrepancy for displacements and less than 10% for force values. Furthermore, calculation methodology shows less than a 4% discrepancy compared to numerical modelling. This close agreement underlines the reliability of the proposed calculation methods and applicability for cable-stayed pedestrian bridges.

References

Abdelaziz, M. M., El-Ghazaly, H. A., & Gomaa, M. S. (2024). Numerical Modeling for Collapse Analysis of Cable-Stayed Bridges using the Improved Applied Element Method. *Iranian Journal of Science and Technology - Transactions of Civil Engineering*, 7, 2891-2904, https://doi.org/10.1007/s40996-024-01343-7

Ali, K., Katsuchi, H., & Yamada, H. (2021). Comparative Study on Structural Redundancy of Cable-Stayed and Extradosed Bridges Through Safety Assessment of Their Stay Cables. *Engineering*, *7*(1), 111–123. https://doi.org/10.1016/j.eng.2020.07.021

Arellano, H., Gomez, R., & Tolentino, D. (2019). Parametric Analysis of Multi-Span Cable-Stayed Bridges Under Alternate Loads. *The Baltic Journal of Road and Bridge Engineering*, *14*(4), 543–567. https://doi.org/10.7250/bjrbe.2019-14.457

Arellano, H., Tolentino, D., & Gómez, R. (2019). Optimum Criss Crossing Cables in Multi-span Cable-stayed Bridges using Genetic Algorithms. *KSCE Journal of Civil Engineering*, *23*(2), 719–728. https://doi.org/10.1007/s12205-018-5736-2.

Atmaca, B. (2021). Size and post-tensioning cable force optimization of cable-stayed footbridge. *Structures*, *33*, 2036–2049. https://doi.org/10.1016/j.istruc.2021.05.050

Atmaca, B., & Ates, S. (2012b). Construction stage analysis of three-dimensional cable-stayed bridges. *Steel and Composite Structures*, *12*(5), 413–426. https://doi.org/10.12989/scs.2012.12.5.413

Bas, S. (2018). Structural Identification (St-Id) Concept for Performance Prediction of Long-Span Bridges. InTech. https://doi.org/10.5772/intechopen.71558

Bassoli, E., Gambarelli, P., & Vincenzi, L. (2018). Human-induced vibrations of a curved cable-stayed footbridge. *Journal of Constructional Steel Research*, *146*, 84–96. https://doi.org/10.1016/j.jcsr.2018.02.001

Baus, U., Schlaich, M., & Boston' Berlin, B. B. (n.d.). Footbridges Construction Design History With photographs by Wilfried Dechau. Birkhauser.

Bayraktar, A., Türker, T., Tadla, J., Kurşun, A., & Erdiş, A. (2017). Static and dynamic field load testing of the long span Nissibi cable-stayed bridge. *Soil Dynamics and Earthquake Engineering*, *94*, 136–157. https://doi.org/10.1016/j.soildyn.2017.01.019

Beivydas, E. (2019). A simplified calculation method for symmetrical loading of a single-span composite string steel structure. *Engineering Structures and Technologies*, *11*(2), 70–73. https://doi.org/10.3846/est.2019.11323

Beivydas, E., Juozapaitis, A., & Paeglite, I. (2023). Experimental and analytical studies of string steel structure for bridges. *Baltic Journal of Road and Bridge Engineering*, *18*(4), 145–165. https://doi.org/10.7250/bjrbe.2023-18.622

Briseghella, B., Fa, G., Aloisio, A., Pasca, D., He, L., Fenu, L., & Gentile, C. (2021). Dynamic characteristics of a curved steel–concrete composite cable-stayed bridge and effects of different design choices. *Structures*, *34*, 4669–4681. https://doi.org/10.1016/j.istruc.2021.10.060

Brownlie, K., Curran, P., & Thompson, S. (2008). Forthside Bridge, Stirling, Scotland. Paper presented at Footbridge 2008 – Footbridges for Urban Renewal, Third International Conference on Footbridges, July 2–4, 2008, Porto, Portugal (p. 161).

Byun, N., Lee, J., Won, J. Y., & Kang, Y. J. (2022). Structural responses estimation of cable-stayed bridge from limited number of multi-response data. *Sensors*, *22*(10). https://doi.org/10.3390/s22103745

Chen, H., Zhuo, Y., Jiao, Y., & Bao, W. (2023). Fatigue Assessment of Cable-Girder Anchorage Zone in a Low Ambient Temperature Environment Based on Extended Finite Element Method. *Applied Sciences*, *13*(17), Article 9990. https://doi.org/10.3390/app13179990

Chen, Y., Wang, S., Huang, K., Zhong, J., & Cheng, H. (2023). Research on Dynamic Response of a Single-Tower Cable-Stayed Bridge with Successive Cable Breaks Based on a 3D Index. *Applied Sciences*, *13*(16), Article 9197. https://doi.org/10.3390/app13169197

Chinchane, A., & Sumant, O. (2020). Bridge Construction Market: Global Opportunity Analysis an Industry Forecst, 2020–2027. *Allied Market Research*: Portland, OR, USA, p. 295.

Cho, S., Yim, J., Shin, S. W., Jung, H.-J., Yun, C.-B., & Wang, M. L. (2013). Comparative Field Study of Cable Tension Measurement for a Cable-Stayed Bridge. *Journal of Bridge Engineering*, *18*(8), 748–757. https://doi.org/10.1061/(ASCE)BE.1943-5592.0000421

Cid, C., Baldomir, A., & Hernández, S. (2018). Optimum crossing cable system in multi-span cable-stayed bridges. *Engineering Structures*, *160*, 342–355. https://doi.org/10.1016/j.engstruct.2018.01.019

Crusells-Girona, M., & Aparicio, Á. C. (2016). Active control implementation in cable-stayed bridges for quasi-static loading patterns. *Engineering Structures*, *118*, 394–406. https://doi.org/10.1016/j.engstruct.2016.03.061

Dlubal RFEM. (2020, September 01). *FEM Structural Analysis Software*. from https://www.dlubal.com/en/products/rfem-fea-software/what-is-rfem

Emanuel Ouni, M. H., ben Kahla, N., & Preumont, A. (2012). Numerical and experimental dynamic analysis and control of a cable stayed bridge under parametric excitation. *Engineering Structures*, *45*, 244–256. https://doi.org/10.1016/j.engstruct.2012.06.018

European Committee for Standardization. (2005). EN 1993-1-1: Eurocode 3 – Design of steel structures – Part 1-1: General rules and rules for buildings. Brussels: European Committee for Standardization.

European Committee for Standardization. (2006). EN 1993-1-1: Eurocode 3 – Design of steel structures – Part 1-11: Design of structures with tension components. Brussels: European Committee for Standardization.

Eriksson, F. (1955). Stromsundsbron [Photo]. https://www.bridgemeister.com/pic.php?pid=2926

Farré-Checa, J., Komarizadehasl, S., Ma, H., Lozano-Galant, J. A., & Turmo, J. (2022). Direct simulation of the tensioning process of cable-stayed bridge cantilever construction. Automation in Construction, *137*, Article104197. https://doi.org/10.1016/j.autcon.2022.104197

Fédération internationale du béton. Task Group 1.2. (2005). Guidelines for the design of footbridges: guide to good practice. International Federation for Structural Concrete.

Ferreira, F., & Simões, L. (2019). Optimum design of a cable-stayed steel footbridge with three dimensional modelling and control devices. *Engineering Structures*, *180*, 510–523. https://doi.org/10.1016/j.engstruct.2018.11.038

Gazzola, F. (2015). *Mathematical Models for Suspension Bridges*. Springer. https://doi.org/10.1007/978-3-319-15434-3

Gimsing, N. J., & Georgakis, C. T. (2011). Cable Supported Bridges: Concept and Design. John Wiley & Sons. https://doi.org/10.1002/9781119978237

Guo, J., & Guan, Z. (2023). Optimization of the cable forces of completed cable-stayed bridges with differential evolution method. *Structures*, *47*, 1416–1427. https://doi.org/10.1016/j.istruc.2022.12.004

Guo, M., Dong, X., & Yang, Z. (2023). Settlement analysis of the giant open caisson during the construction of the Changtai Yangtze River Bridge. *Frontiers in Earth Science*, *10*. https://doi.org/10.3389/feart.2022.1056695

Ha, M. H., Vu, Q. A., & Truong, V. H. (2018). Optimum design of stay cables of steel cable-stayed bridges using nonlinear inelastic analysis and genetic algorithm. *Structures*, *16*, 288–302. https://doi.org/10.1016/j.istruc.2018.10.007

Hassan, M. M. (2013). Optimization of stay cables in cable-stayed bridges using finite element, genetic algorithm, and B-spline combined technique. *Engineering Structures*, *49*, 643–654. https://doi.org/10.1016/j.engstruct.2012.11.036

Hassan, M. M., el Damatty, A. A., & Nassef, A. O. (2015). Database for the optimum design of semi-fan composite cable-stayed bridges based on genetic algorithms. *Structure and Infrastructure Engineering*, *11*(8), 1054–1068. https://doi.org/10.1080/15732479.2014.931976

Hassan, M. M., Nassef, A. O., & el Damatty, A. A. (2012). Determination of optimum post-tensioning cable forces of cable-stayed bridges. *Engineering Structures*, *44*, 248–259. https://doi.org/10.1016/j.engstruct.2012.06.009

Innocenzi, R. D., Nicoletti, V., Arezzo, D., Carbonari, S., Gara, F., & Dezi, L. (2022). A good practice for the proof testing of cable-stayed bridges. *Applied Sciences*, *12*(7), Article 3547. https://doi.org/10.3390/app12073547

Ito, M. (2005). Handbook Of Structural Engineering. CRC Press.

Jana, D., & Nagarajaiah, S. (2021). Computer vision-based real-time cable tension estimation in Dubrovnik cable-stayed bridge using moving handheld video camera. *Structural Control and Health Monitoring*, *28*(5). https://doi.org/10.1002/stc.2713

Janjic, D., Pircher, M., & Pircher, H. (2003). Optimization of Cable Tensioning in Cable-Stayed Bridges. *Journal of Bridge Engineering*, *8*(3), 131–137. https://doi.org/10.1061/(ASCE)1084-0702(2003)8:3(131)

Jutila, A., Järvenpää, E., & Quach, T. T. (2021). Balance and costs of cable-stayed bridges with inclined and curved tower shapes. *Structural Engineering International*, *31*(4), 498–503. https://doi.org/10.1080/10168664.2021.1929666

Kanok-Nukulchai, W., Yiu, P. K. A., & Brotton, D. M. (1992). Mathematical modelling of cable-stayed bridges. structural engineering international, *2*(2), 108–113. https://doi.org/10.2749/101686692780616030

Kaufmann, W., Karagiannis, D., & Widmer, K. (2021). Load factors for permanent actions and cable preload in cable-stayed bridges. *Structural Engineering International*, *31*(1), 10–17. https://doi.org/10.1080/10168664.2019.1667738

Idelberger, K. (2011). The World of Footbridges: From the Utilitarian to the Spectacular. Ernst and Sohn. https://doi.org/10.1002/9783433600849

Kulbach, V., & Idnurm, J. (2006). Discrete and continuous analysis of different cable structures. In III European Conference on Computational Mechanics: Solids, Structures and Coupled Problems in Engineering: Book of Abstracts. Springer Netherlands.

Triplett, R. K, & Schwarzman. A. S. (2012, May 18). *Rare Books: Machinae Novae of 1595.* https://www.nypl.org/blog/2012/05/18/rare-books-machinae-novae

Laumann, J., Feldmann, M., Frickel, J., Krahwinkel, M., Kraus, M., Stranghöner, N., Thomas, & Ummenhofer, T. (2022). Petersen Stahlbau – Grundlagen der Berechnung und baulichen Ausbildung von Stahlbauten (5th ed.). Springer Vieweg. https://doi.org/10.1007/978-3-658-20510-2

Lakshmi Poornima, G., & Bharath, R. (2017). Optimization and analysis of cable stayed bridges. *International Research Journal of Engineering and Technology*, *04* (08), 2307–2312.

Le, L. X., Siringoringo, D. M., Katsuchi, H., & Fujino, Y. (2022). Stay cable tension estimation of cable-stayed bridge under limited information on cable properties using artificial neural networks. *Structural Control and Health Monitoring*. https://doi.org/10.1002/stc.3015

Ma, Y., Song, C., Wang, Z., Jiang, Z., Sun, B., & Xiao, R. (2024). Efficient design optimization of cable-stayed bridges: A two-layer framework with surrogate-model-assisted prediction of optimum cable forces. *Applied Sciences*, *14*(5). https://doi.org/10.3390/app14052007

Machelski, C., & Hildebrand, M. (2021). Cable-stayed bridge loads caused by traffic congestion on the deck measured with bridge monitoring system. *Baltic Journal of Road and Bridge Engineering*, *16*(2), 66–89. https://doi.org/10.7250/bjrbe.2021-16.524

Malinowski, M., Banas, A., Jeszka, M., & Sitarski, A. (2018). Einzigartige Fußgängerbrücke in Mikołajki, Polen. *Stahlbau*, *87*(3), 248–255. https://doi.org/10.1002/stab.201810582

Malwiya, P., & Vahora, F. (2017). Effect of cable arrangment on nonlinear static analysis of cable-stayed bridge. *International Research Journal of Engineering and Technology*. www.irjet.net

Martínez-Rodrigo, M. D., & Filiatrault, A. (2015). A case study on the application of passive control and seismic isolation techniques to cable-stayed bridges: A comparative investigation through non-linear dynamic analyses. *Engineering Structures*, *99*, 232–252. https://doi.org/10.1016/j.engstruct.2015.04.048

Martins, A. M. B., Simões, L. M. C., & Negrão, J. H. J. O. (2020). Optimization of cable-stayed bridges: A literature survey. *Advances in Engineering Software*, *149*, Article 102829. https://doi.org/10.1016/j.advengsoft.2020.102829

McCullough, D. (2012). *The great bridge: the epic story of the building of the Brooklyn Bridge*. Simon and Schuster.

Mozos, C. M., & Aparicio, A. C. (2011). Numerical and experimental study on the interaction cable structure during the failure of a stay in a cable stayed bridge. *Engineering Structures*, *33*(8), 2330–2341. https://doi.org/10.1016/j.engstruct.2011.04.006

Ni, Y. C., Alamdari, M. M., Ye, X. W., & Zhang, F. L. (2021). Fast operational modal analysis of a single-tower cable-stayed bridge by a Bayesian method. *Measurement*, *174*, Article 109048. https://doi.org/10.1016/j.measurement.2021.109048

Nicoletti, V., et al. (2023). The monitoring system of the new Filomena Delli Castelli cable-stayed bridge. In International Conference on Experimental Vibration Analysis for Civil Engineering Structures. Springer Nature Switzerland.

Notkus, A. J. (2010). Tiltų projektavimo pagrindai. Technika. https://doi.org/10.3846/1140-S

Juozapaitis, A., Kutas, R., & Jatulis, D. (2008). Mast behaviour analysis and peculiarities of numerical modelling. *Journal of Civil Engineering and Management*, *14*(1), 61–66. https://doi.org/10.3846/1392-3730.2008.14.61-66

Oliveira Pedro, J. J., & Reis, A. J. (2016). Simplified assessment of cable-stayed bridges buckling stability. *Engineering Structures*, *114*, 93–103. https://doi.org/10.1016/j.engstruct.2016.02.001

Palheriya, M. A., & Kuldeep Dabhekar, M. (2018). Analysis of Hybrid Form of Cable Stayed and Suspension Bridge-A Review. *International Journal of Innovations in Engineering and Science 3* (3), 16–19.

Park, J., Yoon, J., Park, C., & Lee, J. (2023). Studying the Cable Loss Effect on the Seismic Behavior of Cable-Stayed Bridge. *Applied Sciences*, *13*(9), Article 5636. https://doi.org/10.3390/app13095636

Virtanen, P., Gommers, R., Oliphant, E. T., Haberland, M., Reddy, T., Cournapeau, D., Burovski, E., Peterson, P., Weckesser, W., Bright, J.,. van der Walt, J. S., Brett, M., Wilson, J., Millman, K. J., Mayorov, N., Nelson, R. J. A., Jones, E., Kern, R., Larson, E., Carey, CJ., Polat, İ., Feng, Y., Moore, W. E., VanderPlas, J., Laxalde, D., Perktold, J., Cimrman, R., Henriksen, I., Quintero, E. A., Harris, R. Ch., Archibald, M. A., Ribeiro, H. A., Pedregosa, F., van Mulbregt, P., & SciPy 1.0 Contributors. (2020) SciPy 1.0: Fundamental Algorithms for Scientific Computing in Python. Nature Methods, *17*(3), 261–272. https://doi.org/10.1038/s41592-019-0686-2

Pearce, Martin, and Richard Jobson. *Bridge builders*. Wiley-Academy, 2002.

Pipinato, A. Innovative Bridge Design Handbook: Construction, Rehabilitation, and Maintenance; Butterworth-Heinemann: Oxford, UK, 2015.

Pipinato, A., Pellegrino, C., & Modena, C. (2012). Structural analysis of the cantilever construction process in cable-stayed bridges. Periodica Polytechnica Civil Engineering, 56(2), 141–166. https://doi.org/10.3311/pp.ci.2012-2.02

Podolny, W., & Goodyear, D. (2006). Cable suspended bridges. In Structural steel designer's handbook (pp. 15.1–16.91). McGraw-Hill.Pytel,

A., Kiusalaas, J. Mechanics of Materials, Second Edition. Global Engineering, USA, 2012.

Racić, V., Živanović, S., Pavic, A. (2006). FE Modelling and Updating of Unique Fink Truss Footbridge. Proceedings of ISMA 2006. Dynamic Behavior of Civil Structures. p. 1221 – 1232

Robin, C., Datry, J.-B., & de Kosmi, B. (2013). La passerelle du Grand Large à Dunkerque. Travaux, (896), 82–91.

Robin, C., Datry, J.-B., De Cosmi, B. (2014): La Passerelle du Grand Large

Sandovič, G., Juozapaitis, A., & Kliukas, R. (2011). Simplified Engineering Method of Suspension Two-Span Pedestrian Steel Bridges With Flexible and Rigid Cables Under Action of Asymmetrical Loads. The Baltic Journal of Road and Bridge Engineering, 6(4), 267-273. https://doi.org/10.3846/bjrbe.2011.34

Sernizon Costa, R., Cesar Campos Lavall, A., Gomes Lanna da Silva, R., Porcino dos Santos, A., & Francisco Viana, H. (2022). Cable structures: An exact geometric analysis using catenary curve and considering the material nonlinearity and temperature effect. Engineering Structures, 253. https://doi.org/10.1016/j.engstruct.2021.113738

Sharry, T., Guan, H., Nguyen, A., Oh, E., & Hoang, N. (2022). Latest Advances in Finite Element Modelling and Model Updating of Cable-Stayed Bridges. Infrastructures, 7(1). https://doi.org/10.3390/infrastructures7010008

Song, C., Xiao, R., & Sun, B. (2018). Optimization of cable pre-tension forces in long-span cable-stayed bridges considering the counterweight. Engineering Structures, 172, 919–928. https://doi.org/10.1016/j.engstruct.2018.06.061

Song, C., Xiao, R., Sun, B., Wang, Z., & Zhang, C. (2023). Cable force optimization of cable-stayed bridges: A surrogate model-assisted differential evolution method combined with B-Spline interpolation curves. Engineering Structures, 283. https://doi.org/10.1016/j.engstruct.2023.115856

Souza Hoffman, I., Manica Lazzari, B., Campos, A., Manica Lazzari, P., & Rodrigues Pacheco, A. (2022). Finite element numerical simulation of a <scp>cable-stayed</scp> bridge construction through the progressive cantilever method. Structural Concrete, 23(2), 632–651. https://doi.org/10.1002/suco.202100662

Spasojević-Šurdilović, M., Spasojević, A., & Stojić, D. (2014). Modelling of a bridge stay cable for individual strand tensioning. Gradjevinar, 66(6), 549–554. https://doi.org/10.14256/JCE.1019.2014

Stevenson R (1821) Description of bridges of suspension. The Edinburgh Philosophical Journal5(10): 237–256.

Stragys, M. (2019). The preliminary design and technical-economic efficiency of the two-level branched cable-stayed bridge. Engineering Structures and Technologies, 11(1), 17–24. https://doi.org/10.3846/est.2019.8858

Strasky, J. (2007). Stress-ribbon pedestrian bridges supported or suspended on arches. https://www.researchgate.net/publication/242262153

Straupe, V., & Paeglitis, A. (2012). Analysis of interaction between the elements in cable-stayed bridge. Baltic Journal of Road and Bridge Engineering, 7(2), 84–91. https://doi.org/10.3846/bjrbe.2012.12

Svensson, H. (2012). Cable-stayed bridges: 40 years of experience worldwide (454 p.). Ernst & Sohn. https://doi.org/10.1002/9783433601044

Thai, H. T., & Kim, S. E. (2011). Nonlinear static and dynamic analysis of cable structures. Finite Elements in Analysis and Design, 47(3), 237–246. https://doi.org/10.1016/j.finel.2010.10.005

Thai, H. T., & Kim, S. E. (2012). Second-order inelastic analysis of cable-stayed bridges. Finite Elements in Analysis and Design, 53, 48–55. https://doi.org/10.1016/j.finel.2011.07.002

Truong, V. H., & Kim, S. E. (2017). An efficient method of system reliability analysis of steel cable-stayed bridges. Advances in Engineering Software, 114, 295–311. https://doi.org/10.1016/j.advengsoft.2017.07.011

Unitsky, A., 2019: String transport systems: on earth and in space. Minsk, 25 p.

Valdebenito, G., Aparicio, A. (2006). Seismic Behaviour of Cable-Stayed Bridges: Astate-Of-The-Art Review. 4th International Conference on ….

Wai-Fah Chen, E., & Duan, L. (2000). Bridge Engineering Handbook. CRC Press.

Walther, R., Houriet, B., & Izler, W. (1999). Cable stayed bridges (227 p.). Thomas Telford Ltd.

Wang, F., Lv, Z., Gu, M., Chen, Q., Zhao, Z., & Luo, J. (2021). Experimental study on stability of orthotropic steel box girder of self-anchored suspension cable-stayed bridge. Thin-Walled Structures, 163, 107727. https://doi.org/10.1016/j.tws.2021.107727

Wang, F.-Y., Xu, Y.-L., Sun, B., & Zhu, Q. (2018). Updating Multiscale Model of a Long-Span Cable-Stayed Bridge. Journal of Bridge Engineering, 23(3). https://doi.org/10.1061/(ASCE)BE.1943-5592.0001195

Wang, X., Wang, H., Zhang, J., Sun, Y., Bai, Y., Zhang, Y., & Wang, H. (2021). Form-finding method for the target configuration under dead load of a new type of spatial self-anchored hybrid cable-stayed suspension bridges. Engineering Structures, 227, 111407. https://doi.org/10.1016/j.engstruct.2020.111407

Wang, Z., Zhang, W., Fang, R., & Zhao, H. (2021). Dynamic Model Testing of Low-Gravity-Center Cable-Stayed Bridges with Different Girder-to-Tower Connections. Journal of Bridge Engineering, 26(1). https://doi.org/10.1061/(ASCE)BE.1943-5592.0001649

Wei, S., Gong, W., Wu, X., & Zhang, Z. (2023). Nonlinear Stress-Free-State Forward Analysis Method of Long-Span Cable-Stayed Bridges Constructed in Stages. Buildings, 13(7). https://doi.org/10.3390/buildings13071735

Wen, Y., & Zhou, Z. (2022). Qualification of the Ernst formula for modeling the sag effect of super-long stay cables in the long-span railway cable-stayed bridges. Structures, 45, 99–109. https://doi.org/10.1016/j.istruc.2022.09.002

Wu, J., Frangopol, D. M., & Soliman, M. (2015). Geometry control simulation for long-span steel cable-stayed bridges based on geometrically nonlinear analysis. Engineering Structures, 90, 71–82. https://doi.org/10.1016/j.engstruct.2015.02.007

Wu, Z., & Wei, J. (2019). Nonlinear Analysis of Spatial Cable of Long-Span Cable-Stayed Bridge considering Rigid Connection. KSCE Journal of Civil Engineering, 23(5), 2148–2157. https://doi.org/10.1007/s12205-019-0071-9

Xiaoyu, L., Yue, W., Airong, C., Bo, L., & Haibo, L. (2021). Form Finding and Aesthetic Design for Pylons of Cable-supported Bridges. Structural Engineering International, 31(4), 468–476. https://doi.org/10.1080/10168664.2020.1870056

Xie, G. hua, Yin, J., Liu, R. gui, Chen, B., & Cai, D. sheng. (2017). Experimental and numerical investigation on the static and dynamic behaviors of cable-stayed bridges with CFRP cables. Composites Part B: Engineering, 111, 235–242. https://doi.org/10.1016/j.compositesb.2016.11.048

Xu, X., Xu, Y.-L., Ren, Y., & Huang, Q. (2021). Site-Specific Extreme Load Estimation of a Long-Span Cable-Stayed Bridge. Journal of Bridge Engineering, 26(4). https://doi.org/10.1061/(ASCE)BE.1943-5592.0001700

Yang, B. (2025). Changtai Yangtze River Bridge in Changzhou [Photo]. https://news.global-ce.com/n/202408/26/135722.html

Zhang, Y., Zhao, Y., Zhou, Y., & Yang, X. (2022). Calculation Method of Rotational Constraint Stiffness for a New Tower-Pier Connected System. Applied Sciences (Switzerland), 12(21). https://doi.org/10.3390/app122111221

Zheng, J., Fang, G., Wang, Z., Zhao, L., & Ge, Y. (2023). Shape optimization of closed-box girder considering dynamic and aerodynamic effects on flutter: a CFD-enabled and Kriging surrogate-based strategy. Engineering Applications of Computational Fluid Mechanics, 17(1). https://doi.org/10.1080/19942060.2023.2191693

Zhou, J., Ruan, X., Shi, X., & Caprani, C. C. (2019). An efficient approach for traffic load modelling of long span bridges. Structure and Infrastructure Engineering, 15(5), 569–581. https://doi.org/10.1080/15732479.2018.1555264

List of scientific publications by the author on the topic of the dissertation

Papers in reviewed scientific journals

Dabrila, P., & Juozapaitis, A. (2024). Calculation of prestressed cable-stayed steel bridge with intersecting cable stays = Berechnung einer vorgespannten Schrägseilbrücke aus Stahl mit sich kreuzenden Schrägseilen. *Bauingenieur*, 99(3), 78–89. https://doi.org/10.37544/0005-6650-2024-03-38

Dabrila, P., & Juozapaitis, A. (2024b). Numerical and experimental investigation of a new cable-stayed string steel bridge = Numerische und experimentelle Untersuchung einer neuen Schrägseilen-Saiten Stahlbrücke. *Bauingenieur*, 99(12), 396–405. https://doi.org/10.37544/0005-6650-2024-12-46

Dabrila, P. (2021). Behavior of pre-stressed intersecting cable steel bridge. *Engineering Structures and Technologies*, 13(1), 19–25. https://doi.org/10.3846/est.2021.18402

Papers in other editions

Dabrila, P., & Juozapaitis, A. (2022). Design of pre-stressed intersecting cable string steel bridge. *In IABSE Congress Nanjing 2022 – Bridges and Structures: Connection, Integration and Harmonisation* (pp. 872–879). International Association for Bridge and Structural Engineering (IABSE). https://doi.org/10.2749/nanjing.2022.0872

Dabrila, P., & Juozapaitis, A. (2021). Shape-finding and behavior of the pre-stressed hybrid cable-stayed string steel bridge. In M. A. Giżejowski, A. Kozłowski, M. Chybiński, K. Rzeszut, R. Studziński, & M. Szumigała (Eds.), *Modern trends in research on steel, aluminium and composite structures: Proceedings of the XIV International Conference on Metal Structures (ICMS 2021)*, Poznań, Poland, 16–18 June 2021 (pp. 278–283). Taylor & Francis. https://doi.org/10.1201/9781003132134-34

Summary in Lithuanian

Įvadas

Problemos formulavimas

Vantiniai tiltai su kryžminais vantais yra santykinai nauji ir pasižymi geometriškai netiesine elgsena. Anksčiau publikuotų darbų literatūrinė apžvalga atskleidė skaičiavimo metodikos ir detalių projektavimo gairių šiai konstrukcijai trūkumą. Be to, panaudojus įtemptą stygą vietoj sijos, konstrukcijos elgsena tampa dar sudėtingesnė. Šiuo metu išlieka šie klausimai, susiję su kryžminių vantų tilto sistema:

- nėra žinomi racionalūs sistemos formos parametrai: tarpmazgių (pilonų) kiekis, pilonų kontūro forma ir kt.;
- nėra parengtos skaičiavimo metodikos, leidžiančios apskaičiuoti poslinkius bei įtempius šiems tiltams;
- nėra išsamiai ištirta, kaip ši tilto konstrukcija elgiasi veikiant asimetrinėms pėsčiųjų apkrovoms;
- nėra apibrėžta netiesinė tilto elgsena veikianr simetrinėms ir asimetrinėms apkrovoms.

Darbo aktualumas

Augant gyventojų skaičiui pasaulyje, didėja poreikis tvariai plėtoti infrastruktūrą: mažinti gamtinių išteklių naudojimą, anglies dioksido pėdsaką ir užtikrinti visuomenės, besinaudojančios šia infrastruktūra poreikius. Šiems tikslams įgyvendinti būtina užtikrinti efektyvius sprendimus visuose proceso etapuose.

Vantiniai tiltai yra išskirtiniai dėl efektyvių konstrukcinių sprendinių ir išraiškingos architektūros, jie tinka ne tik transportui bet ir pėstiesiems. Visgi šie tiltai turi keletą trūkumų. Pirma, jie yra jautrūs veikiant netolygiai apkrovai, todėl reikalingos santykinai masyvios standumo sijos. Antra, vantinių tiltų efektyvumą riboja mažiausias galimas vantų įrengimo kampas. Be to, dėl urbanistinių ar ekonominių veiksnių gali būti ribojamas pilonų aukštis, taip mažinant visos sistemos pritaikomumą.

Ieškant racionalių parametrų, siūlomi nauji sprendiniai, tokie kaip standumo siją pakeisti styga arba taikyti kryžminių vantų išdėstymą (kartais vadinamą apverstąja Finko santvara). Toks susikertančių vantų sprendinys leidžia geriau išlaikyti pradinę tilto formą esant asimetrinėms apkrovoms, efektyviai perskirstant jas ir taip mažinant medžiagų sąnaudas. Tačiau tokia konstrukcija dar mažai tyrinėta – pasaulyje pastatyta vos keletas tokių tiltų. Nepaisant galimo sistemos taikymo, vis dar nėra išplėtotos skaičiavimo metodikos šio tipo konstrukcijoms. Be atitinkamų skaičiavimo metodų ar eksperimentinių duomenų, sunku racionaliai projektuoti tokius tiltus, parinkti jų parametrus.

Tyrimo objektas

Disertacijos tyrimo objektas - vantinio su kryžminiais vantais ir iš anksto įtempta styga pėsčiųjų tilto įtempių ir deformacijų būvis.

Darbo tikslas

Sukurti naujos formos plieninio vantinio-styginio pėsčiųjų tilto su kryžminiais vantais konstrukciją ir ištirti jos įtempių ir deformacijų būklę.

Darbo uždaviniai

Siekiant įgyvenfinti darbo tikslą, turi būti sprendžami šie uždaviniai:

1. Suformuoti naujos formos vantinio-styginio tilto konstrukcinę schemą ir ištirti jos elgseną.
2. Parengti laikančiųjų elementų poslinkių ir įrąžų inžinerines skaičiavimo metodikas vantiniam tiltui su (1) standumo sija ir su (2) styga.
3. Atlikti naujos vantinio tilto konstrukcijos elgsenos skaitinę analizę, veikiant statinėms simetrinėms ir asimetrinėms pėsčiųjų apkrovoms.
4. Atlikti eksperimentinį tiriamos plieninio vantinio-styginio tilto konstrukcijos modelio tyrimą.
5. Atlikti gautų duomenų palyginimą su BEM rezultatis.

Tyrimų metodika

Tyrime taikyti šie metodai: statinė sistemos analizė, įtraukiant geometrinį netiesiškumą; skaitinis modeliavimas, taikant baigtinių elementų metodą, bei fiziniai eksperimentiniai bandymai.

Darbo mokslinis naujumas

Rengiant disertaciją, statybos inžinerijos mokslų srityje gauti šie nauji rezultatai:

1. Pasiūlytas naujos formos vantinė-styginė tilto konstrukcija.
2. Parengta kryžminių vantų pėsčiųjų tilto su standumo sija ir su styga laikančiųjų elementų inžinerinė skaičiavimo metodika įrąžoms ir poslinkiams apskaičiuoti.
3. Atliktas eksperimentinis naujos formos vantinis-styginio plieninio tilto modelio tyrimas.

Darbo rezultatų praktinė reikšmė

Sukurtas naujas kryžminių vantų su iš anksto įtempta styga tiltas. Parengta kryžminių vantų tilto inžinerinė metodika leidžia parinkti racionalią geometrinę formą bei tinkamus laikančiųjų elementų skerspjūvius. Ji supaprastina racionalios konstrukcinės schemos komponavimą, padeda parengti skaitmeninį modelį ir sutrumpina pirminį projektavimo etapą.

Ginamieji teiginiai

Remiantis tyrimo rezultatais, formuluojami šie ginamieji teiginiai:

1. Kryžminių vantų pėsčiųjų tiltai efektyviai perskirsto netolygią pėsčiųjų apkrovą, sumažindami poslinkius ir lenkimo momentus standumo sijoje, lyganant su įprastiniais vantiniais tiltais.
2. Tinkamas susikertančių vantų ir stygos išankstinis įtempimas yra būtinas tilto pradinei formai užtikrinti.
3. Vantinių su sija bei vantinių ir styginių tiltų skaičiavimo metodikų rezultatai nuo skaitinės analizės skiriasi mažiau nei 4 %, todėl galima pakankamai tiksliai įvertinti tilto įtempius ir poslinkius veikiant simetrinėms ir asimetrinėms apkrovoms.
4. Vantinių tiltų prototipo baigtinių elementų analizė patvirtina eksperimento rezultatus. Įtempių ir poslinkių vertės skiriasi ne daugiau kaip 9–10 %, taip pagrindžiant modeliavimo metodo patikimumą.

Darbo rezultatų aprobavimas

Disertacijos tema yra paskelbti 5 moksliniai straipsniai recenzuojamuose mokslo žurnaluose, iš kurių du *Web of Science* duomenų bazės leidiniuose, turinčiuose citavimo indeksą; vienas straipsnis kitų tarptautinių duomenų bazių leidiniuose; du straipnisi mokslinių konferencijų rinkiniuose. Autoriaus publikacijų sąrašas pateiktas 97 puslapyje. Disertacijoje atliktų tyrimų rezultatai buvo pristatyti dviejose mokslinėse konferencijose:

- 14-oje tarptautinėje konferencijoje „XIV International Conference on Metal Structures (ICMS, 2021) “, Poznanėje, Lenkijoje.
- IABSE 2022-ųjų metų kongrese „Bridges and Structures: Connection, Integration and Harmonisation“, Nankine, Kinijoje.

Disertacijos struktūra

Disertaciją sudaro įvadas, trys pagrindiniai skyriai, išvados, literatūros sąrašas, autoriaus publikacijų disertacijos tema sąrašas. Disertacijos apimtis (be priedų) – 121 puslapis, 102 formulės, 64 iliustracijos ir 16 lentelių.108 literatūros šaltiniai buvo naudojami rašant disertaciją.

Padėka

Autorius nuoširdžiai dėkoja savo moksliniam vadovui prof. Algirdui Juozapaičiui už suteiktą pagalbą ir mentorystę.

Ypatinga padėka skiriama „Peikko Lietuva“ ir IDDO už medžiagas, būtinas tilto modelio eksperimentui.

Galiausiai autorius dėkoja šeimai ir draugams už nuolatinį palaikymą ir padrąsinimą.

1. Vantinių ir styginių tiltų konstrukcijų apžvalga

Pirmajame disertacijos skyriuje atlikta literatūros šaltinių disertacijos tematika apžvalga. Didelę šio skyriaus dalį sudaro vantinių tiltų istorijos ir dabartinių jų tyrimų aptarimas. Apžvelgiama vantinių tiltų netiesinė elgsena, analizės metodai. Aptarta vantų elgsena, jų įtempimas, išdėstymas. Apibrėžta dabartinių tyrimų kryptis patikimumo, būklės stebėjimo, optimizacijos srityse. Apžvelgiami ir pėsčiųjų vantiniai tiltai, jų specifika. Skyriuje aptariamos pagrindinės skaičiavimo metodikos ir jų taikymas tokio tipo konstrukcijoms.

Pirmieji vantinių tiltų variantai buvo pasiūlyti ganėtinai anksti. Idėja naudoti vantais palaikomas standumo sijas buvo minima jau XVI a. literatūroje. Venecijos išradėjo Fausto Verenzio veikale „Machine Novae“ pavaizduotas dviejų pilonų tiltas su grandinėmis palaikomomis sijomis (Triplett, 2012). Nors šis tiltas niekada nebuvo pastatytas, pateikta koncepcija atskleidžia pažangią tiltų statybos sampratą, net prieš kelis šimtus metų (1.3 pav.).

XIX amžiuje tiltų statyba tapo sudėtingesnė, o projektuose dažnai buvo derinamos kabamųjų ir vantinių tiltų formos. Ankstyvieji kabamieji tiltai, tokie kaip Dryburgh Abbey tiltas (Stevenson, 1821) ir Bruklino tiltas (McCullough, 1972), turėjo papildomų vantų, siekiant stabilizuoti formą.

Šiuolaikiniai vantiniai tiltai pradėti statyti apie 1950 metus. Jie pasirodė ypač tinkami dideliems tarpatramiams dengti dėl ekonomiškos statybos, ypač aktualios pokario laikotarpiu, kai išaugo tiltų paklausa, o statybinės medžiagos buvo ribotos. Pirmasis toks tiltas – Stromsundo tiltas Švedijoje – buvo pastatytas 1955 m., suprojektuotas Franz Dischinger ir pastatytas bendrovės AB Skånska Cementgjuteriet (Wai-Fah, 2000). Tiltą sudaro trys tarpatramiai: pagrindinis – 182,6 m, ir du šoniniai – po 74,7 m.

Priklausomai nuo konstrukcinio tipo, visame pasaulyje statomi įvairūs pėsčiųjų tiltai (Strasky, 2005). Tarp jų ypač išsiskiria vantiniai tiltai – dėl savo estetinio patrauklumo, vizualinio lengvumo, ekonomiškumo ir statybos proceso paprastumo (Atmaca, 2021).

Pėsčiųjų tiltai suteikia glaudesnę sąveiką su juos naudojančiais žmonėmis, kadangi pėstieji tiesiogiai eina, liečia ir atidžiai juos apžiūri, skirtingai nei kelių ar geležinkelių tiltus (Svenson, 2012). Šis tiesioginis ryšys turi didelės reikšmės jų projektavimui, ypač atsižvelgiant į žmogaus mastelį. Skirtingai nei kelių ir geležinkelių tiltai, kurių tikslas

dažniausiai yra kuo tiesiau sujungti du taškus, pėsčiųjų tiltai leidžia nukrypti nuo šio tiesmuko požiūrio. Tokie sprendimai kaip pakeliami tiltai, išlenkti ir lynais palaikomi, ar tarpusavyje susikertantys keli paklotai, gali sukurti unikalią erdvinę patirtį (Idelberger, 2011).

Atsiradus pažangiems projektavimo metodams ir didelio stiprumo medžiagoms, pėsčiųjų tiltai tapo vis grakštesni. Dėl šios priežasties jie tapo jautresni dinaminėms vibracijoms, kurias sukelia pėsčiųjų eismas, kas gali paveikti jų patogumą ir tinkamumą naudoti (Bassoli, 2017).

Nepaisant apžvalgoje minėtų klausimų, novatoriški metodai, tokie kaip standumo sijų pakeitimas stygomis (Unitsky, 2019; Pipinato, 2015) ir kryžminių vantų panaudojimas, suteikia reikšmingų pranašumų prieš tradicinius sprendinius (1.1S pav.). Kryžminiai vantai padidina konstrukcijos pradinės formos stabilumą esant asimetrinėms apkrovoms (Pearce & Jobson, 2002). Nepaisant perspektyvių rezultatų, ši konstrukcija tebėra gana menkai ištirta, o įgyvendintų pavyzdžių yra nedaug (1.1S lentelė).

1.1S lentelė. Susikertančių vantų tiltai

Tiltas	Šalis	Pagrindinio tarpatramio ilgis [m]	Statybos metai
Royal Victoria Dock Pedestrian	JK	127,5	1998
Forthside	JK	88,2	2009
Passerelle du Grand Large	Prancūzija	112,425	2014
Frank Gehry	Ispanija	76,9	2014
Moody Pedestrian Bridge	JAV	42,4	2015
Zhangjiatang	Kinija	55,0	2018
Grand Canal	Kinija	150,0	2024
Hickory Riverwalk	JAV	105,0	2024

1.1S pav. Passerelle du Grand Large (Janberg, 2022)

Yra keletas kryžminių vantų tiltų, detaliau apžvelgtų literatūroje, pavyzdžiui, *Royal Victoria Dock* tiltas Jungtinėje Karalystėje (Pearce & Jobson, 2002), *Passerelle du Grand Large* tiltas Diunkerke (Robin et al., 2014) ir *Taiping North Road* pėsčiųjų tiltas Kinijoje (Brownie et al., 2008).

Vis dėlto, pastebima šių konstrukcijų skaičiavimo metodikų stoka (Racić, 2006). Projektuojant šio tipo racionalių parametrų tiltus, susiduriama su iššūkiais dėl analitinių, skaičiavimo metodų ir eksperimentinių tyrimų duomenų trūkumo. Inžinieriai apskaičiuoja reikalingus elementų skerspjūvius ir vantų įtempimą remdamiesi priartėjimu. Siekdami išvengti vantų atsipalaidavimo, vertinanamas tinkamumo ribinis būvis, leidžiant centrinių vantų atsipalaidavimą nagrinėjant saugumo ribinį būvį. Toks supaprastintas modeliavimas, vertinant tiltą kaip dvi atskiras sistemas, lemia netikslų poslinkių ir įtempių vertinimą, todėl būtini išsamesni tyrimai (Robin et al., 2014).

2. Inovatyvus vantinis plieno tiltas

Antrajame darbo skyriuje pateikta autoriaus sukurta metodika, leidžianti apskaičiuoti vantinės ir sijinės sistemos įlinkius ir įrąžas. Pirmojoje skyriaus dalyje buvo atlikta skaitinė analizė, lyginant skirtingų pilonų aukščių kryžminių vantų tiltus ir klasikinį vantinį tiltą.

Analitiškai nagrinėjama tilto sistema, susidedanti iš standumo sijos, susikertančių vantų ir keturių tarpinių pilonų, kaip pavaizduota 2.1S pav. Laikoma, kad tilto inkariniai vantai yra fiksuojami į guolius, įvertinant jų horizontalų poslinkį. Analizuojamas tiltas, siekiant nustatyti kintamuosius, priklausomus nuo vantų ir sijos sąveikos.

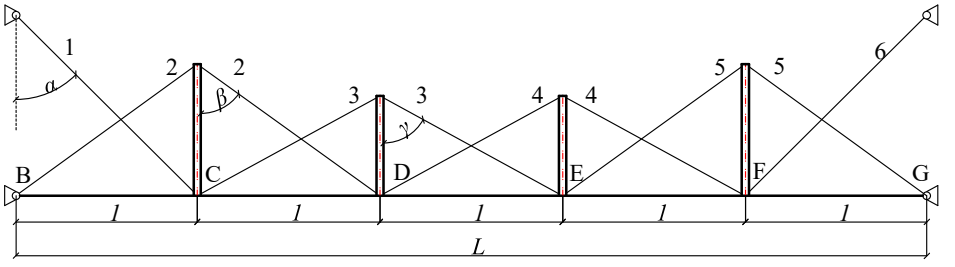

2.1S pav. Kryžminių vantų su tarpiniais pilonais tilto schema

2.2S pav**.** Vantinio tilto deformuota schema veikiant simetrinei apkrovai (a), veikiant asimetrinei apkrovai (b). Apkrova tolygiai paskirstyta ant standumo sijos. Pagrindiniai nežinomieji (tiesinio skaičiavimo atveju) yra poslinkiai vantų ir sijos jungties taškuose (Δ_c, Δ_d, Δ_e, Δ_f), sijos lenkimo momentai M ir vantų ašinės jėgos N_i. Taip pat papildomi nežinomieji yra siją palaikančiosios vantų jėgos F_1, F_2, F_3 ir F_4 (2.16 pav.).

Sudarius skaičiavimo metodiką vantinei ir sijinei sistemai (2.1–2.52 lygtys) buvo pasiūlytas metodas, kuris gali būti pasirinktas įvertinant sistemos elgseną.

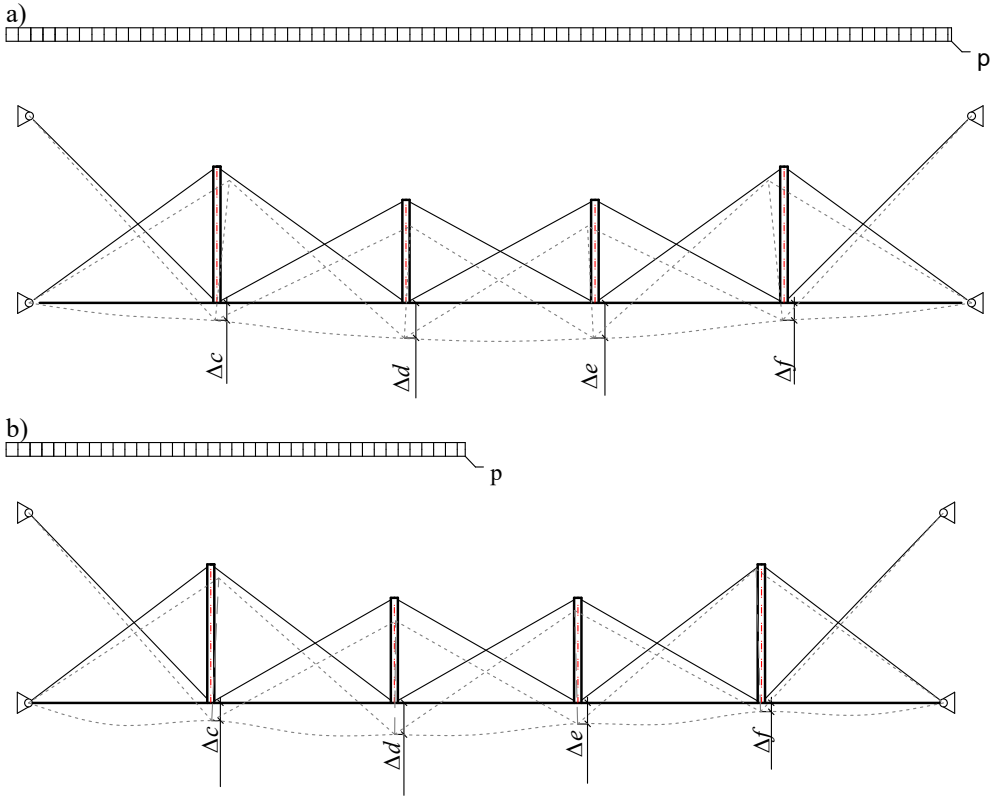

2.2S pav. Deformuoto tilto išvaizda: simetrinis apkrovimas (a), asimetrinis apkrovimas (b)

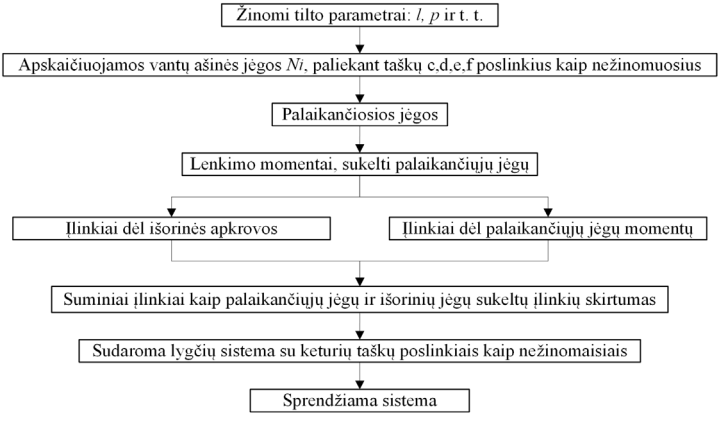

2.3S pav. Skaičiavimo eiga vantinei-sijinei konstrukcijai

Laikantis 2.3S pav. aprašytos sekos buvo apskaičiuota vantinė ir sijinė sistema (2.4S pav.) su profilių duomenimis, nurodytais 2.1 lentelėje, o gauti rezultatai palyginti su Dlubal RFEM skaitiniu modeliavimu. Šio palyginimo duomenys pateikti 2.1S ir 2.2S lentelėse.

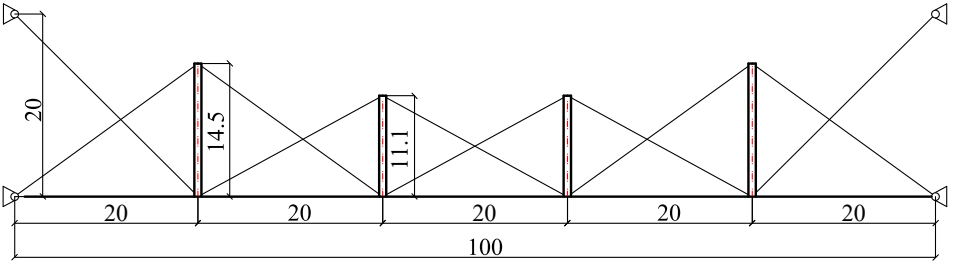

2.4S pav. Analizuotos kryžminių vantų sistemos matmenys

2.1S lentelė. Vantinio-sijinio tilto įrąžos ir įlinkiai esant simetriniam apkrovimui

Sija							Vantai
	Maksimalus lenkimo momentas [kNm]		Įlinkiai [m]				Didžiausioji ašinė jėga [kN]
	M+	*M-*	Δ_c	Δ_d	Δ_e	Δ_f	
BEM	772	1214	0,142	0,306	0,306	0,142	2225
Skaič. metodika	745	1170	0,144	0,318	0,318	0,144	2285
Skirtumas [%]	3,50	3,62	1,39	3,77	3,77	1,39	2,63

2.2S lentelė. Vantinio-sijinio tilto įrąžos ir įlinkiai esant asimetriniam apkrovimui

Sija							Vantai
	Didžiausioji ašinė jėga [kN]		Įlinkiai [m]				Didžiausioji ašinė jėga [kN]
	M+	*M-*	Δ_c	Δ_d	Δ_e	Δ_f	
BEM	773	1181	0,116	0,231	0,206	0,087	1966
Skaič. metodika	791	1140	0,115	0,229	0,203	0,087	1983
Skirtumas [%]	2,28	3,47	0,862	0,866	1,46	0	0,86

Taip pat, sudarius skaičiavimo metodiką vantinei ir styginei sistemai (2.53–2.72 lygtys) buvo pasiūlytas metodas, kuris gali būti pasirinktas apskaičiuojant šios sistemos įrąžas ir poslinkius, 2.5S pav. pavaizduota šio skaičiavimo seka.

Vantinė ir styginė sistema (2.4S pav.), kurios vantų ir pilonų skerspjūviai pateikti 2.1 lentelėje, buvo apskaičiuota taikant 2.5S pav. aprašytą metodiką ir palyginta su skaitinio modeliavimo Dlubal RFEM rezultatais. Pasirinktas stygos skerpjūvis – $A_{string} = 78{,}5\ \text{cm}^2$. Šio palyginimo duomenys pateikiami 2.3S lentelėje.

Nustačius kryžminio vantinio tilto skaičiavimo metodikas, galima nagrinėti naujoviško styginio tilto projektavimą ir racionalius parametrus sijinei sistemai. Parabolinis pilonų išdėstymas reikšmingai sumažina lenkimo momentus sijoje, palyginti su vienodo aukščio pilonų konfigūracija. Siekiant nustatyti racionalias pilonų apybraižos formas buvo panaudotas L-BFGS algoritmas. Analizės metu paaiškėjo, kad išoriniai pilonai aukštėja, o viduriniai žemėja, susidarant paraboliniam aukščių pasiskirstymui, kurį lemia tarpmazgių plotis arba išankstinis įtempimas.

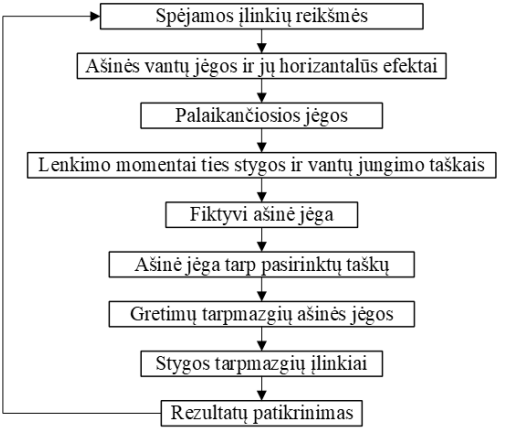

2.5S pav. Skaičiavimo eiga vantinei-styginei sistemai

2.3S lentelė. Vantinio-styginio tilto įrąžos ir įlinkiai esant simetriniam apkrovimui

Styga						Vantai
	Didžiausioji ašinė jėga [kN]	Įlinkiai [m]				Didžiausioji ašinė jėga [kN]
		Δ_c	Δ_d	Δ_e	Δ_f	
BEM	6683	0,423	1,134	1,134	0,423	3761
Skaič. metodika	6475	0,415	1,120	1,120	0,415	3741
Skirtumas [%]	3,11	1,92	1,25	1,25	1,92	0,53

Nelyginis tarpmazgių skaičius yra racionalus sprendinys dėl tolygesnio įtempių pasiskirstymo, tą patvirtina ir jau įrengti kryžminių vantų tiltai. Tinkamas kryžminių vantų ir stygų išankstinis įtempimas labai svarbus palaikant konstrukcijos pradinę formą bei mažinant poslinkius. Vis dėlto vantinis-styginis sprendinys generuoja didesnes atramines reakcijas, todėl pamatų projektavimui turi būti skiriamas ypatingas dėmesys. Apibendrinant galima teigti, jog vantinio-styginio tilto pranašumai – galimos mažesnės sąnaudos ir geresnis konstrukcijos atsparumas asimetrinėms apkrovoms, pasiektas parenkant racionalų pilonų konfigūraciją bei tinkamai reguliuojant išankstinius įtempius.

3. Eksperimentinis vantinio-styginio plieno tilto modelio tyrimas

Trečiajame skyriuje pateikti fizinio modelio ekperimentų rezultatai. Modelį sudarė 5 tarpmazgiai, skirtingo aukščio pilonai, kuriuos laiko iš anksto įtempta plieninė styga. Vietoje tradicinių pagrindinių (šoninių) pilonų šiame modelyje naudojamos standžios atramos, skirtos galimiems horizontaliiems minėtų pilonų poslinkiams riboti eksperimento metu (3.1S pav.). Iš anksto įtemptos stygos galai taip pat buvo inkaruoti į tas pačias standžias atramas.

3.1S pav. Vantinio tilto modelis

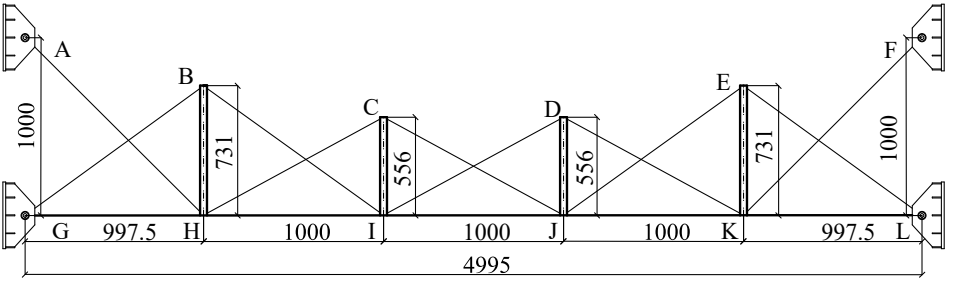

3.2S pav. Vantinio-styginio tilto modelio geometriniai parametrai

Tilto modelio ilgis – 4995 mm. Viduriniai tarpmazgiai tarp pilonų po 1000 mm, o išoriniai tarpmazgiai po 997,5 mm. Išorinių pilonų aukštis siekia 731 mm, o vidinių – 556 mm. Tarpinių pilonai išdėstyti pagal parabolinę kreivę. Vertikalus atstumas tarp viršutinių atramų ir apatinio įtvirtinimo – 1000 mm (3.2S pav.). Atstumas tarp stygų plane – 320 mm. Stygos ir kraštiniai (inkariniai) vantai įtvirtinami į atraminius guolius, kurie gali suktis apie horizontaliąją ašį (3.3S pav., a).

a) b)

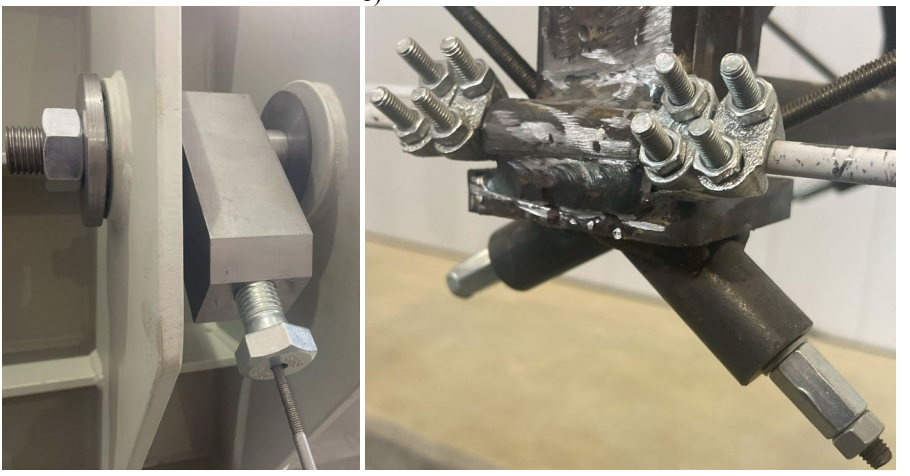

c)

3.3S pav. Inkarinio vanto tvirtinimas „A“ (a); pilono apatinė jungtis „I“ (b); atrama „L“ (c)

Styga suprojektuota kaip ištisinis plieninis strypas, siekiant užtikrinti tolygų šio elemento įtempimą. Visi vantų ir stygų galai turi sriegį, skirtą surinkimui ir įtempimui. Stygos įtempimas pasiekiamas naudojant inkarinius varžtus ant lankstinių atramų. Kryžminiai vantai prie pilonų jungiami per prailgintas veržles, užsukamas ant nusriegtų jų galų. Pilonai paremti ant stygos, pervertos pro jų įvores, o prie stygos jie pritvirtinami U formos varžtais. Taip užtikrinama, kad pilonai nepasislinks išilgai stygos (3.3S pav., b).

Styga ir kryžminiai vantai suprojektuoti iš apvalaus d = 6 mm strypo. Pilono elementams parinktas 40×40×3 mm stačiakampis vamzdis. Tokie skerspjūvio matmenys pasirinkti siekiant panaikinti galimas ašines pilono deformacijas ir taip sumažinti jų įtaką bendroms tilto deformacijoms. Inkarnių vantų atramos (3.3S pav.) suprojektuotos taip, kad būtų įmanoma įtempti inkarinį vantą ir stygą, nesukeliant papildomų (daugiausia sukimo) įtempių. Išankstinis vantų ir stygos įtempimas šiame modelyje yra itin svarbus, kadangi jis užtikrina nuolatinį kryžminių vantų tempimą. Taip pat, esant tam tikrai apkrovimo reikšmei, kraštiniai stygos tarpatramiai gali būti gniuždomi. Modelio elementų išankstinis įtempimas buvo suteikiamas palaipsniui.

Eksperimentu ir skaitiniu modeliavimu (BEM) gauti stygos poslinkių duomenys pateikti 3.1S lentelėje. Iš jų matyti, kad didžiausi skirtumai tarp eksperimentiškai bei BEM būdu nustatytų stygos poslinkių siekia apie 9–10 %, nepriklausomai nuo taikytos simetrinės ar asimetrinės apkrovos. Pažymėtina, kad tik vidinio stygos tarpmazgio eksperimentiniai poslinkiai yra didesni už skaitiniu būdu nustatytus; visuose kituose tarpmazgiuose skaitiniu metodu gautos poslinkių reikšmės buvo didesnės.

3.1S lentelė. Įlinkių palyginimas

Apkrovimas	Žingsnis	Įlinkiai	Tarpmazgis (G-H)	Tarpmazgis (H-I)	Tarpmazgis (I-J)
			Įlinkiomatis 3	Įlinkiomatis 5	Įlinkiomatis 7
Simetrinis	1	Eksp. [mm]	16,05	14,96	15,95
		BEM [mm]	17,70	14,40	14,40
		Skirtumas [%]	9,3	3,7	9,7
	2	Eksp. [mm]	20,97	15,30	17,50
		BEM [mm]	20,20	16,00	16,00
		Skirtumas [%]	2,7	4,4	8,6
Asimetrinis	1	Eksp. [mm]	16,00	16,20	10,04
		BEM [mm]	17,30	15,30	10,40
		Skirtumas [%]	7,5	5,6	3,5
	2	Eksp. [mm]	20,40	18,00	12,26
		BEM [mm]	19,60	17,00	11,80
		Skirtumas [%]	3,9	5,6	3,7

Eksperimentiškai ir BEM būdu nustatytos stygos ir kryžminių vantų ašinės jėgos pateiktos 3.2S lentelėje. Iš duomenų matyti, kad abiejuose apkrovimo etapuose skaitiniu būdu apskaičiuotos stygos tarpmazgių jėgos yra didesnės už eksperimentiškai gautas. Didžiausių reikšmių skirtumai išoriniame stygos tarpmazgyje neviršija 7 %, o viduriniame stygos tarpmzdyje maksimalus poslinkių skirtumas pirmajame apkrovimo etape siekia 19 %; padidinus apkrovą (2 etape), šis skirtumas sumažėja iki 7 %.

Analizuojant vantų įtempių reikšmes nustatyta, kad tik viduriniams vantams BEM duomenys rodo mažesnes jėgas nei eksperimentiškai išmatuotos. Didžiausias šių verčių skirtumas užfiksuotas antrajame apkrovos etape. Nesutapimai rezultatuose greičiausiai kyla iš minėtų neatitikimų tarp skaitinio ir realaus tilto modelio.

3.2S lentelė. Ašinių įrąžų palyginimas

Apkrovimas	Žingsnis	Ašinė jėga	Tarpma zgis (G-H)	Tarpma zgis (H-I)	Tarpma zgis (I-J)	Ink. vantas (A-H)	Viduriniai vantai (C-J, I-D)	
			Tenzojutiklis 1	Tenzojutiklis 2	Tenzojutiklis 3	Tenzojutiklis 7	Tenzojutiklis 11,12	
Po įtempimo		Eksp. [kN]	2,93	2,35	1,68	0,49	1,02	
		BEM [kN]	2,81	2,13	1,51	0,38	1,13	
Simetrinis	1	Eksp, [kN]	4,013	4,76	5,03	2,26	0,68	
		BEM [kN]	4,26	5,49	6,02	2,13	0,03	
	2	Eksp, [kN]	4,53	5,35	6,67	2,63	0,51	
		BEM [kN]	4,69	6,26	6,94	2,50	0,02	
Asimetrinis	1	Eksp, [kN]	3,88	4,06	3,67	1,24	1,01	0,72
		BEM [kN]	4,29	4,81	4,27	1,85	0,84	0,08
	2	Eksp, [kN]	4,32	4,61	4,53	1,66	0,93	0,52
		BEM [kN]	4,76	5,44	5,78	2,15	0,87	0,01

Taip pat svarbu paminėti, kad eksperimento metu tiek stygai, tiek inkariniam vantui nebuvo pasiektos BEM nustatytos įrąžų vertės, išskyrus vidurinius skersinius vantus.

Bendrosios išvados

Apibendrinus analizės rezultatus, galima teigti, kad:

1. Sukurtas nauja vantinio tilto konstrukcinė schema su kryžminiais vantais ir iš anksto įtempta styga. Jos elgsenai analizuoti sukurta skaičiavimo metodika. Ji leidžia racionaliai parinkti konstrukcijos parametrus. Remiantis pasiūlytomis išraiškomis, galima nustatyti racionalią pilonų aukščių konfigūraciją ir vantų įtempimą.

2. Kryžminis vantinis tiltas pasižymi puikiomis savybėmis veikiant asimetriniam apkrovimui. Eksperimentinė, skaitinė ir analitinė analizės parodė, kad tokie tiltai efektyviai perskirsto netolygias pėsčiųjų apkrovas. Šis perskirstymas padeda sumažinti standumo sijos ar stygos poslinkius ir įrąžas, išlaikant jas ne aukšesnes nei esant simetriniam apkrovimui.
3. Netolygus poslinkių pasiskirstymas kryžminių vantų tilte pabrėžia būtinybę tinkamai parinkti stygos ir vantų išankstinį įtempimą. Bandymų rezultatai parodė, kad tiek simetrinės, tiek asimetrinės apkrovos atvejais didžiausi poslinkiai pasireiškia kraštiniuose stygos tarpmazgiuose (pvz., G-H ir K-L), o mažesni – viduriniuose tarpmazgiuose (pvz., I-J). Todėl svarbu tinkamai parinkti išankstinio
   įtempimo reikšmes inkariniuose ir kryžminiuose vantuose, siekiant išvengti didelių įlinkių ir užtikrinti pradinę konstrukcijos formą.
4. Eksperimentiniai rezultatai ir baigtinių elementų analizė patvirtina naujos vantinės-styginės tilto sistemos įgyvendinamumą. Eksperimentinių ir skaitinių modelių palyginimas simetrinio ir asimetrinio apkrovimo atvejais rodo, kad poslinkių neatitikimas neviršija 9 %, o jėgų reikšmės skiriasi mažiau nei 10 %. Be to, skaičiavimo metodika, lyginant su skaitiniu modeliavimu, parodė mažesnį nei 4 % neatitikimą. Šie rezultatai patvirtina siūlomų skaičiavimo metodų taikymą kryžminių vantų pėsčiųjų tiltams.

Povilas DABRILA

STRUCTURAL ANALYSIS OF INNOVATIVE STEEL CABLE-STAYED-STRING BRIDGE

Doctoral Dissertation

Technological Sciences,
Civil Engineering (T 002)

INOVATYVAUS VANTINIO-STYGINIO PLIENO TILTO KONSTRUKCIJŲ ANALIZĖ

Daktaro disertacija

Technologijos mokslai,
Statybos inžinerija (T 002)

Lietuvių kalbos redaktorė Dalia Markevičiūtė

Anglų kalbos redaktorė Jūratė Griškėnaitė

2025 05 05. 10,5 sp. l. Tiražas 20 egz.
Leidinio el. versija *https://doi.org/10.20334/2025-026-M*
Vilniaus Gedimino technikos universitetas
Saulėtekio al. 11, 10223 Vilnius
Spausdino UAB „Ciklonas“,
Žirmūnų g. 68, 09124 Vilnius